ABSTRACT

Moment Analysis Methods of Ultrasonic Waveforms to Characterize the Internal Temperature and Melt Transition Boundary for Materials with Irregular Porosity

Tyler R. Watson, M.S.M.E.

Mentor: David A. Jack, Ph.D.

The utilization of acoustic measurements occurs frequently in a multitude of industries. Monitoring the internal thermal and phase states of materials is of particular interest to the petro-chemical, food, and polymer processing industries, and ultrasound has found limited investigation within the literature for such applications. In this thesis, ultrasound is shown to be useful for monitoring spatial thermal variations through the thickness of a material system without the need to access the interior of the medium in question. The research presented within this thesis will show how the characterization of the internal thermal state of a structure containing random and irregularly shaped internal voids is possible using the internal moments of the captured acoustic waveform. Studies are presented to demonstrate the sensitivity of the resulting analysis to variations in the experimental configuration. The results of this research demonstrate how the proposed methodology is capable of quantifying the internal thermal and phase states of porous mediums with thermal gradients and approximating the two-dimensional variation of the temperature from ultrasonic waveforms.

Moment Analysis Methods for Ultrasonic Waveforms to Characterize the Internal Temperature and Melt Transition Boundary for Materials with Irregular Porosity

by

Tyler R. Watson, B.S.M.E.

A Thesis

Approved by the Department of Mechanical Engineering

_____

Paul Ro, Ph.D., Chairperson

Submitted to the Graduate Faculty of
Baylor University in Partial Fulfillment of the
Requirements for the Degree
of

Master of Science

Approved by the Thesis Committee

_____

David A. Jack, Ph.D., Chairperson

_____

Douglas E. Smith, Ph.D.

_____

Ian Gravagne, Ph.D.

Accepted by the Graduate School

August 2021

_____

J. Larry Lyon, Ph.D., Dean

Page bearing signatures is kept on file in the Graduate School.

TABLE OF CONTENTS

LIST OF FIGURES

ACKNOWLEDGMENTS

I want to thank my mentor, Dr. David Jack, for all the wisdom he has poured into me. It is true to say he has been my primary educator in the field of ultrasonics. However, this is not the wisdom I am referring to. Dr. Jack goes beyond the role of an educator to become whatever it is his students need. Specifically, he provides encouragement to those who've lost all courage in themselves. I could not have reached the place I stand now without his guidance.

I want to also thank my parents, Doug and Karla Watson, my brother and sister-in-law, Travis and Samantha Watson, and all of my friends who have remained at my side from the moment they met me. If it were not for the constant reminder that I have an infinite supply of support from each of these people, I don't know where I'd be today, much less how little I would have accomplished. So, thank each of you for the extended phone calls day after day.

Thank you, Sandia National Laboratories, for the funding of this work, but thank you all the more David Moore and Sarah Stair for the direction you have provided along the way. The work displayed in this thesis is progressed tremendously by the efforts of these two individuals.

I cannot talk of encouragement, guidance, direction, and support without mentioning the God above. For in every meeting my mentor was tied up in, every phone call to family and friends that was left unanswered, and every time my sponsors could not be reached for direction, I was never alone. Thank you, Jesus, for never allowing me to be without the encouragement, guidance, direction, and support you knew I so desperately needed.

DEDICATION

To the God of all creation, who spoke into existence the very scientific laws the authors of this work humbly attempt to describe.

CHAPTER ONE

Introduction

The intent of this thesis is to present a new methodology to quantify the internal temperature across phase transitions of materials containing a high degree of irregular porosity using ultrasound. High porosity materials are inherently difficult to characterize using acoustic techniques due to the nature for sound to scatter off any non-uniform surface or material boundary change. For this reason, the desire for new methods of thermal characterization is not unique to this thesis [1,2]. One of the early attempts to characterize porous materials found within the literature dates back to 1990 when Nagy utilized slow wave propagation to analyze rock formations [1]. Recently, Nori and Venegas commented on the general lack of methodology centered around characterization of porous materials [2].

Although the history on this field of research is limited, it has potential for use within industry. Thermal characterization of any material using ultrasound would allow for the ability to quantify the temperature of a medium which may be deemed inaccessible. The inaccessibility of the medium can vary from physical constraints to concerns of material handling due to sanitary limitations. Ultrasound techniques do not require direct access to a material to perform analysis. Industries who share an interest in the development of the research described include, but are not limited to, the petro-chemical industry, the food industry, and the polymer processing industry. Applications in the petro-chemical and food industries would tend to center around materials transport,

whereas the polymer processing industry would benefit from manufacturing controls and process monitoring. The benefit of the thermal quantification described is expanded by attributing these concepts to a broader range of material types. The interpretation of sound waves will be expanded in order to further the development of material characterization.

1.1 Thesis Overview

A porous material is presented and analyzed using techniques intended for materials of uniform, homogeneous structure. Chapter Three will introduce this porous material and contrast it with a material of homogeneous structure with a similar melting temperature that has been previously investigated by the same research team from which the author is a member of. The nonporous material is investigated, and the results align with previous studies. The same techniques are applied to the porous material and the results presented are unsatisfactory. The purpose of this comparison is to demonstrate the need for, and benefits of, new interpretations for acoustic signals. The analysis covered in Chapter Three will also lead to the desire to characterize a material based on the entirety of an acoustic waveform.

In order to characterize a material based on the entire waveform requires experimental considerations which could previously be ignored using the existing characterization techniques. Chapter Four presents these additional considerations and provides possible solutions to address the new challenges when investigating highly porous materials. Signal resolution shall be the priority in each adaptation made to experimentation. The entirety of a signal cannot be used for analysis if it is polluted with distortions. Several factors which commonly distort a signal are identified. The solutions

suggested by the author are different than typical methods employed to enhance signal clarity due to the highly attenuative and ringing nature of the captured waveform due to the high degree of internal scatter. The solutions presented within this thesis are intended to be preliminary to testing. While this process is intended for thermally characterizing materials, these discoveries can be attributed to other applications including flaw detection (see e.g., [3]).

Chapter Five discusses each proposed expansion to signal interpretation once a proper experimental test setup is completed and the data has been collected. Several methods to extract the relationship between the acoustic waveform and the internal thermal profile are presented and are compared against each other. Embedded thermocouples are used for validation of each analysis method. First, the energy of the captured waveform is studied. For the porous material studied throughout this thesis, the proposed signal energy analysis provides results for approximating the transition temperatures similar to the results obtained from differential scanning calorimetry. The interpretations of ultrasonic signals are further expanded to include an analysis on statistical central moments of a waveform. The central moments of a captured waveform are shown to be capable of identifying the transition between phase states of a material, however, their utility for thermal characterization is shadowed by that of energy. The central moments of waveforms are useful for describing the shape of each signal and relaying information about the quality of the scans to the analyst. The discussion covering central moments proposes potential uses for future studies.

The main contribution of this thesis pertains to the discovery of how the first raw moment of an acoustic soundwave can be used to thermally characterize materials of

irregular porosity. This discovery leads to a surrogate representation of the material property, speed of sound. Employing the same calculations as are typically done to characterize the speed of sound, the first raw moment will be shown to return what shall be termed as the centroidal speed of sound. The calculated centroidal speed of sound possess a monotonic, piecewise continuous relationship with temperature. To demonstrate this, data will be collected while the material experiences thermal equilibrium and is used to define a relationship between the centroidal speed of sound and temperature for ranges encompassing the material's transition temperature. The relationship defined for the solid region will be preferred over prior relationships based on inspection methods proposed for homogeneous materials in Chapter Three. The generation of the preferred relationships will be proven to be repeatable and applicable to industry in Chapter Six.

Chapter Six introduces experimentation which tests the applicability of the proposed inspection methodology. Two tests are involved within this chapter. The first test shall observe the material as it uniformly cools while the second shall observe nonuniform cooling. An experimental overview will be given for each of the experimental configurations. Both tests attempt to validate the capability of the centroidal speed of sound for effective internal temperature quantification of porous materials across a two-dimensional rectangular plane. Signal energy will also be provided to examine its ability to identify the time a material begins its transition of phase during continuous testing. All information obtained from ultrasonic data collection will be verified using internally positioned thermocouples. Finally, a temperature profile will be approximated for two-dimensional representations of internal temperature along the

distance of channel lines. The results presented show the temperature using the estimated thermal profile based upon the acoustic waveform are typically within 5℃ of the actual temperatures characterized using internal thermocouples.

The final chapter is a conclusion discussing each scientific contribution made throughout this thesis and the broader significance to the scientific community. The thesis provides a discussion on potential areas of future work to increase the understanding of the inspection methodologies proposed and to test their limitations.

CHAPTER TWO

Literature Review

This chapter is intended to inform the reader on the basic principles of the research contained within this thesis. The information presented within this brief review is expanded upon in each individual chapter throughout this thesis as the various topics arise. Section 2.1 and Section 2.2 are intended to provide the reader with answers to how and why the authors are investigating new methodology for the thermal characterization of materials containing randomly dispersed and sized internal voids, and Section 2.3 and Section 2.4 will narrow the scope to the fundamental information required to achieve our goal.

2.1 Thermal Characterization of Homogeneous Materials

Section 2.1 introduces the history of material characterization for materials of uniform structure. The reader will be informed on the work completed by previous members of the research group and the methodologies used for characterization at that time. Understanding how materials were previously characterized is paramount to understanding the desire for additional characterization techniques. To achieve this understanding, the experimental procedures performed by previous researchers will be described. The material structures these experimental procedures are capable of successfully characterizing are reported. The processes used in signal analysis for material characterization, both inside and outside the present research group, will be discussed. Similar testing procedures will be adapted in Chapter Three based upon the

works of prior researchers. It is important to understand the calculations used in previous characterization techniques to further the understanding of how interpretations found in Chapter Five differ from previous researchers.

The research contained within this thesis is a continuation of efforts performed previously by Stair, Gregg, Jost, and Jeffrey [4-7] who each analyzed homogeneous materials without irregular internal porosity. An inspection technique for the characterization of homogeneous materials was proposed, or performed, by each of these researchers. Stair analyzed a soy-based candle wax as it experiences internal alterations to temperature and phase state in [4]. An inspection technique involving a strong focus on the onset to the time of flight of a signal was proposed. In the work of Stair, a signal's time of flight corresponds to the length of time required to send an acoustic waveform through a medium. The onset to the time of flight loosely refers to the first instance at which the acoustic waveform arrived in the recorded a-scan data. Determining the exact location for the onset to the time of flight continues to be a disputed topic (see e.g., [8]). For the inspection technique proposed by Stair, determining the exact location of the onset to the time of flight was of less importance than the ability to be consistent between data sets. This inspection technique uses the distance traveled by the signal through the homogeneous material and divides it by the given time of flight to produce a bulk speed of sound for a given temperature. The results demonstrated that the location determined as the onset to the time of flight for each waveform needs to be consistently chosen rather than exactly. For example, selecting the initial time that correlates to signal arrival by hand is subject to human error, but the time corresponding to 20% of the peak amplitude yielded consistent results across data sets (see e.g., [9]). Selecting the time of fight in the

previous studies, [4-7], was performed using a detection threshold technique within a custom software written in the MATLAB environment.

The previous work conducted by Gregg [5] involved the thermal analysis of a homogeneous soy-based wax over temperature ranges encompassing phase transitions. The material mentioned is of uniform structure and exhibits no signs of porosity during the solidification process. Experimentation found in [5] involves directing heat flow through a material contained within a rectangular structure. As the internal temperature of the studied material increased, transducers aligning the walls of the rectangular container continuously collected ultrasonic data. Speed of sound was calculated for the material over the duration of testing based on the onset to the time of flight as estimated by Stair [4]. The speed of sound data was compared to thermocouple data obtained during testing to identify the relationship between speed of sound and internal temperature. Stair and Gregg [4,5] both identified a nonlinear relationship between the speed of sound and temperature for select homogeneous materials as the phase of the materials transitioned.

Research conducted by Jost in [6] focused on addressing the nonlinear relationships identified by Gregg and Stair. Jost selected another soy-based material to analyze during phase transitions. Waveforms received from experimentation by Gregg and Stair experienced alterations beyond the expected shifting of the onset to the time of flight. The waveforms additionally experienced changes in their general structure, such as amplitude and the overall lifetime of the signal, as temperature changed. Jost's discovery plays a direct role throughout the remainder of this thesis. He addresses the changes in waveform structure by assigning a normalized gain for all waveforms collected. Experimentation performed by Jost closely resembled that of Gregg and Stair, however,

Jost collected the ultrasonic data while continuously renormalizing the gain. Normalizing the gain for all scans allowed Jost to identify the relationship between speed of sound and temperature to be a bi-linear function, specifically a pair of linear functions that intersected each other at a point. The hypothesis proposed in [6] states the location where the two linear relationships meet corresponds to the melt temperature of the material. The hypothesis is supported by a study conducted by Tariq et al [10]. Tariq investigates material hardness of aluminum alloys using ultrasound. Several alloys were heat treated in order to render different levels of expected hardness. The material speed of sound was concluded to be proportional to the material's degree of hardness [10]. Jost's hypothesis is based on a drastic transition in material hardness, therefore the fundamental change in the rate of change of the speed of sound as a function of temperature would change at the transition of phase. The material containing irregular porosity analyzed throughout this thesis will be observed in Chapter Three, and it also possess two different functional forms for the speed of sound as a function of temperature. Results will show that the temperature at which the relationship changes from one functional form to another is also near the transition temperature. Dissimilar to previous work on this project, Jost does not use the bi-linear relationship between speed of sound and temperature to quantify the internal temperature of the homogeneous material. Instead, the relationship is approximated into a step function to relate the speed of sound to the phase of a material.

Jost also briefly addresses the fourth moment, often termed the statistical kurtosis, of a signal to be beneficial for identifying a material's phase transition. Lau et al [44] use the statistical moments of an ultrasonic signal to investigate changes in the signal as they relate to changes in the internal temperature of a material. It is concluded that central

moments, moments that are about the centroid, are capable of identifying when a signal is saturated with high levels of noise. Lau additionally proposes that the higher order statistical moments may be useful in identifying the phase transition of a material. The present research will accept the claims posed by Lau et al, however, we will expand upon them as well in Section 5.3. Our analysis techniques using statistical moments will differ from Jost and Lau by analyzing ultrasonic data taken in independent isothermal material states instead of during continuous thermal testing of the studied materials.

Jeffrey combines information provided by Stair, Gregg, and Jost in order to thermally characterize the soy-based, homogeneous material for internal temperature and phase state [7]. The proposed experimental procedures used to collect ultrasonic data for quantifying the speed of sound of the homogeneous material differs from the work performed previously. Ultrasonic data is collected while the material experiences thermal equilibrium. Continuous data collection is no longer utilized to estimate the relationship between the speed of sound and the temperature. This removes the need to estimate or average the temperature for the material system, and instead the entire material system is held in thermal equilibrium for several hours prior to data collection for each data point. Once the speed of sound is quantified for a set temperature, the material's internal temperature is incremented and again held isothermally to allow thermal equilibrium to return before collecting data again. Performing data collection in this manner allowed Jeffrey to create a smooth and continuous bi-linear equation for the material's speed of sound relationship with internal temperature. As expected, the relationship for speed of sound became bi-linear near the material's transition temperature as proposed by Jost [6,7].

Quantifying the sound propagation of a material by collecting ultrasonic data during thermal equilibrium is not unique to Jeffrey's thesis [11,12]. D'Arrigo and Paparelli are able to quantify the sound propagation speeds of water-ethanol mixtures at low temperatures using a similar experimental setup to Jeffrey's [11]. D'Arrigo and Paparelli immersed a cell containing the material of interest into a "large volume thermostat" [11]. The thermostat used in their experimentation was capable of uniformly distributing temperature throughout the material with a sensitivity of ± 0.1℃. Ultrasonic data was collected only during times of thermal equilibrium experienced by the material. The results from quantifying the speed of sound using this experimentation technique led to a "substantial agreement" with estimates found for the solutions at room temperature [11]. Li et al conduct experimentation similarly in order quantify temperature effects on backscattered energy [12]. Ultrasonic data was collected by Li et al for distilled water in thermal equilibrium at various temperatures verified by thermocouple data. The use of thermocouples to verify a material is in thermal equilibrium is similar in setup to that of Jeffrey's [7] experimentation. Chapter Three of this thesis attempts to quantify the speed of sound of a material with irregular porosity based on the experimental procedures described by Jeffrey and advocated by D'Arrigo, Paparelli, and Li.

Jeffrey uses the bi-linear relationship she obtained from the quasi-isothermal studies to calculate the internal variations of temperature of the soy-based wax contained within a cylindrical geometry in a non-isothermal state [7]. Thermocouples were positioned internally to the medium to observe the accuracy of the analysis performed using exclusively the captured ultrasonic data. An aluminum heater block centered in the cylindrical container provided internal heat generation to the material. The internal heat

source introduced thermal gradients into the material as ultrasonic data was continuously collected. Similar experimentation is utilized in Chapter Six by containing a material with irregular porosity inside a rectangular geometry containing two internal heater blocks. For materials not in thermal equilibrium, Jeffrey's previously defined relationships for quantifying temperature returned the effective, or average, internal temperatures of the material. Jeffrey combines the defined bi-linear relationship of the soy-based wax with the geometry of the cylindrical containment vessel to create a two-dimensional temperature approximation across a circular plane. The plane was equal in depth to the transducers used during data collection. Jia et al similarly expand the one-dimensional effective temperatures returned from speed of sound relationships to two-dimensional temperature fields [13]. Jia et al collect ultrasonic data using multiple transducers in order to observe the effective temperatures of the material along intersecting acoustic pathways. The reconstruction method used rejected the least squares method (see e.g., [14]) and focused on the radial basis function approximation and singular value decomposition. The reconstruction method proposed by Jia et al resulted in a nominal increase to accuracy over the least squares method [13]. Jeffrey's method for constructing two-dimensional temperature fields also relies on the crossing of acoustic pathways. Additionally, Jeffrey's method relies on the generation of temperature profiles along the acoustic pathways calculated using the boundary conditions of the cylindrical container [7]. For the purposes of the present research, ultrasonic analysis will conclude with similarly generated temperature profiles along the acoustic pathways but has not yet been expanded to temperature fields for a two-dimensional rectangular plane.

The previous methods determined by the research group [4-7] studying the homogeneous soy-based wax are reintroduced in Chapter Three and are investigated for a porous material. Characterization using the previous methodology on the porous material will assist in identifying the limitations of the prior method. Chapter Six utilizes experimentation similar to Jeffery's for approximating temperature profiles in order to express the scalar interpretation of internal temperature in a two-dimensional representation.

2.2 Historical Characterization of Materials with Irregular Porosity

Section 2.2 discusses the historically limited advancements for characterization of materials defined by porosity. Material characterization for materials exhibiting high porosity in solid forms has been expanded by researchers outside the present research group. The history of characterization for materials of similar structure will be explained. Understanding the limitations other researchers have experienced characterizing similar material structures shall provide reasoning for the interests taken by the research group. These interests include taking additional steps to increase signal resolution found in Chapter Four and formulating new interpretations to ultrasonic data found in Chapter Five. The research will propose a material inspection methodology conducive for use during thermal analysis which stands apart from previous contributions to the field. It is imperative to understand how the proposed methodology stands apart from the standards of characterization set by other researchers.

Material structures defined by irregular porosity are notoriously illusive to characterization. For this reason, limited resources are exhausted toward the effort. The characterization of a porous material for the purpose of internal temperature

quantification and phase state identification is even further nuanced. These statements are substantiated by the general lack of literature regarding the concept. Of the relevant literature pertaining to porous materials, the majority consists entirely of predictive model theory without experimental representations. Very few researchers attempt thermal characterization on porous materials and instead focus on the ability to propagate sound through these materials at all.

Consider the work of Herskowitz et al in [15]. Alterations in ultrasonic attenuation for porous materials in the presence of dispersed microbubbles are predicted. Biot's approach, or the Biot theory, is used to numerically simulate a system to observe the changes in ultrasonic wave propagation and attenuation. The authors conclude, based upon the numerical simulation, that a correlation exists between the porous features of a material and the attenuation of ultrasound based on frequency ranges [15]. In Chapter Three, experimental results are used to draw similar conclusions about waveform manipulation due to the presence of porosity.

Experimentation to prove the conclusions drawn from works similar to Herskowitz et al is not simplistic. Voids along the surface of a porous material are likely to cause complete signal loss. The authors propose the lack of experimental validation represented throughout literature is a reflection of the limitations of ultrasonic hardware used to collect data across porous media. The effort presented in Chapter Four is an effort to maintain signal resolution while characterizing materials of irregular porosity. Nagy et al address the issue of acoustic propagation through porous materials in [1]. A common solution to signal retention in porous media mentioned by Nagy is to fill the porosity with a higher viscosity material than air, such as water. Since our interests are analyzing

mediums enclosed in inaccessible containers, it was not practical for us to consider such an experimental configuration. Nagy et al propose the use of slow wave propagation as a solution to propagating sound in the presence of porosity [1]. The slower waveforms do not experience the same drastic change in attenuation and scatter between solids and gases, therefore the signal does not completely disperse upon traversing the pores. The frequency of the slow waveform is selected based on pore size in order to receive a signal at all [1], and for the system studied in this thesis a 500 kHz transducer was found to penetrate through the porous medium investigated. The transducer frequency would need to be adjusted based upon the size of the porous structure being investigated.

The addition of experimental data to support anticipated acoustic behaviors for porous materials is needed within this field of research. This thesis will contribute to furthering the scientific communities understanding of acoustic behavior by providing several series of experimental data. Of the literature mentioned within this section, neither considered the effects of temperature on porous materials. Very few researchers have attempted to perform the thermal characterization of porous materials. The limited literature regarding this topic within the thesis is a reflection of the limited information available to the authors. The advancements proposed for thermal characterization are truly separate from previous research.

The history of material characterization for both homogeneous and porous materials has been discussed. The direction for the research made by the authors throughout this thesis follow the guidelines set before. Utilizing similar characterization techniques to prior researchers of the field will provide the incentive to propose differing techniques.

2.3 Basics of Ultrasound

Section 2.3 begins to narrow the scope of discussion by introducing the basic principles of ultrasound. Raw ultrasonic data is commonly represented in three unique forms, each of which are discussed in this section. The expression of raw data each representation provides to an analyst renders unique information regarding the waveforms, so an explanation for each representation is included. How the raw data obtained from ultrasound is observed will be imperative for all proceeding chapters. Three common hardware configurations exist for collecting ultrasonic data, and each option is discussed in detail. Information on why a given data collection method is preferred over another will form a basis for the presentation in Chapter Four. Additionally, the proposed inspection methodology relies heavily on waveform structure and propagation. Ultrasonic transmission generates different waveforms defined by their propagation. Therefore, it is important to understand what types of waveforms exist and which ones are applicable to the present research. Chapter Four relies on specific waveform isolation to achieve proper characterization. Section 2.3 concludes on the basic calculations used previously for characterization that will serve as the basis for the presented contributions.

The fundamentals of ultrasound are built upon to allow the research to take on different forms. For example, there exists three different plotting techniques continually used to represent the raw data collected from ultrasound [16]. The first technique uses the raw waveform captured as the ultrasonic signal arrives and is recorded in what is known as an a-scan. The a-scan is often represented on an oscilloscope for voltage as a function of time. The voltage amplitude oscillates with time until it dampens out entirely. Voltage

represented in a-scan data is in response to acoustic soundwaves. Soundwave propagation occurs after an electrical current sent to piezoelectric crystals located inside the transducer is dispersed. The dispersion causes ultrasonic mechanical vibrations at the transducer face which propagates waveforms across a media. The reception of soundwaves by a transducer performs the same actions in reverse. Mechanical vibrations displace the receiving transducer's face and are recorded as a voltage, effectively recording the resultant soundwave [16]. Unaltered, raw a-scan data presents the purest form of an ultrasonic wave. Jost and Jeffrey collected a-scans while normalizing gain values in [6,7]. In the present research, the unaltered structure of the waveform is paramount in importance for the alternative inspection methodology proposed.

The second method often used to interpret the resulting acoustic information is the representation of ultrasonic data displayed using b-scans, where the a-scan is plotted as a function of time or space based upon the system being investigated. B-scans are commonly seen in applications pertaining to flaw detection [16-18]. Zhang et al demonstrate a common application of b-scans used to identify defects in composite materials for the aerospace industry [18]. A-scan information can often be used, based upon the b-scan to identify an area of concern, to identify defects through the depth of the composite part. The b-scan representations reported in the work of Zhang et al align a-scans recorded along a unidirectional displacement of the part and display amplitude intensities. The b-scans identify defects including delamination, resin rich layers, and waviness along a horizontal displacement of a composite part [18]. Traditional presentations of b-scan data involve the a-scan flight time displayed on the lateral axis and the scan location displayed on the longitudinal axis [17]. The lateral axis may also be

converted from a-scan flight time to depth of the part (see e.g., [18]). The contributions of this thesis are not centered on flaw detection, however, a presentation of ultrasonic data similar to the b-scan form described will be presented in Chapter Six, but instead of the a-scans plotted as a function of position as a transducer is run across a surface, the a-scans are plotted as a function of experimental time. The proposed inspection methodology found within this thesis pertains to the thermal characterization of materials and not flaw detection, so b-scan data will instead be understood in terms of lateral a-scan flight time corresponding to longitudinal test time. In Chapter Six, a material is cooled throughout the duration of a test while a-scan data is continuously collected. Each a-scan waveform is aligned along the longitudinal axis chronologically. B-scan presentation in this format allows the analyst to observe alterations to waveform structure across time corresponding to thermal and phase state changes (see e.g., [7]).

The final common representation for raw ultrasound data is known as the C-scan. C-scan data presentation involves a similar data collection requirement to traditional b-scans. Traditional b-scan representations require data collection to occur along a unidirectional displacement. C-scan representations require scans to be performed in a raster pattern in order to represent waveform intensity as a function of depth. The lateral and longitudinal axes each represent the scan location on the part of interest [17].

The process of collecting ultrasonic data is also considered for this research. Ultrasonic data collection may be performed using through-transmission, pulse-echo, or pitch-catch. Pulse-echo requires a single transducer to operate. For a set transducer positioning, an acoustic waveform is emitted, reflected off a backwall, and returned to the same transducer to record the a-scan data [17]. Transducers used in a pulse-echo

configuration are both the transmitter and receiver of soundwaves. Pulse-echo setups are often preferred because they only require access to one side of the desired media and use less hardware compared to the other setups. A downfall of pulse-echo configurations involves the reliance of the transmitted soundwave to return to the original transducer location. Snell's law states the direction of reflection for ultrasonic waveforms is dependent upon the geometry of the backwall [16]. Consider the cylindrical containment vessel used by Jeffrey [7]. Decerning the location of the reflected ultrasonic waveforms would greatly affect the accuracy of the methodology. The difficulty of quantifying thermal and phase state changes for any material greatly increases in the presence of unknown geometries. Using the pulse-echo configuration is not conducive to experimentation used throughout this thesis.

The pitch-catch configuration utilizes two transducers while collecting data. One transducer emits the acoustic wave into the media and a second transducer receives the resulting waveform at a separate location [16]. Prior knowledge of how the waveform will reflect is necessary for positioning the receiving transducer. The advantage of the pitch-catch configuration is similar to pulse-echo. Only access to one side of the media is required to operate in a pitch-catch configuration. However, the same issue also arises while trying to use this configuration for thermal characterization of materials. Tracking the location of a reflection wave becomes proportionally difficult to increasing geometric complexity. Schmerr suggests the angle of reflection for waveforms is a function of speed of sound [16]. As the results show in the present thesis, the speed of sound of the investigated materials is also a function of temperature. Therefore, the reflected waveform will eventually no longer be observable from a transducer's original placement

as temperature changes while using the pitch catch configuration without moving the receiving transducer throughout the study.

Through-transmission is the final configuration to discuss and is the standard configuration used for all experimentation contained within this thesis. Through-transmission requires two transducers, a transmit and a receive, in order for data collection to ensue. Additionally, two separate sides of a media must be accessible. Through-transmission propagates an acoustic soundwave from one transducer in a straight line to the second transducer [17]. This configuration requires less preprocessing of the signal before analysis due to the simplistic acoustic pathways compared to the pitch-catch configuration.

Ultrasonic transmission is also capable of producing four distinct waveforms that may appear in an a-scan. Waveforms are defined by their differences in propagation. A shear wave will propagate through a media while its particle motion fluctuates perpendicular to the direction of propagation [19]. For example, consider constantly whipping one end of a long piece of string vertically. The visible waveform expressed is a representation of a shear wave. Shear waves require special acoustic coupling gel in order to propagate and will not be used for characterization in the present work. The importance of selecting an appropriate coupling gel will be expanded upon in Chapter Four.

The remaining three forms of waveform propagation are all useful in material characterization and do not require unique transducer coupling. Lamb, or plate, waves experience a complex form of propagation that is exclusively exhibited in material thicknesses less than the wavelength sent by the transducer [19]. The applicability to

industrial use is a major factor which directs this research. Most industries desire to quantify temperature across broad areas. For example, the petro-chemical industry cannot scan through a pipeline and return lamb waves because the signal must travel a great distance to traverse the pipe and the lamb waves are incapable of penetrating into the desired material system. For this reason, lamb waves were not considered applicable for the desired applications of the research.

Unlike shear and lamb waves, surface waves are capable of being received during acoustic transmission for the present studies. Surface, or Rayleigh, waves exclusively propagate around the exterior of a material [19]. For the studies conducted in this thesis, the media under study is always housed within a confined vessel. Therefore, surface waves are only capable of characterizing the material of the container and not the media of interest within the vessel. Section 4.1 is dedicated to the dampening of surface waves in order to increase the resolution of the desired waveform.

Longitudinal waves, commonly referred to as pressure waves, are the only waveforms studied as part of our characterization. Longitudinal waves propagate directly from a transducer's face with its particle motion moving in the same direction [19]. For example, consider fixing one end of an extended slinky and repeatedly pushing on the opposite end. The resulting waveform is an example of a longitudinal wave. Longitudinal waveforms are selected as the desired form of sound propagation to capture. Waveforms of this type are capable of characterizing the media of interest across long distances while exhibiting predictable propagation patterns. The use of surface and lamb waves for material characterization is expanded upon in Chapter Three.

The predictability of propagation found in longitudinal waves assists in speed of sound calculations. A pair of transducers set across from one another are commonly referred to by their channel listing. The channel lines, or acoustic pathways, can be defined as the path a signal must take through the media before reaching the receiving transducer. For through-transmission of longitudinal waves, the channel lines can be approximated as the shortest path from one transducer to the next. The length of an acoustic pathway can be used in conjunction with the arrival time of a signal in a-scan data to calculate a material's speed of sound (see e.g., [20]).

$$c_a = \frac{d_a}{t_a} \tag{2.1}$$

where c_a represents the speed of sound for the scan, d_a represents the length of the channel line, and t_a is the time of arrival obtained from a-scan data.

The accuracy of the speed of sound for a material is increased by only considering the time the signal spent within the medium of study. Lopez-Haro et al demonstrate this technique in [20] where they utilized an immersion transducer with pulse-echo configuration to propagate a waveform through water and into a biological tissue sample. The speed of sound for water is known prior to experimentation. The study intended to only characterize the tissue sample. To accomplish this, Equation 2.1 was rewritten for time as a function of speed of sound. The distance the signal traveled through water was used in conjunction with its known speed of sound to calculate the time the signal exclusively spent within that material. The time the signal spent exclusively in the tissue sample could be calculated using a similar relation seen in Equation 2.2 (see e.g., [20]).

$$t_m = t_a - t_w \tag{2.2}$$

where t_m represents the time spent within the material of study and t_w represents the time spent within the material of known speed of sound.

Using the actual time of flight for a material to calculate the respective speed of sound gives a recasting of Equation 2.1 as follows:

$$c_m = \frac{d_m}{t_m} \tag{2.3}$$

where c_m represents the material speed of sound and d_m represents the distance the signal traverses through the respective media.

The methodology for obtaining the material speed of sound will be similarly conducted in Chapter Three. The containers housing the desired media for characterization will be of known speed of sound in order to follow the prescribed procedures.

2.4 Thermo-analyzers

The literature review concludes in Section 2.4 by introducing several of the thermal characterization devices used within the thesis. These devices and machines assist in thermal characterization and are often termed as thermo-analyzers. The thermo-analyzers are used in the validation of the proposed inspection methods. The ability to interpret the information presented by each thermo-analyzer will be discussed within this section. Understanding the potential information that may be acquired from each thermo-analyzer, and how to obtain that necessary information, shall assist in validating the techniques proposed by the author throughout the thesis.

Three devices are utilized throughout this thesis to validate the proposed inspection methodology for thermal characterization. It is important to understand the information provided by each of these thermo-analyzers and their degree of accuracy in

order to ensure the reliably of our discoveries to the reader. The most common thermo-analyzers used to validate methods for quantifying temperature are thermocouples. A thermocouple simply registers changes in voltage at the end of a probe due to a mismatch in materials of the thermocouple wire. A datalogger then uses the change in voltage to correlate back to changes in temperature. The value reported by the datalogger is a scalar for the temperature at the end of the thermocouple probe. K-type thermocouples are connected to a Graphtec midi LOGGER GL820 during the studies contained in Chapter Three, Chapter Five, and Chapter Six. Up to eighteen thermocouples are used simultaneously within the presented research and their results are recorded on the datalogger during testing shown in this thesis. For most tests, thermal data is collected every two minutes for the continuous testing shown in Chapter Six. The Graphtec midi LOGGER GL820 reports temperature to the tenth of a degree Celsius and an error of ± 1.0℃ for K-type thermocouples [22].

The next thermo-analyzer, the differential scanning calorimeter (DSC), is used to approximate the transition temperature of two different materials in Chapter Three. DSC testing begins by encapsulating a weighed sample of the desired material in a Tzero sample pan and loading it into the machine. The DSC then heats and cools the system containing the material while recording heat flow values as the temperature of the environment changes. Curves for heat flow as a function of environmental temperature are useful for approximating the melt temperature and temperature of solidification of the material. Jin et al use a DSC to determine the melt temperature range of several phase changing materials [21]. The accuracy of DSC measurements is affected by the sample weight according to Jin [21]. However, it is suggested to use the range of temperatures

encompassing the peaks of DSC curves to approximate the melt temperature of a material. Jeffrey refers to a “valley” on DSC curves as being useful for selecting melt temperature ranges. The valley corresponds to the temperature at which the slope of heat flow decreases prior to reaching the peak [7]. In Chapter Three, DSC plots are displayed for two separate materials. Further explanation on interpreting the information provided by a DSC is provided at that time.

A thermogravimetric analyzer (TGA) is employed in Chapter Four to investigate acoustic coupling gel performance. The TGA Q50 manufactured by TA Instruments used for this research is capable of measuring the mass of a sample to the tenth of a microgram with an error of ± 0.1% of reported mass [23]. TGA testing involves loading a material sample into a furnace and observing the thermal effects on the material’s mass. Mass is recorded as a percentage of the material’s original weight from the start of the test. TGA experimentation relays a material’s resilience to varying levels of thermal exposure. Section 4.2 is dedicated to observing thermal effects on acoustic coupling gels. Three different acoustic coupling gels are subjected to two TGA tests which increase the heat of the environment and analyze weight changes in the materials. Since the pertinent field of research requires prolonged exposure to high temperatures, the coupling gel must not sufficiently deteriorate during data collection. As TGA testing is introduced in Chapter Four, further explanation of the testing processes will be explained.

CHAPTER THREE

Characterization of High-Porosity Materials with Traditional Methodologies

The material studied during this thesis is a wax developed for aiding in the fabrication and casting of metallic components. This particular material is selected due to its propensity to form large, random, internal voids as it solidifies from a molten state as shown in Figure 3.1. It is the presence of these voids that cause traditional inspection methods significant difficulty and what advances the present work above that of previous authors studying the coupling effects between acoustics and thermal quantification. The tradename of the casting wax selected for the present study is Rigidax® and will be referred to throughout the remainder of this thesis as a "machinist wax" as it is often used as an aid during the machining of parts and tools. The characterization of this material is strictly for the benefit of expanding the horizon of analysis on materials which exhibit similar structural characteristics in solid phases, with a specific interest in highly porous material systems with a random distribution to the internal voids as demonstrated by the machinist wax structure shown in Figure 3.1. This material responds quite differently to acoustic transmission than that of a homogeneous material.

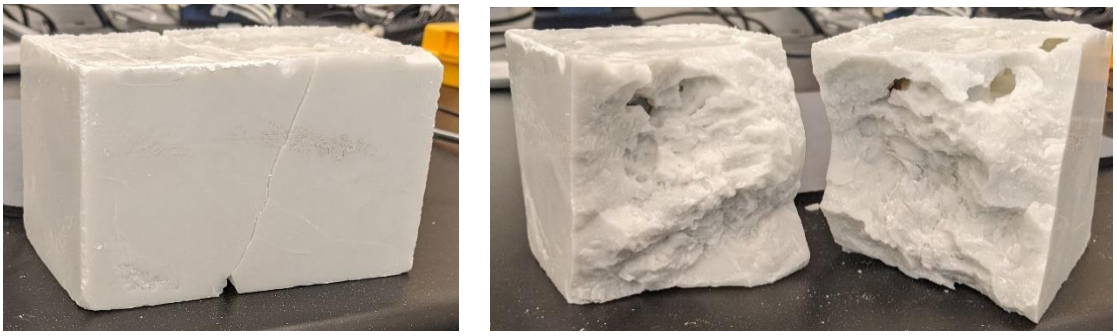

(a) (b)

Figure 3.1. Solid 127 mm x 76 mm x 84 mm (5.0” x 3.0” x 3.3”) block of machinist wax, (a) external view, and (b) internal view highlighting non-uniform, porous structure

The highly porous machinist wax system will be studied in this thesis against a wax system for which no identifiable internal voids occur. The comparison material studied is a wax marketed to the candle making industry, the CBL-125 EcoSoya®. This candle wax solidifies into a homogeneous structure without any detectable voids or variations in the internal microstructure allowing for a smooth acoustic transmission of the generated ultrasonic waves used in this study.

3.1 DSC Results and Comparison to Homogeneous Structures

To better understand the thermal behavior of the materials studied, differential scanning calorimetry (DSC) is employed. The DSC will be utilized to identify temperatures at which phase changes occur, thermal repeatability under repeated thermal loadings, and estimates for the energy required for a phase change. The homogeneous candle wax was analyzed and reported on in a previous study in Taylor Jeffrey’s thesis [7], and those results are used in the present study for comparison. For the DSC testing, Jeffrey sectioned samples of the candle wax that ranged from 5 – 15 mg. Each individual sample was placed into a Tzero DSC sample pan, cooled to -20°C, and then held

isothermally for five minutes. Then, the sample was heated at a rate of 2℃/min until the sample reached 125℃. The sample was then cooled to -20℃ at a rate of -2℃/min. This process was repeated five times to identify signs of hysteresis of the material if there were any. For the 13.91 mg sample Jeffrey studies in [7], the results are replotted in Figure 3.2. Tests two through five returned identical information for this material. The first sweep returned data affected by the previous cooling rate it experienced during manufacturing. The first resulting graph containing repeatable data is displayed.

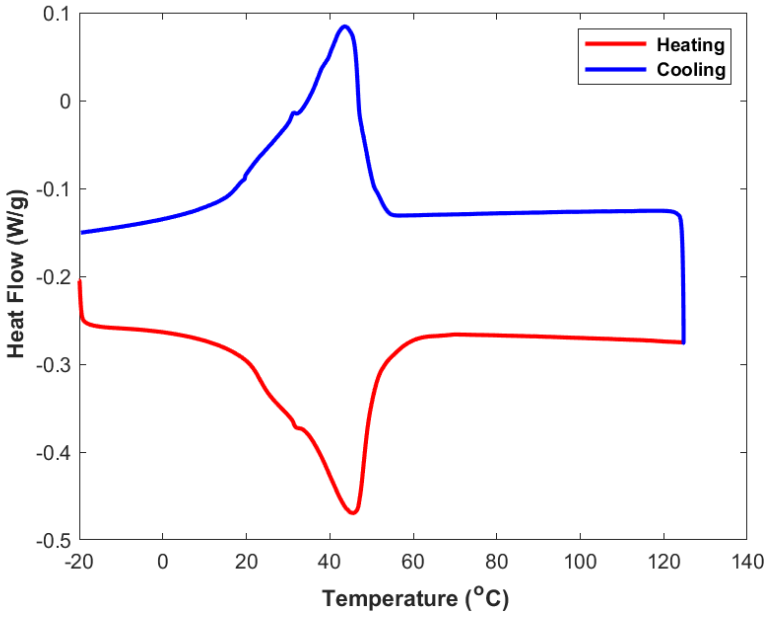

Figure 3.2. Heating and cooling profiles of candle wax given by DSC (data from [7])

The DSC machine returns values for heat flow as a function of temperature. Two separate curves are shown in Figure 3.2. The lower curve represents the material's reaction to heating while the upper curve corresponds to cooling. When a material is cooled, the heat flows outward, an exothermic process, and into the system. Higher values of heat flow in DSC plots correlate to heat being relocated from the material to the

surroundings. That is why cooling curves returned from DSC processes return higher values for heat flow than heating curves. During the heating of a material, heat is absorbed, an endothermic process, by the material from the surroundings resulting in lower values for heat flow. DSC analysis is capable of approximating a material's melt temperature and its temperature of solidification from the heating and cooling curves returned respectively. These transitional temperatures of phase may be approximated by identifying the "valley" of each curve's peak (see e.g., [7]). Based on heating and cooling valleys similarly observed in Figure 3.2, Jeffrey identifies the range between 45°C and 50°C to correlate to the melt and solidification zones for the candle wax. It can be assumed from this point that the major transition temperatures operate independently from heating direction. Therefore, the major transition from either phase state is considered 47°C for the purposes of this chapter. Additionally, the heating and cooling curves both show significant changes in heat flow between 20°C and 55°C. A gradual change between phases is preferred for characterization because ultrasound is affected by a material's internal structure. For instance, a molten material will have a slower speed of sound than when the same material is solid. The DSC indicates the candle wax will gradually soften or harden before its full transition. Therefore, the relationship between speed of sound and internal temperature for this material can also be expected to gradually change as it approaches the transition temperature. The material's SoS as a function of temperature will likely not include a sudden sharp change as it encounters a transition of phase. The bi-linear relationship described by Jost is expected to occur [6], however, the transition from one slope to the next is likely continuous near the melt temperature.

Similar DSC testing was conducted on the nonuniformly porous machinist wax following the same thermal profile as that of the candle wax sample. For the result shown here, a 14.38 mg sample was taken for testing that was a blend from multiple flakes of the machinist wax. In obtaining samples from multiple flakes, the DSC output curves were homogenized. The sample was initially cooled to -20℃ and held isothermally for five minutes. The sample was then heated at a rate of 2℃/min until the sample reached 125℃. The sample was then cooled to -20℃ at a rate of -2℃/min. This process was repeated five times in order to investigate the possibility of changes brought about from the material sample being heated and cooled repeatedly. The results from the fifth heating cycle can are shown in Figure 3.3.

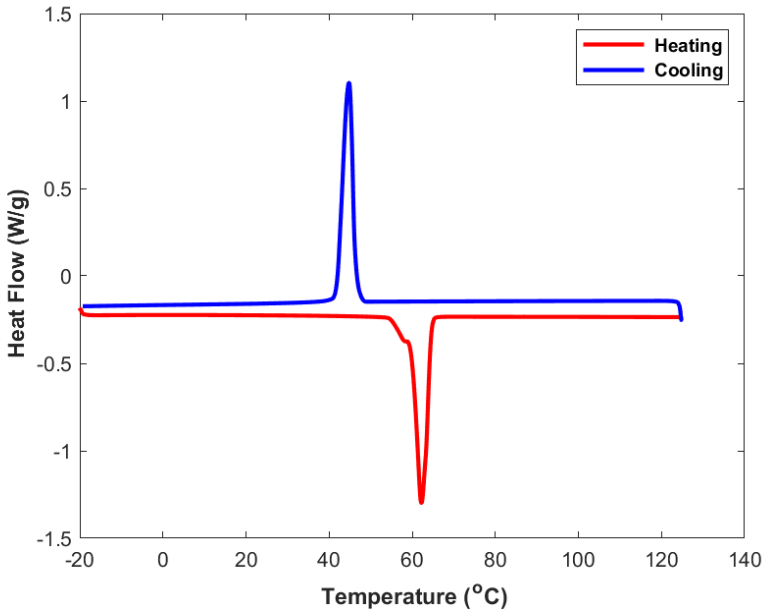

Figure 3.3. Heating and cooling profiles of machinist wax given by DSC

The DSC plot for the machinist wax can be interpreted similarly. The heating and cooling profiles provided by the DSC for the machinist wax appear as heat flow spikes rather than smooth curves, therefore the temperature at the valleys and peaks are

approximately the same. The peaks represented in Figure 3.3 are used to determine the machinist wax's transition temperatures. The heating peak corresponds to the melt temperature of 62℃, and the cooling peak at 45℃ corresponds to solidification. These peaks do not align with each other at a single temperature, as was the case for the candle wax sample. In addition, the transition between the solid form to the molten form state, nor the molten form to the solid form state, does not occur gradually as did the previously studied candle wax. Note the discrepancy found in the machinist wax's heating peak. The curve plateaus briefly before continuing its descent. This plateau experienced during the heating cycle resembles a softening stage as opposed to a complete change of state. A significant point of interest is that the corresponding values for the temperature of solidification and melting are no longer identical as they were for the candle wax noted from Figure 3.2. This observation implies the need for separate plots for time of flight and speed of sound based on the internal temperature's incremental direction in order to fully characterize the material based on traditional methodology. The heating and cooling profiles not only encompass different ranges of temperatures, but they also both encompass a very small range of temperatures. This correlates to the amount of energy that must be absorbed or released by the material to complete a transition between the solid and molten state. A transition of state which occurs quickly between one temperature and the next creates several challenges for characterization. The speed of sound likely has two piecewise functions of temperature which depend on state. If the transition is sudden, a discontinuity may be observed requiring a higher fidelity around the phase change temperatures. Additionally, from the perspective of time and energy, in order for the machinist wax to transition between solid and molten phases, significantly

higher energy will be required for longer durations as the internal temperature nears the determined transition temperatures. Essentially, the specific heat of this material will rise drastically around these temperatures. As the results will later show, ultrasonic data collection around these temperatures is also quite difficult.

In summation, from the findings of the DSC results it is expected that the characterization of the machinist wax should vary greatly from the candle wax. The variations stem from the differences discovered in each material's thermal profiles. The machinist wax shall require prior knowledge of heating direction in order to complete characterization since it contains two separate transition temperatures. However, the larger issue resides with the fact that the transitions of phase cover such short ranges. From the recognition that the melt transition is a function of whether the sample is being heated or cooled, the subsequent ultrasonic studies will investigate the acoustic behavior of the material both during heating and during cooling, and results will show that the onset of the time of flight of the acoustic wave over the intermediate temperatures between the two melt temperatures is sensitive to the state of the material.

3.2 Initial Quasi-isothermal Investigation for Determining Speed of Sound

The quasi-isothermal study, one of the key scientific contributions of the present work, presents the acoustic profile of the machinist's wax as a function of increasing and decreasing temperature. The methodology presented can be applied over a wide range of material systems and is not limited to the specific material investigated. The study is coined "quasi-isothermal" as the entire system is brought to thermal equilibrium prior to any data collection. The material of interest is placed inside some container with access to the top. Thermocouples are then inserted into the material at constant depths in random

locations throughout the container in order to verify the entire material is at thermal equilibrium. Examples of several setups are shown in Figure 3.4. Data is collected at a series of isothermal states and is allowed to come to equilibrium at each selected temperature for several hours prior to data collection as suggested by Jeffrey, D'Arrigo, Paparelli, and Li [7,11,12], respectively.

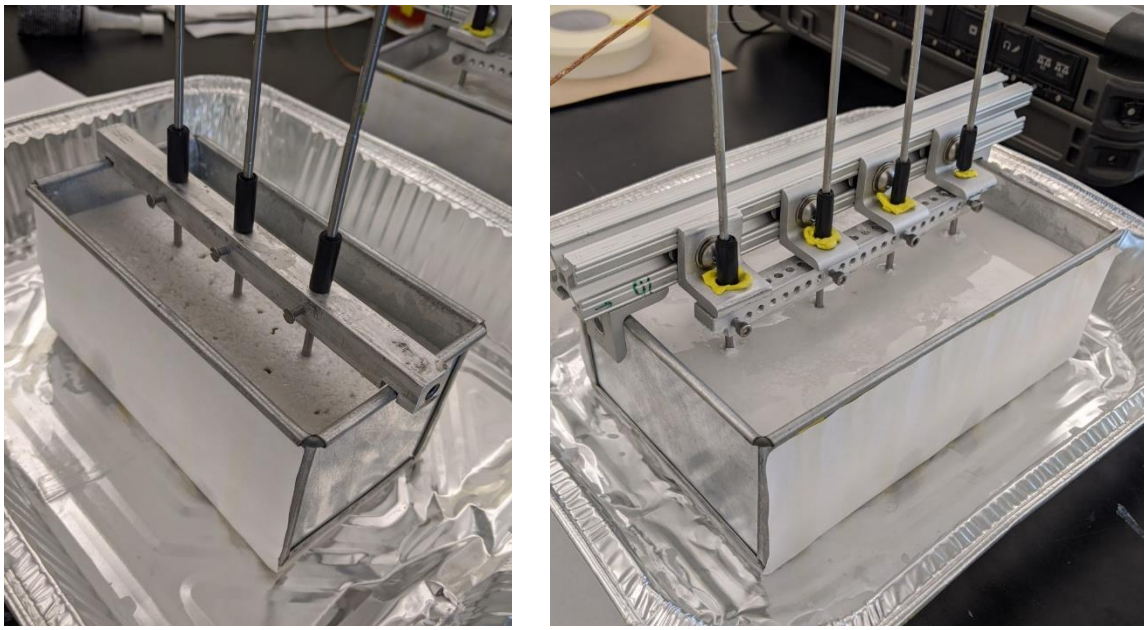

(a) (b)

Figure 3.4. Examples of quasi-isothermal setups with, (a) 152 mm (6") long axis tin container, and (b) 203 mm (8") long axis tin container

Observed from the figure, the methodology was performed using containers with various sizes to show an independence of the acoustic path length. The investigators also have studied the choice of material system for the container, and as long as the container material information is known, specifically the wall thickness and speed of sound, the time of flight of the acoustic wave in the wax can be extracted (see e.g., [7,20]).

The first quasi-isothermal study will be conducted on both the candle and machinist waxes and analyzed using the traditional methodologies of calculating the speed of sound based on the onset of the time of flight. These methods for determining temperature of an inaccessible medium vary on which acoustic signal to capture as described in Section 2.3. Lamb waves have been used for structural health monitoring [24], electromagnetic (EM) waves have been used on oil pipelines [25], and the utilization of longitudinal waves is often found in a variety of applications. Applications which record longitudinal waves are quite varied. Two specific examples related to the present study are their use in deriving thermodynamic properties [26] and in monitoring the cure state of thermosetting resins [27-29]. Lionetto et al address the importance of thermal analysis using longitudinal waves as it relates to the polymer processing industry [27,28]. They suggest using air-coupled ultrasound to propagate soundwaves. Air-coupled ultrasound is appealing for use on porous materials as well because the signal is less likely to disperse upon traversing porosity. Unfortunately, the results of the studies shown in [27,28] suggest that air-coupled transducers still lack the consistency and accuracy exhibited by traditional contract transducers.

Longitudinal wave analysis is the focus of the various studies presented in this thesis. It is important to collect and analyze a-scan data using the traditional longitudinal onset methods from the literature for the machinist wax in order to express the need for alternatives to these methodologies. It will also be useful to compare these results to the results of the candle wax as it undergoes the same data collection process and analyzation. The purpose of this is for verification of the applicability of the technique for

uniform materials and pointing out where the technique faulters for porous, nonuniform materials such as our machinist wax.

A containment vessel was created with dimensions 138 mm x 88 mm (5.44” x 3.47”) with a height of 108 mm (4.26”) and a wall thickness of 6 mm (0.22”). When a wax material was subjected to the quasi-isothermal study, it was poured into the containment vessel at approximately 80% capacity and three thermocouples were inserted non-symmetrically into the wax at a molten state. These three thermocouples reported the internal temperature of the material at random points but of equal depth. The thermocouple positioning points were randomly placed to confirm that the material entered an isothermal state. Once the material hardened, the internal thermocouples were secured into place. Two additional thermocouples were placed outside of the containment vessel to record the air temperature within the convection oven as seen in Figure 3.5.

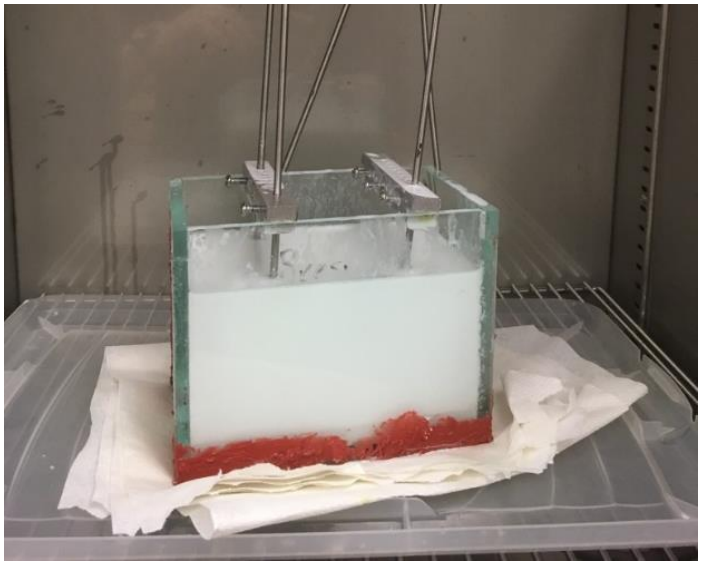

Figure 3.5. 138 mm x 88 mm x 108 mm (5.44” x 3.47” x 0.22”) containment vessel used during initial quasi-isothermal study

Previous researchers have utilized similar systems when attempting to characterize materials based on speed of sound changes with temperature. Most notably, the use of a thermal bath [11,12,30] has become increasingly common. The use of an oven in place of a thermal bath provides an ease for post-processing the a-scan data. At the beginning of each quasi-isothermal study, the wax was placed inside the oven and held isothermally at a set temperature, ranging between 20 – 100℃, for a minimum of three hours to reach equilibrium before the internal and external thermocouple readings were recorded. Once each of the thermocouples were within 0.5℃ of each other, through-transmission a-scan data was collected using 25 mm (1”) diameter 0.5 MHz Olympus, or Panametrics equivalent, VideoScan transducers [31] on both the long and short axes of the containment vessel. The temperature would then be incremented by 2 – 5℃ and the process of waiting for thermal equilibrium would be repeated. Recall from the previous DSC study in Section 3.1 that whether the material is heating or cooling has an impact on its material state during the melt transition for the machinist wax. It should be noted that the machinist wax was heated from room temperature up to 100°C, and the test was repeated a second time starting at 100°C and then cooling to room temperature. However, only the test observing the machinist wax cooling from 100℃ to room temperature is shown for the purposes of this chapter.

The present study investigates the correlation between the internal thermal state and the longitudinal waves of a captured acoustic signal, however, an evaluation technique found in the literature involves analyzing the lamb waves [24]. Scalea and Salamone were successful in monitoring the thermal effects of an isotropic plate using Lamb waves [24]. Unfortunately, the results cannot be repeated for the current study due

to the required signal travel distance. Recall the discussion from Section 2.3 on the requirements for obtaining lamb wave data in an a-scan. Lamb wave analysis is not possible for any of the studies contained within this thesis due to the thickness of the mediums under study. Lamb, or plate, waves are only useful in the analysis of materials whose thicknesses are less than the wavelength introduced through ultrasound [19]. Similar to lamb waves, surface waves, often referred to as Rayleigh waves, are useful for characterization (see e.g. [32]) but are unfortunately unapplicable for the given study. Any surface waves detected by the transducers would have traveled around the exterior of the containment vessel, never reaching the waxes under study. Any information extracted from the resulting waveforms only contributes to the characterization of the container harboring the waxes, but not the waxes themselves. Fortunately, the container created for use in the current study is not conducive to the travelling of surface waves. Surface wave transmission is inhibited because each wall of the container is a separate piece of material, thus making it difficult for the wave to transition from one surface to the next. Surface wave dampening is covered in greater detail in Chapter Four.

After experimentation concluded for each of the waxes, a-scan data for select temperatures along the range were in possession and ready for analysis. Traditional analysis methodology involves capturing and tracking the onset of the signal, termed the time of flight (ToF), and evaluating its changes with temperature. The distance travelled by the acoustic signal is then divided by this ToF and the material property speed of sound (SoS) is acquired as it relates to each temperature. Acquiring the onset of the a-scan signals is generally accomplished in one of two ways. The first method, often used in coding applications, involves using threshold detection based on a set desired

percentage of the maximum amplitude. The following approach is inspection of the a-scan data by hand for the signal onset, but this leads to inconsistencies due to human error as explained in Section 2.1. However, the purpose for characterizing each material within this chapter is not for generating a repeatable function, but for comparing the outcomes of the suggested inspection method between homogeneous and porous materials While obtaining the signal onset by hand is less consistent than using detection threshold, this method allows for the investigators to select a ToF closer to the actual onset. The signal onset in this case is defined as the time at which the a-scan signal deviates from the zero value to the first acoustic peak. Each individual a-scan was examined and a ToF was chosen by hand for the current quasi-isothermal study. In Chapter Five and Chapter Six, detection threshold is used due to the increase in consistency described in Section 2.1. The selected ToF data is used to create Figure 3.6 and Figure 3.7. These plots were generated using the data collected from the candle wax study performed in collaboration with a previous researcher on the present project [7]. This is done by subtracting off the time the acoustic wave spends within the walls of the containment vessel from the acquired ToF. The ToF information represented in Figure 3.6 is characterizing the wax and not the container as suggested in [7,20] and represented by Equation 2.3.

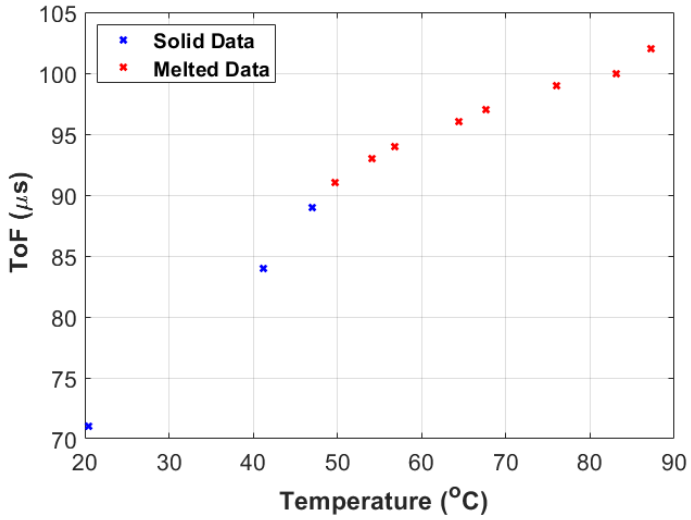

Figure 3.6. Time of flight as a function of the internal temperature of the investigated candle wax (data originally published in [7])

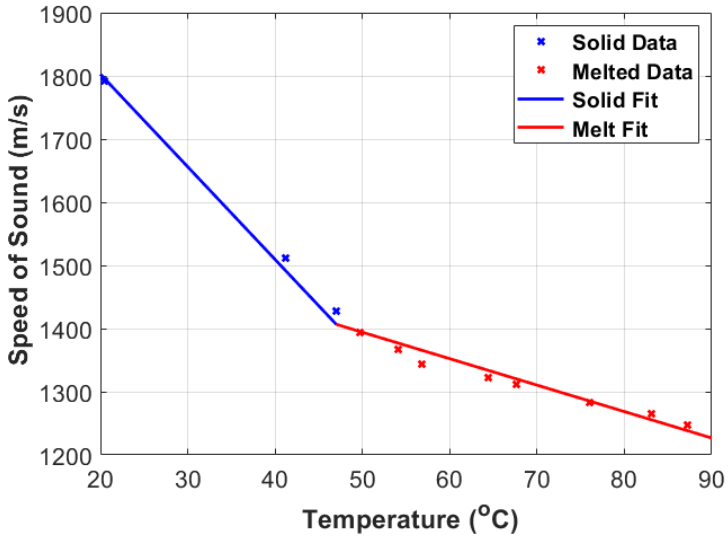

Figure 3.7. Speed of sound as a function of the internal temperature of the investigated candle wax (data originally published in [7])

Utilizing the measured SoS that has been obtained, a piecewise linear regression is performed on the resulting data set. Notice that there is a clear bend in the curve at the melt temperature of 47°C, and the relationship between speed of sound of the material

and temperature is well represented with two piecewise functions. that relate speed of sound to the internal temperature of the material.

The selected piecewise linear function model used for fitting is

$$c_{solid}(T) = a_1 + b_1 T \tag{3.1}$$

$$c_{molten}(T) = a_2 + b_2 T \tag{3.2}$$

Subject to the constraint

$$c_{solid}(T_{melt}) = c_{molten}(T_{melt}) \tag{3.3}$$

This equation is solved using least squares regression yielding coefficients of

$$a_1 = 2100 \text{ (m/s)} \qquad b_1 = -14.7 \text{ (m/s°C)} \tag{3.4}$$

$$a_2 = 1600 \text{ (m/s)} \qquad b_2 = -4.19 \text{ (m/s°C)} \tag{3.5}$$

where the resulting speed of sound, c_{solid} or c_{molten}, will be in units of m/s and T is expressed in °C. Figure 3.7 shows this fitted piecewise function with a slope discontinuity at the melt temperature.

Internal temperature as a function of material speed of sound is recast from Equation 3.1 and Equation 3.2 using the constraint defined in Equation 3.3.

$$T_{solid}(c) = 143 - 0.068c \tag{3.6}$$

$$T_{molten}(c) = 383 - 0.239c \tag{3.7}$$

where Equation 3.6 is only applicable for $c \geq 1428$ m/s and Equation 3.7 is only applicable for $c \leq 1428$ m/s. The speed of sound of 1428 m/s corresponds to the melt temperature of the material using either Equation 3.6 or Equation 3.7.

These results for the candle wax are similar in form to that of pervious materials characterized by other researchers [4-7,10-11,20,27-30,33]. The bi-linear relationship defined for temperature is continuous across all values of speed of sound. A downfall of

using the onset inspection method for the candle wax is the resulting narrow slope for temperature quantification in the solid region as shown in Equation 3.6. Quantifying temperature using a narrow slope decreases the accuracy of the approximation based on issues regarding signal resolution. When an acoustic waveform is flooded with noise, the onset may fluctuate by several microseconds, therefore reducing the accuracy of the temperature approximation greater in solid regions.

The process of selecting the onset to the ToF by hand was repeated for the a-scan data collected during the quasi-isothermal study on the machinist wax. The time the acoustic waveforms spend in the containment vessel walls is subtracted off as described in Equation 2.3. The resulting ToF used for characterizing the machinist wax according to the previously suggested material inspection methodology is used to create Figure 3.8 and Figure 3.9.

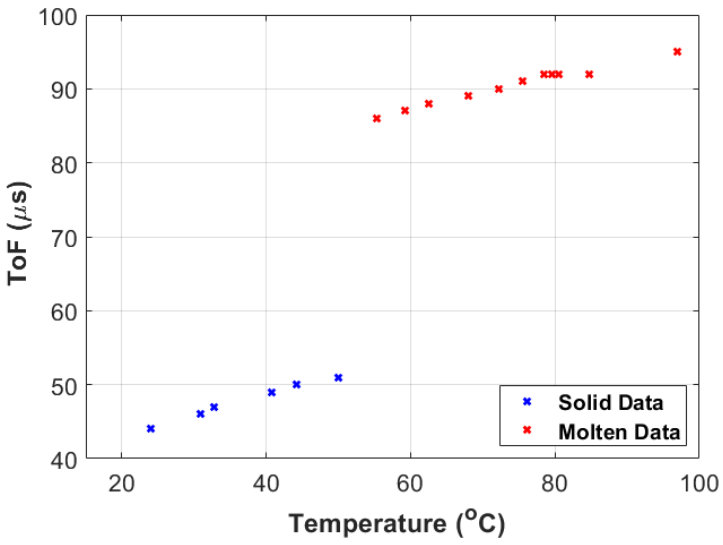

Figure 3.8. Time of flight as a function of the internal temperature of the investigated machinist wax during cooling

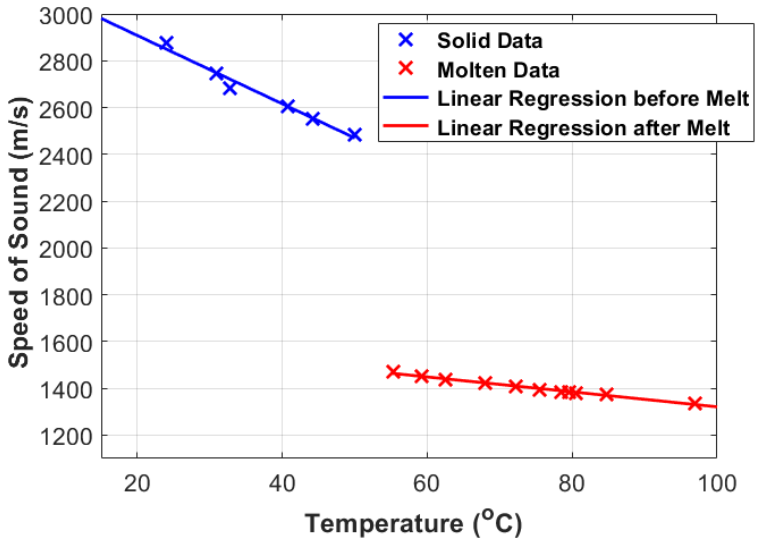

Figure 3.9. Speed of sound as a function of the internal temperature of the investigated machinist wax during cooling

While least squares regression can be utilized once again to quantify the curves above and below the melt temperature, the relationship will no longer be piecewise continuous like it was for the homogeneous candle wax but will instead be a discontinuous function around the melt transition. The reason for this is a result of the nonlinear behavior occurring around the melt temperature. Furthermore, since the resulting curves are piecewise discontinuous, there exists a gap in information between 50 – 55℃. The selected piecewise linear function model for the machinist wax of speed of sound as a function of temperature is shown in Equation 3.1 and Equation 3.2, however, the constraint defined in Equation 3.3 does not apply to these models. The equations are solved for using least squares regression yielding coefficients of

$$a_1 = 3200 \text{ (m/s)} \qquad b_1 = -14.6 \text{ (m/s℃)} \tag{3.8}$$

$$a_2 = 1640 \text{ (m/s)} \qquad b_2 = -3.19 \text{ (m/s℃)} \tag{3.9}$$

where $c_{solid}(T)$ is only applicable for values of $T \leq 50$℃, and $c_{molten}(T)$ is only applicable for values of $T \geq 55$℃. The discontinuity near the transition temperature shown in Figure 3.9 is represented in Equation 3.8 and Equation 3.9.

Similarly, the internal temperature of the machinist wax as a function of speed of sound is recast from Equation 3.1 and Equation 3.2 without using the constraint defined in Equation 3.3.

$$T_{solid}(c) = 219 - 0.069c \tag{3.10}$$

$$T_{molten}(c) = 514 - 0.313c \tag{3.11}$$

where $T_{solid}(c)$ is only applicable for values of $c \geq 2428$ m/s corresponding to $T \leq 50$℃ using the coefficients from Equation 3.8 in Equation 3.1, and $T_{molten}(c)$ is only applicable for values of $c \leq 1470$ m/s corresponding to $T \geq 55$℃ using the coefficients from Equation 3.9 in Equation 3.2.

A primary observation to extract from Equation 3.10, Equation 3.11, and Figure 3.9 is the drastic shift in time of the signal onset as the temperature increases from 50℃ to 55℃. This feature was not present in the candle wax. The discontinuity shown in Figure 3.9 is alternatively represented in Figure 3.10. Observing the discontinuity in this format additionally allows the analyst to observe the change in waveform structure with increasing temperature. A-scan data representing higher temperatures past the point of discontinuity show increases in the resulting general waveform structures, such as the overall lifetime of the signal itself.

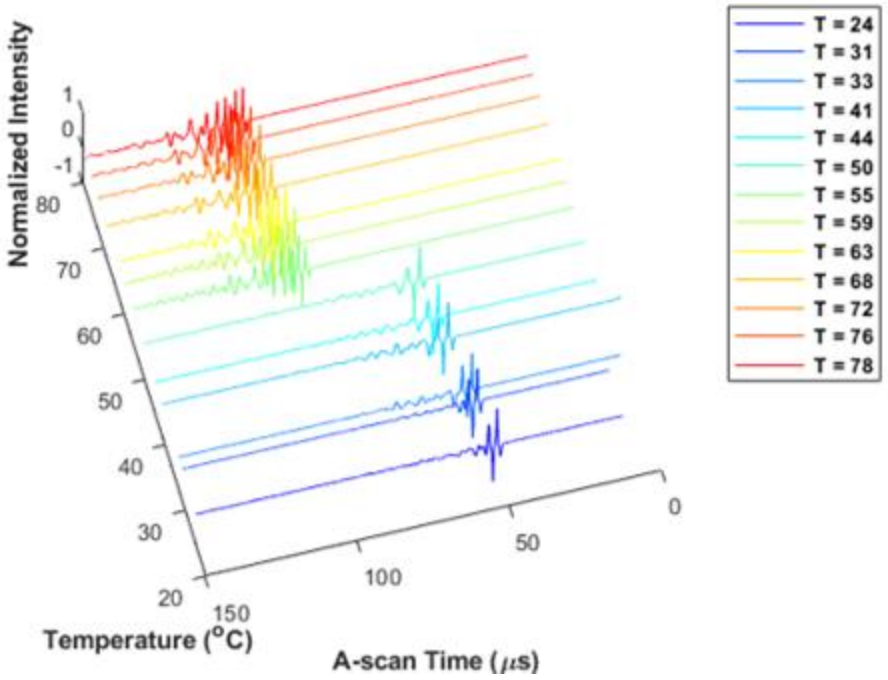

Figure 3.10. A-scans from select isothermal step changes of the machinist wax (Temperature in units of ℃)

In conclusion, the quantification of the internal temperature of the porous, nonuniform machinist wax using the traditional methodology of relating back to the material's onset to the time of flight, has proven to be less useful than when performed on the homogeneous candle wax. The discontinuity found while relating the material's speed of sound to temperature results in uncertainties for thermal quantification. Neither Equation 3.10 nor Equation 3.11 can be used for speed of sound values between 2428 m/s and 1470 m/s. Therefore, if the machinist wax returns a speed of sound value within this range during analysis, we cannot quantify the internal temperature. Additionally, Equation 3.6 and Equation 3.10 equally share narrow slopes for temperature as a function of speed of sound during solid phases. The accuracy of estimates made when using such narrow slopes often decreases. This is because a slight miscalculation in the speed of sound produces larger shifts in temperature approximations for these regions. The authors

consider the discontinuity discovered while characterizing the machinist wax and the narrow temperature slopes for both materials during solid phases to be justification in pursuing additional inspection methods for thermal characterization. Figure 3.10 provides valuable insight on possible correlations between the returned ultrasonic waveform and internal temperature. The signal onset was previously the only consideration in characterization of homogeneous material. If instead attention is paid to the remaining portions of the signal, it is observed in Figure 3.10 that as temperature increases, the time it takes for the signal to return to the baseline noise level also increases. These considerations shift the focus from the signal's onset to the entirety of the signal itself. Considering the full waveform in analysis typically involves tracking the waveforms changes in attenuation. Ono compiles the work of several researchers in [34] to describe how waveform attenuation is commonly used to characterize homogeneous materials. Additionally, Techavipoo [35] tracked the changes in signal attenuation as a function of temperature. During early studies of the present research investigation, the correlation between signal attenuation and the temperature was not monotonically increasing or decreasing for the investigated machinist's wax, thus the use of attenuation to estimate the internal temperature state would yield a multiplicity of solution sets. The inability to define a relationship between attenuation and temperature for the machinist wax led to a desire to propose new ultrasonic interpretations of full waveforms. The observations gathered from Figure 3.10 implied a relationship between general waveform structure and temperature and led to the desire to create a relationship between the material's internal temperature and the signal's energy and its statistical moments.

CHAPTER FOUR

Experimental Considerations for Signal Retention of a Parent Signal

The intention of Chapter Four is to address changes in experimental procedures when shifting the focus of analysis from the onset of a soundwave to the full waveform. Waveform structure can be altered by the introduction of reflection waves and surface waves from the propagated ultrasound. Section 4.1 proposes solutions for negating the effect of reflection and surface waves on the captured waveform structure. Additionally, the importance of selecting proper acoustic coupling gels for experimentation involving prolonged exposure to high temperatures is relayed in Section 4.2. Thermogravimetric analyzer (TGA) testing methods to perform on coupling gels is suggested with results explained.

4.1 Considerations for Maintaining Full Waveform Resolution

To analyze relationships between internal temperature and a signal's energy or its moments requires a second quasi-isothermal study. The new study needs to be conducted in a manner which accommodates the preservation of the resulting acoustic signal during its entire lifetime. Primarily, the section of the resulting acoustic signal which requires preservation will be referred to as "the parent signal". The parent signal will be defined as the resulting longitudinal signal gated in time from the initial onset to the time at which its amplitude returns the baseline noise signal without disruption. Refer to Figure 4.1 for a visualization of the parent signal. This is an important factor not considered in the prior quasi-isothermal study which only required preservation of a signal's onset. Before

initiating the second round of tests for the quasi-isothermal study, several factors need to be addressed. For example, Jost proposed in [6] to renormalize gain values for each scan when attempting to thermally characterizing a homogeneous material. By continuously normalizing the gain values as temperature changes, the structure of the captured waveform is untraceably altered. For the inspection methods proposed in Chapter Five, ultrasonic data collection will require a set gain value in order to track changes in full waveform behavior. The information collected in the quasi-isothermal study found in Section 5.1 will be gathered at several different predetermined gain values per incremented temperature by changing the LABVIEW coding used during data collection.

4.1.1 Exclusion of Internal Reflection Wave

The containment vessel housing the material of interest is extended in order for data to be collected over greater distances than in the prior study. There are two major reasons for doing this. When characterizing porous, nonuniform materials, the authors suggest traveling over several lengths for validation purposes. This ensures the relationships discovered during the various studies are repeatable for a variety of distances. Using a variety of differently sized containment vessels increases applicability for industry use. Additionally, reflection waves from the propagated soundwaves have the potential to crash into the parent signal before it completes resonating. The reflection waves can interfere with the patent signal if the distance between the transmit and receive transducers is inadequately spaced. Figure 4.1 depicts an instance where both the parent signal and its reflection wave are present and not colliding.

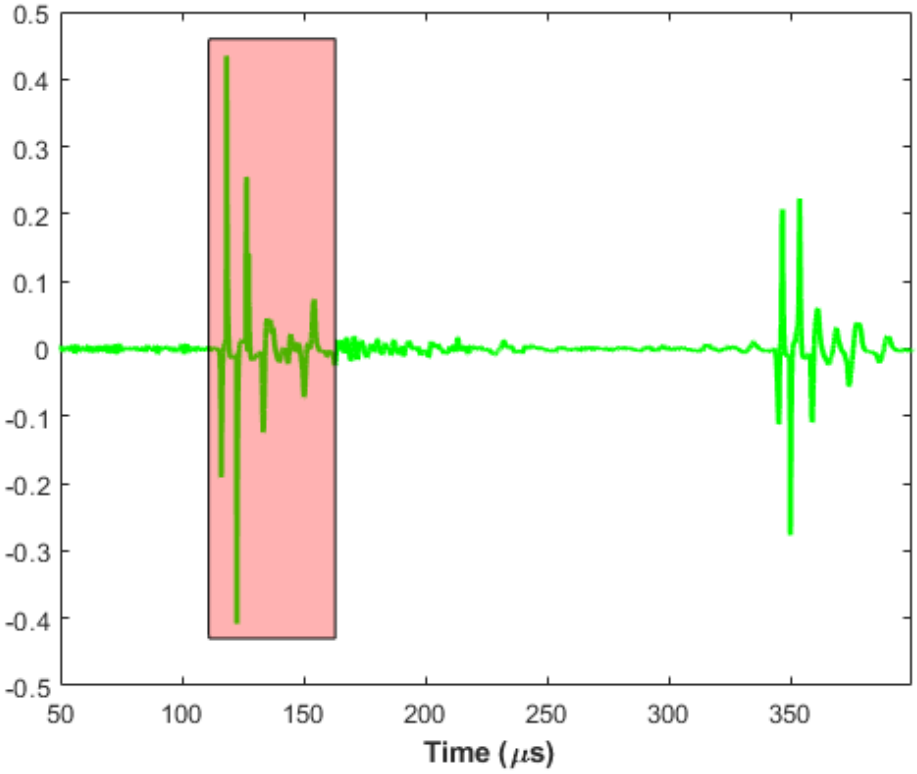

Figure 4.1. Presence of uninterrupted parent signal (highlighted) and its reflection wave due to appropriate spacing using through-transmission across 152 mm (6”) long axis

The a-scan shown in Figure 4.1 was captured for the machinist wax during a molten state at 0 dB over a 152 mm (6”) axis between the transmit and receive transducers. This 152 mm (6”) span is considered by the authors to be an acceptable distance for a signal to travel through the porous material under study in order to avoid disruption by its reflection wave. The studies described in the remainder of this thesis do not utilized a distance less than 152 mm (6”) between each transducer on the same channel. Containment vessels used during the second quasi-isothermal study possessed a long axis of the range 203 – 254 mm (8 – 10”). The reflection wave is the result of the original longitudinal wave sent by the transmitter after traversing the media between each transducer three times. However, while signal reflections may be a source of disruptive

longitudinal waves, they are not the only disruptive waves overall. Surface waves are encountered more frequently and can also distort the desired longitudinal signal being collected. Unlike the reflection waves, increasing signal travel distance will not solve this problem.

4.1.2 Surface Wave Dampening

The intent of this Section 4.1.2 is to provide a means for increasing signal resolution. Found throughout most literature, signal resolution is commonly enhanced on the backend of data collection and during analysis. A common practice is to incorporate wavelet transforms (see e.g., [36,37]). The issue with using transforms is the need to know what the ideal signal should look like. This concept is explained in [36] when deciding which mother wavelet to choose from in order to filter out unwanted waveform frequencies. In the case of this research, it is unclear how to define the parent signal as the results shown previously and through the remainder of this thesis show that the fundamental nature of the waveform varies with temperature and is inconsistent with each subsequent cooling. This variation with cooling is speculated to be caused by the random nature of the internal porosity giving rise to changing scattering paths for each individual acoustic path traversed. In this present study we focus on signal resolution before data collection. Zhou touches on this concept with the use of the MLS-modulated continuous wave in [38]. However, Zhou also explains how this technique is intended for echo suppression. The longitudinal wave reflection, or echo, will not interfere with data collection in the present case since the travel distance has been optimized prior. This creates the opportunity to propose a methodology for increasing signal resolution prior to testing. A major problem experienced during ultrasonic data collection involves receiving

undesired surface waves as shown in Figure 4.3a. The proposed solution to this problem involves nullifying the effects surface waves have on the desired parent signal. The results of attributing the proposed surface wave dampening technique on a five-gallon steel bucket, shown in Figure 4.2, are reported in Figure 4.3.

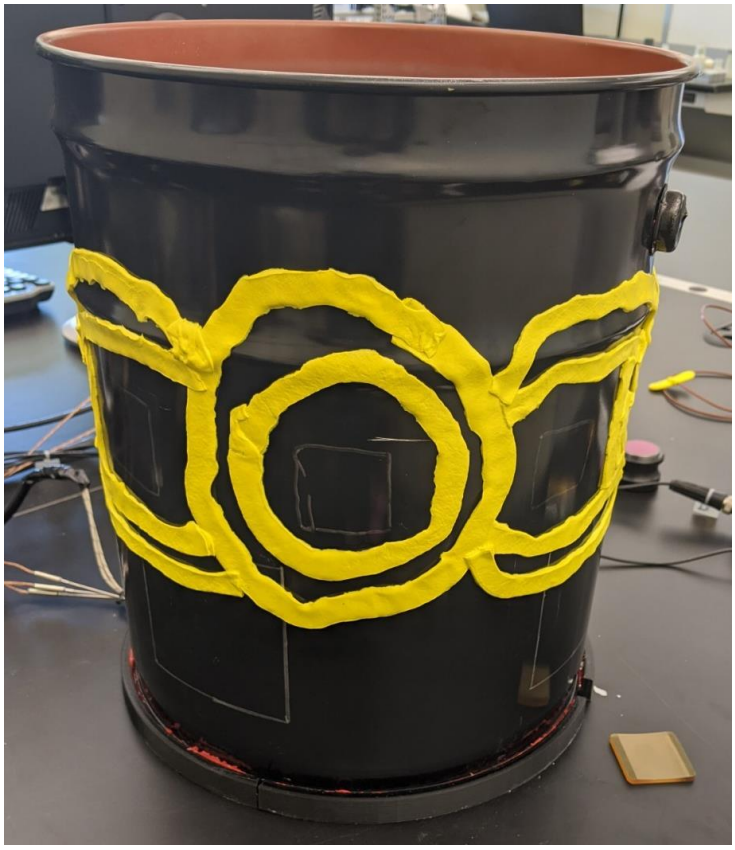

Figure 4.2. Proposed surface wave dampening methodology attributed to five-gallon bucket

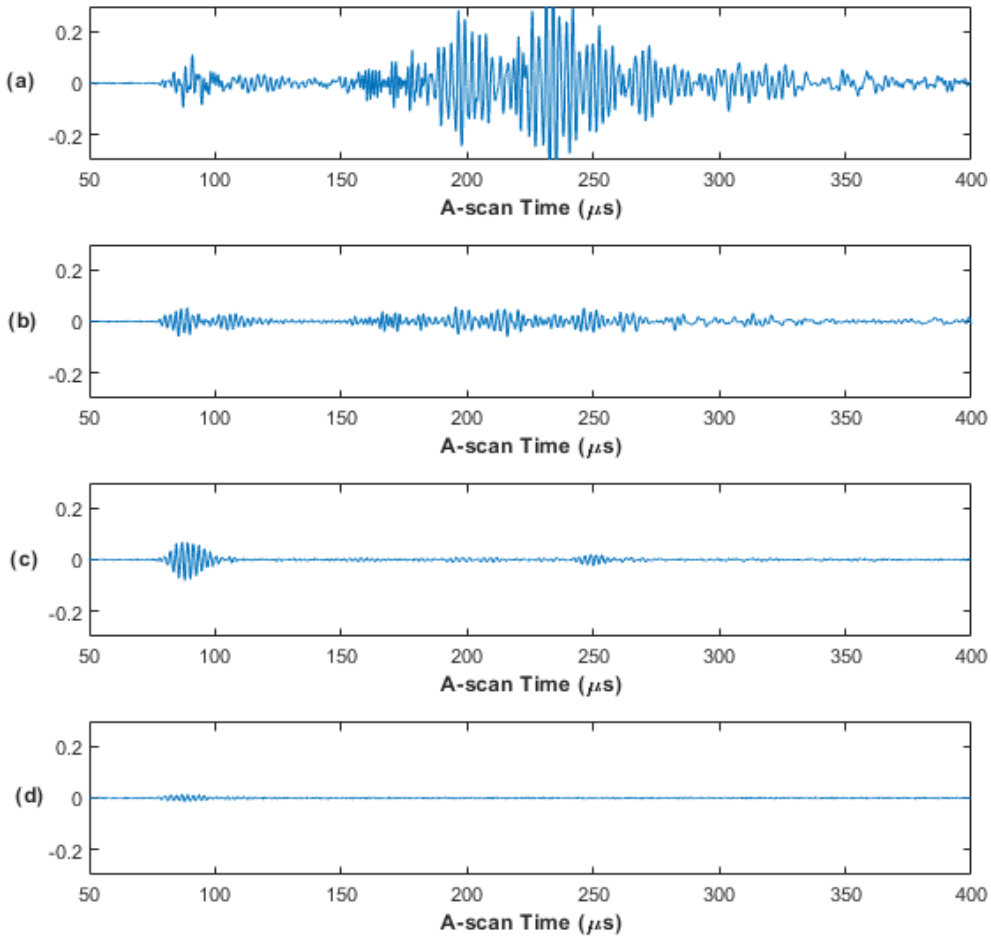

Figure 4.3. Results of attributing the proposed surface wave dampening methods to a five-gallon bucket for (a) no dampening, (b) one ring of gum-tape, (c) two rings of gum tape, and (d) all prior rings of gum-tape with paper and insulation

Figure 4.3 shows the resulting signals before dampening was applied (Figure 4.3a), after a single dampening ring was applied (Figure 4.3b), after two dampening rings were applied (Figure 4.3c), and after paper and insulation were applied (Figure 4.3d). It is important to note that each of these scans were collected with the same gain and plotted with the same amplitude axis.

The process to achieve the surface wave dampening displayed in Figure 4.3 required extensive testing and began with material selection. Selecting the appropriate

material for the containment vessels proved to be crucial in alleviating the impact surface waves possessed on the returned waveforms as they travelled around the outside of the containers and were observed by the receivers. The obtained surface waves overlap with our longitudinal signal and are not easily extracted, thus effecting the accuracy of our results. This causes a problem with the analysis of the acoustic wave, specifically the component of the captured wave that is of the acoustic signal that passes through the thermally heated material itself. In Section 3.2, it was determined to subtract off the time a signal spends while passing through the walls of a containment vessel. The signal at that time was characterizing the material of the container walls. The collected surface waves similarly characterize materials other than the machinist wax. When a surface wave is present in the collected a-scan, there is an issue of determining which onset belongs to which material. The surface waves will characterize the material of the container and not the waxes held inside. To study this, three materials are chosen as potential candidates for housing the machinist wax during the quasi-isothermal study with the intention of limiting surface wave interactions. The three materials were glass, polycarbonate, and tin. Glass was observed to propagate the surface waves from one transducer to the next with the greatest amplitude since it has a lower attenuation than polycarbonate and tin. For this reason, glass was used to attribute several different dampening techniques to. The process of attributing a dampener to the glass container and scanning for surface wave reception was conducted in order to gauge each dampening technique's effectiveness. If the surface waves could be dampened in glass, then they could be further dampened in the remaining materials with higher attenuations. Figure 4.*4* is the result of a multitude of the different dampening techniques attempted.

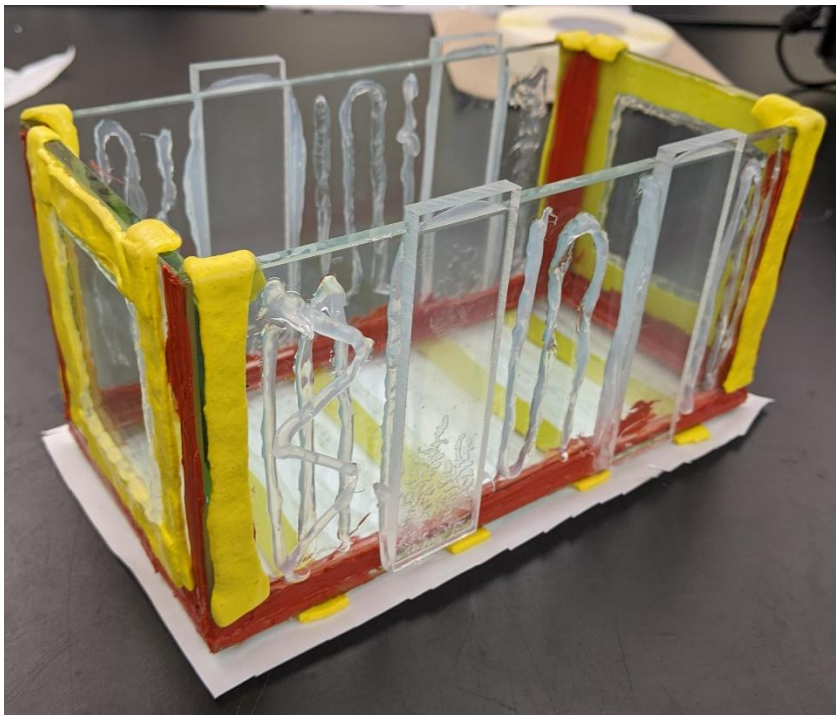

Figure 4.4. Various surface wave dampening techniques attributed to a glass containment vessel

After each dampening technique was applied to the glass container, a-scans were collected using through transmission while the container held either air or water at room temperature. Using air meant the longitudinal signal within the container was dampened completely by the acoustic mismatch between the solid and gas along with the attenuative properties of the air itself. Therefore, the resultant signal received is entirely from the surface waves which had travelled along the outside walls of the containment vessel. Surface wave dampening is attempted using three different materials adhered to the exterior of the container which obstruct the surface wave's path to the receiver. The interceptive materials include clear RTV sealant, 25 mm (1") wide polycarbonate strips, and gum-tape commonly used in laminate fabrication. The interceptive materials are selected for their viscous structures and ability to withstand the high temperatures of the

quasi-isothermal study. It can be seen in Figure 4.4 that several different patterns of adhesion were tested for each material. The polycarbonate and gum-tape were applied in singular thin strips while the RTV sealant was applied in both a raster pattern and in a continuous layup which layered over itself. While each method showed promise, dampening peaked in response to having several thin segments of a material interrupt the direct path of the surface waves repeatedly rather than using a single slab of material to absorb the vibrations. The gum-tape, provided and manufactured by ACP Composites having part number AT-200Y [48], proved to be the greatest dampener when laid in thin strips. The maximum recommended temperature of 204℃ for the gum-tape [48] is above the desired temperature range for the testing included within this thesis, so this dampener is not expected to deteriorate throughout its use on any testing apparatuses to appear in the following chapters. The final discovered method for dampening surface waves occurred incidentally. Since the gum-tape has a tenacious grip to whatever it touches, a simple sheet of printer paper is applied to the bottom of the container. It was discovered later that the application of a uniform material layered over the strips of gum-tape dampened the signal further. The use of gum tape, placed along the surface path of the acoustic wave in offset parallel strips is used for the results throughout the remainder of this thesis.

For example, the results for the five-gallon bucket made of steel utilized concentric rings of the gum-tape placed around the location where each transducer is mounted as depicted in Figure 4.2. Experimentation is performed on the five-gallon bucket to observe the progression of surface wave dampening and the results are shown in Figure 4.3. The results from Figure 4.3 are of the steel bucket that was scanned while

empty in order to focus the analysis on the received surface waves on the receiving transducer similar to the experimental procedures performed on the glass container. The insulation mentioned in Figure 4.3d dampens the surface waves similarly to the paper. The insulation was added with the primary purpose of maintaining the thermal energy within the containment vessel, however, the dampening effects provided the additional benefit of further dampening the acoustic signal passing within the steel bucket walls.

Containment vessels used in the quasi-isothermal studies contained in Chapter Five utilize the surface wave dampening methods, specifically the use of parallel bands of gum-tape placed on any acoustic path emanating from the transmitting transducer, proposed from this analysis.

4.2 TGA Analysis of Acoustic Gels

The next and final consideration for altering experimental procedures to be conducive for parent signal analysis involves reevaluating which acoustic coupling gel to use. The choice of coupling gel has less of an impact on the quasi-isothermal studies in Chapter Five. Although the choice of coupling gel may apply additional surface wave dampening, the decision to utilize a different coupling gel has a greater impact on testing conducted in Chapter Six.

All prior testing to this point of the thesis has taken little consideration on the type of acoustic gel used whenever data collection occurred. Unfortunately, it was never recorded in the notes of testing procedures for the studies discussed in Chapter Three which acoustic coupling gel was utilized. However, the results of Chapter Five and Chapter Six all utilize the VersaSonic® acoustic gel Section 4.2 advocates for. In early studies, two separate acoustic gels were used interchangeably and without consideration

as to the circumstances to the selection of one versus the other. The first, and less viscous of the two coupling gels, is known as Ultragel® II while the second is known as EchoPure™. Previously, the selection of acoustic coupling gel relied entirely on the level of relative viscosity. It was observed in early experimentation that as testing temperatures increased throughout continuous experimentation, over time the signal clarity was lost. Initially, this was accepted as a result of the porous material's reluctancy to change phase. After analyzing the resultant residue of the gel after a long test it became apparent that the gel had undergone a transition and had reduced in volume. This loss of material as a function of time and temperature is then studied using thermogravimetric analysis (TGA). Ultragel® II and EchoPure™ each have a particular application as stated by their manufacture's provided applications document at [39] and [40]. The operable temperature range of 20°C to 90°C used in the present thesis falls within the application window for both the EchoPure™ and Ultragel®, but there is not a discussion as to the application time window for the respective temperature range of interest.

4.2.1 Isothermal Hold TGA Testing

Two separate TGA tests were performed. The first test initially investigated the abilities of Ultragel® II and EchoPure™ coupling gels to sustain high temperatures for long periods of time. The point of this isothermal holding test is to see how long it takes for the selected material to evaporate or vaporize at a set temperature. This knowledge is imperative to the research being conducted. If the acoustic coupling gel deteriorates while ultrasonic data is being collected, the signal clarity will eventually disappear completely because no longitudinal signal will reach the receiving transducer. A ~10 mg sample from each gel was loaded into the TGA and taken to 50°C, 60°C, and 100°C near

instantaneously to be held isothermally until the gels sufficiently deteriorated below 50% weight. These temperatures were chosen to loosely represent the transition temperatures of the machinist wax as well as the maximum temperature used during quasi-isothermal studies. Figure 4.5 and Figure 4.6 show the results from the isothermal holding tests for Ultragel® II and EchoPure™, respectively.

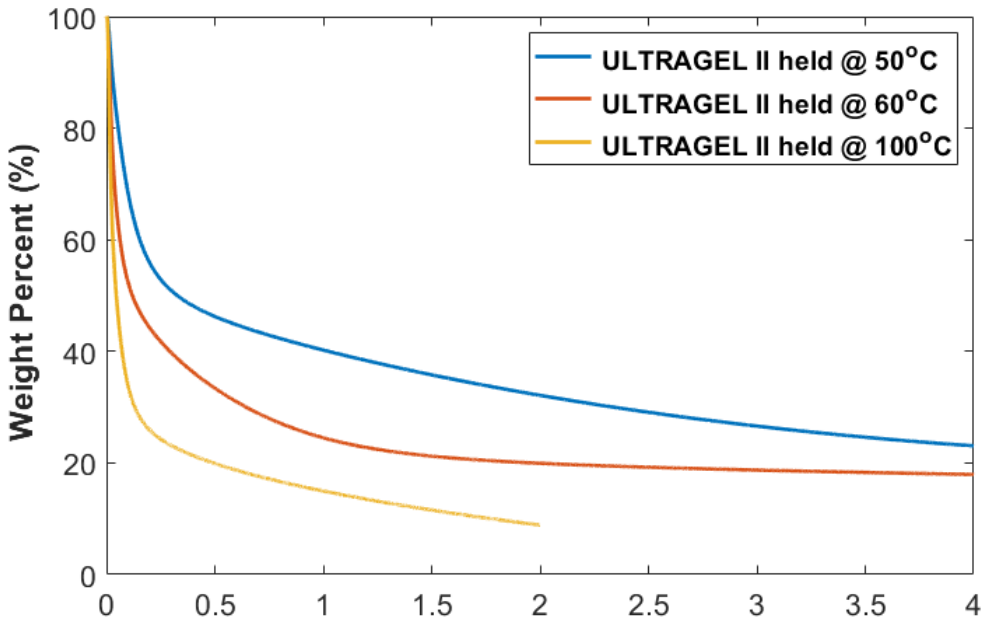

Figure 4.5. Results of isothermal hold testing using the TGA for Ultragel® II

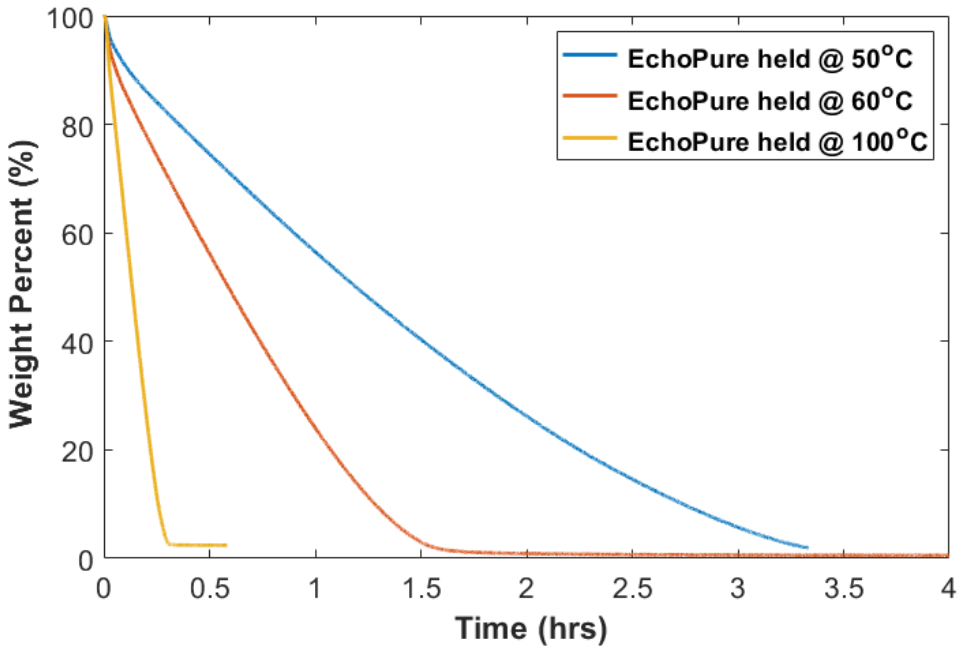

Figure 4.6. Results of isothermal hold testing using the TGA for EchoPure™

The samples sizes used for testing each gel range from 4 – 14 mg, which is within a range of recommendation given by [23]. The plots seen above only cover a maximum of four hours into testing. A few of the tests were stopped before reaching the fourth hour. An arbitrary acceptable minimum of 70% of the gel's weight was selected by the authors to remain in order to continue a-scan data collection on all future studies. Ultragel® II falls below the arbitrary 70% weight minimum for all measured temperatures long before the first half-hour. This means even at 50°C, the acoustic coupling Ultragel® II should not be applied for any duration exceeding thirty minutes or the a-scan data may be at risk of losing signal completely. EchoPure™ does show improvements during the burn-off tests in other aspects, however. This gel lasts longer at the same temperatures. The test at 100°C evaporated completely before the first half-hour, while the 50°C and 60°C tests dropped below the 70% weight marker between thirty minutes to one hour into testing. Essentially, using EchoPure™ as opposed to Ultragel® II only has the potential to

extend testing time by a maximum of thirty minutes which is too short for experimentation conducted in Chapter Six. Since neither the Ultragel® II nor the EchoPure™ coupling gels returned satisfactory results for the experimental intensions of the future studies listed in Chapter Five and Chapter Six, a third acoustic coupling gel was selected for similar TGA testing.

After looking at several different specification pages, it was determined that VersaSonic®, at both the high and medium viscosities, would likely be sufficient for our desired operating temperature range. The specifications for VersaSonic® are found at [41]. Even though the published operating range for this material is well within the bounds of testing, the isothermal hold testing was carried out on the TGA for verification. Figure 4.7 and Figure 4.8 show the results of the isothermal hold tests performed on medium and high viscosity VersaSonic® gels, respectively.

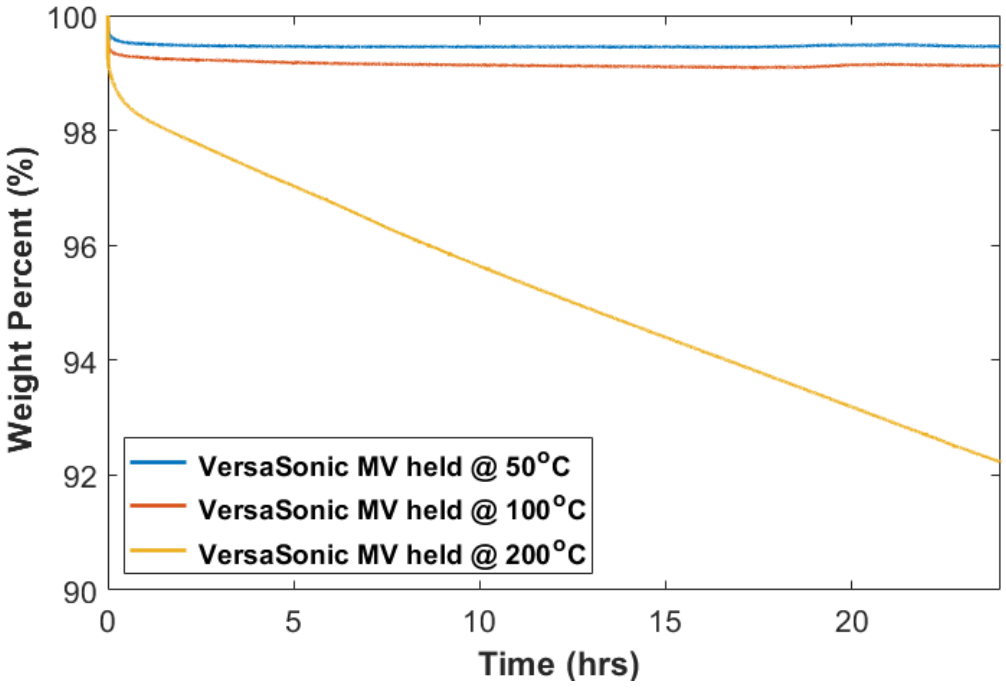

Figure 4.7. Results of isothermal hold testing on the TGA for VersaSonic® Medium Viscosity

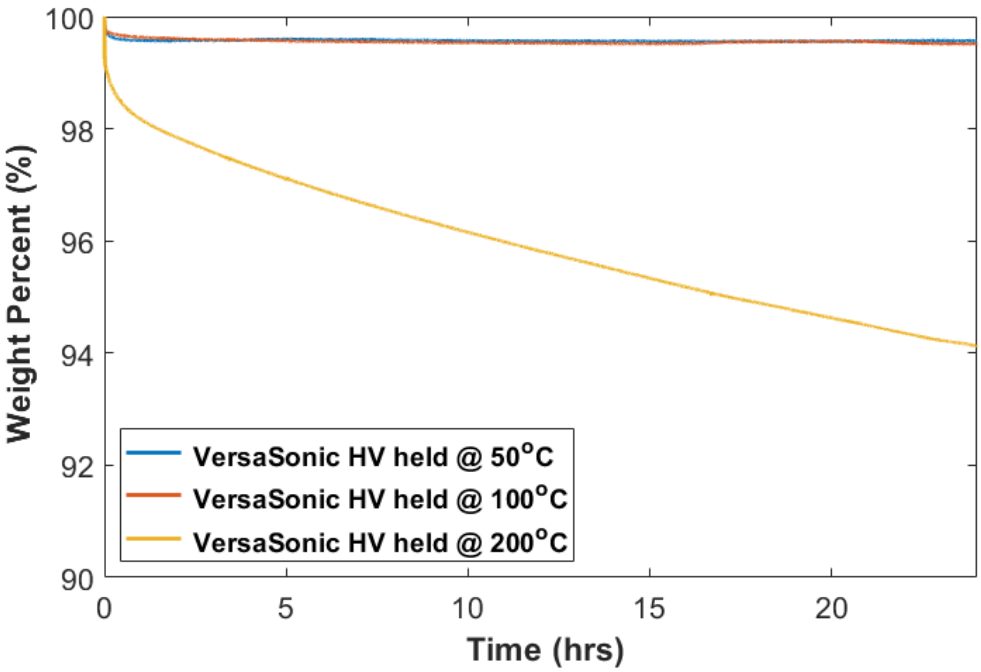

Figure 4.8. Results of isothermal hold testing on the TGA for VersaSonic® High Viscosity

The isothermal holding tests for both viscosity options performed exceptionally well at 50℃ and 100℃, not even dropping below 99% weight. For this reason, the final isothermal holding test doubled the previous maximum temperature of interest. Even at 200℃, both viscosities lasted twenty-four hours of testing without dropping below 90% weight.

4.2.2 Temperature Ramp TGA Testing

Isothermal tests are not the greatest representation of how a material reacts to sustaining high temperatures. This is due to the fact that isothermal tests bring the system from room temperature to the desired temperature in less than five minutes. This simulation poorly portrays the thermal effects the coupling gels will experience during testing. It does however provide good insight on how fast these acoustic coupling gels

will deteriorate while in use for the quasi-isothermal experiments. Since a-scan data is only collected during short bursts of time whereas the material system is held for many hours at fixed and elevated temperatures, the gel is not applied until each instance the material reaches thermal equilibrium. This means the gel warms from room temperature to the temperature of the containment vessel walls in less than a minute and the gel is held at that temperature for less than five minutes for even the longest of the quasi-isothermal studies. Unfortunately, for the slow heat and cooling tests performed in Chapter Six, the system will be held at an elevated temperature well above 50°C for many hours and even days in some studies. Thus, there is a need for a coupling gel better equipped to sustain high temperature for long periods of time.

In order to simulate the gradual heating of the acoustic coupling gels, a temperature ramping test is conducted using the TGA. For the Ultragel® II and EchoPure™ coupling gels, the material was ramped from room temperature, near 20°C, to 200°C at ramping rates of 2°C/min and 10°C/min for a total of four tests. Figure 4.9 and Figure 4.10 show the results of the TGA temperature ramping tests for Ultragel® II and EchoPure™, respectively.

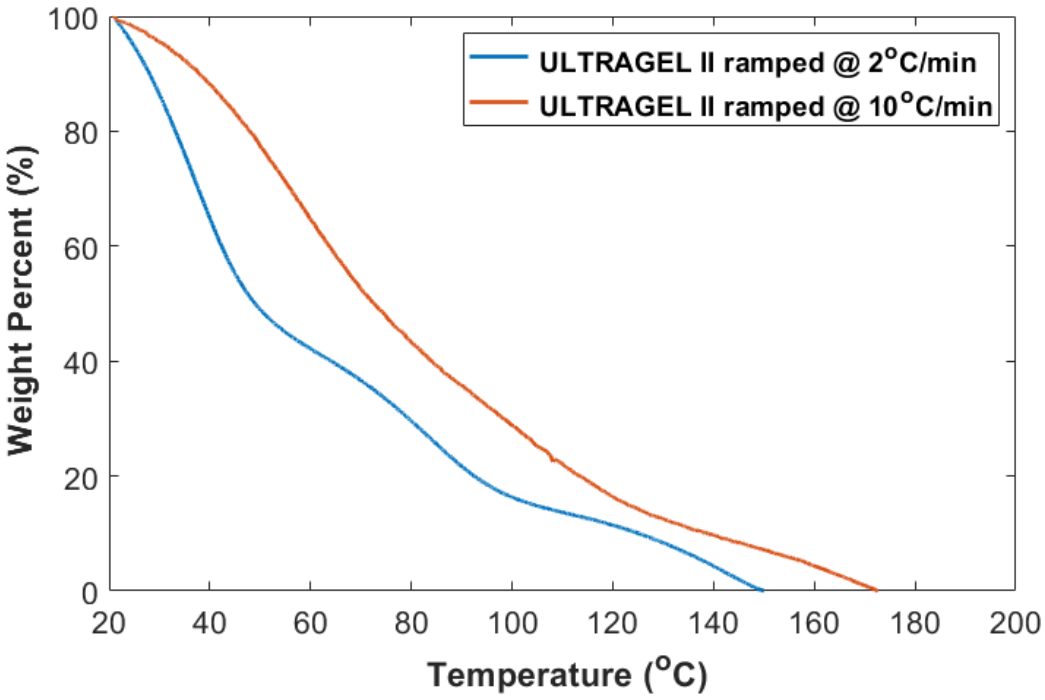

Figure 4.9. Results of temperature ramp testing on the TGA for Ultragel® II

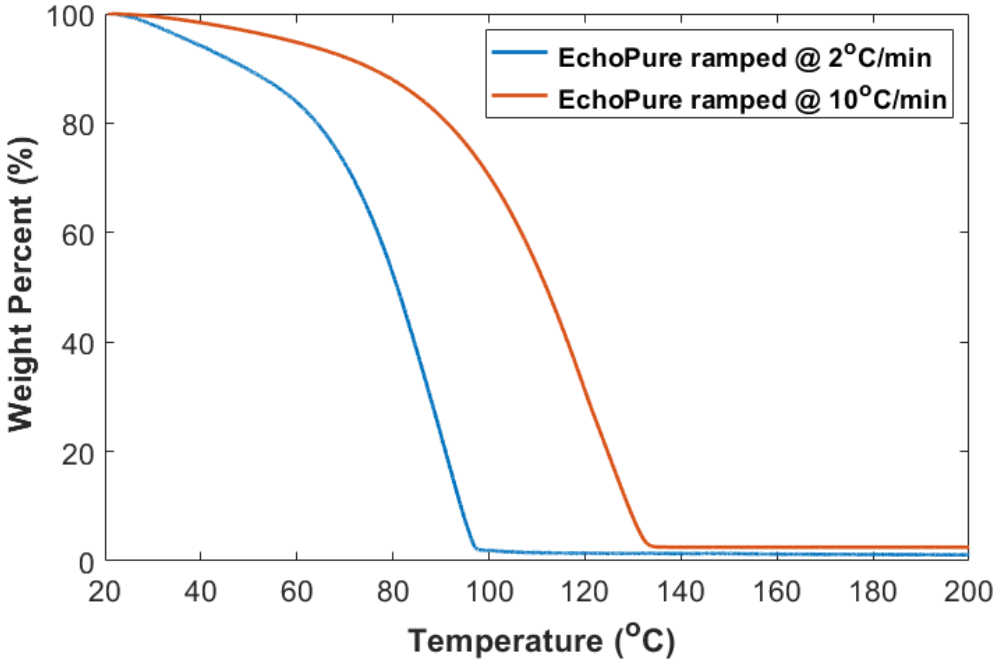

Figure 4.10. Results of temperature ramp testing on the TGA for EchoPure™

The sample sizes for each of these materials ranged from 5 – 8 mg. Notice in each case, the gels deteriorated at lower temperatures when temperature increased at a slower rate. This confirms the conclusion from earlier that these gels begin to evaporate or vaporize the moment they come in contact with temperatures even slightly above room temperature. The ASTM E2550 standard [46] states the onset of material decomposition is obtainable from the TGA curves given in Figure 4.9 and Figure 4.10. Using the TGA curves corresponding to each respective gel being heated at a controlled rate between 1℃/min and 20℃/min, the departure from the initial mass baseline corresponds to the material's decomposition temperature. If the percent weight begins to decline immediately at the start of testing, as observed for both the Ultragel® II and EchoPure™ coupling gels in Figure 4.9 and Figure 4.10, then the material is releasing vapors and is not conducive for use in the desired temperature range [46].

Let's consider the exposure time required for Ultragel® II to drop below an arbitrary 70% weight. Take the temperature at which this weight percentage occurs to be 40℃ for the 2℃/min ramp rate. The difference between room temperature and the temperature at which the material's weight percentage falls below 70% is 20℃. Therefore, Ultragel® II dropped below the accepted value for weight percentage after just ten minutes of exposure. The exposure time for this material to reach 70% weight at the 10℃/min heating rate is calculated similarly. It only took three and a half minutes before the gel drops below the arbitrary 70% weight marker for this heating rate. Repeating these calculations for EchoPure™ extends acceptable exposure time to a maximum of less than thirty minutes using the 2℃/min heating rate. In conclusion, the Ultragel® II

and EchoPure™ coupling gels are insufficient for collecting a-scan data over the desired range of temperatures.

For the VersaSonic® coupling gels, examining the same ramping test as used with the prior two coupling gels would be redundant, so the end temperature was increased in 400°C. Figure 4.11 and Figure 4.12 show the TGA temperature ramping results for VersaSonic® at medium and high viscosity, respectively.

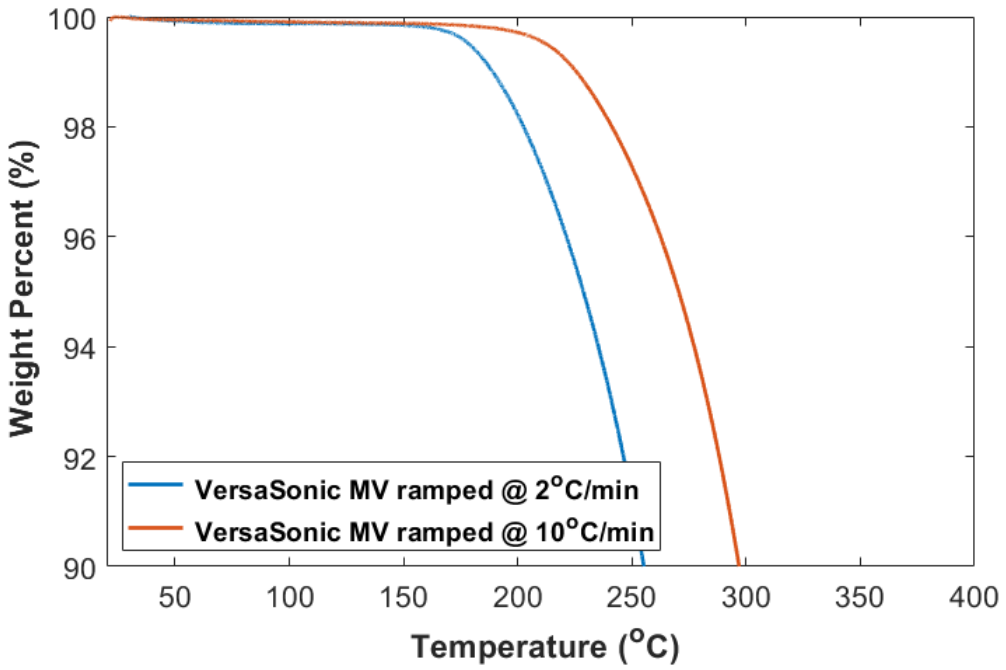

Figure 4.11. Results of temperature ramp testing on the TGA for VersaSonic® Medium Viscosity

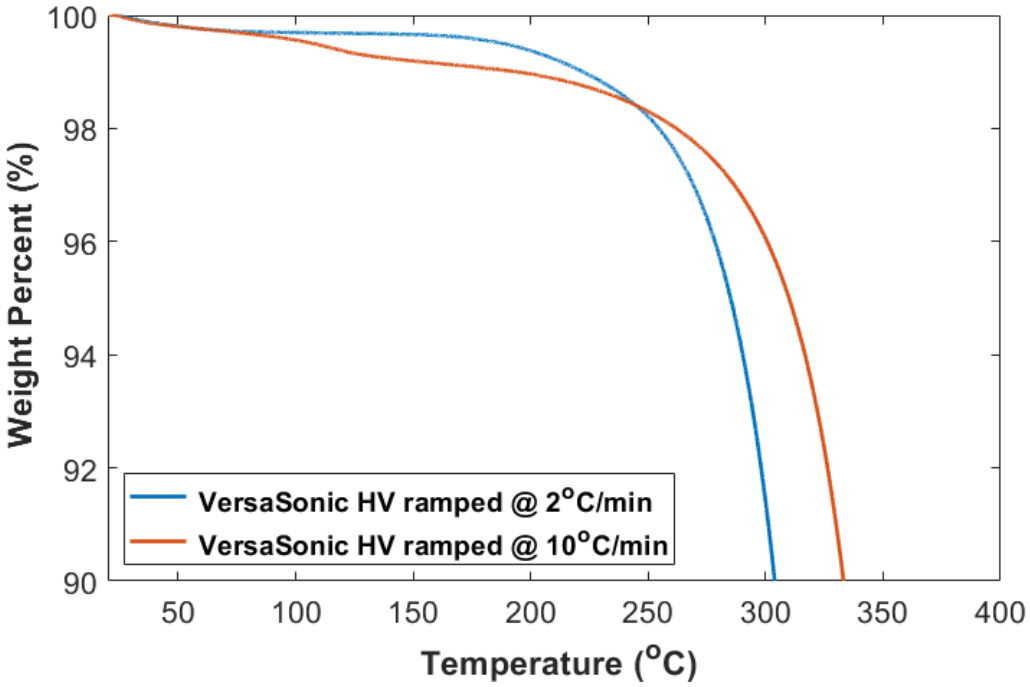

Figure 4.12. Results of temperature ramp testing on the TGA for VersaSonic® High Viscosity

The high viscosity VersaSonic® coupling gel appears to let off vapors initially, however, the majority of decomposition for the gel does begin until after 150°C. At the point of which either of the VersaSonic® coupling gel viscosities reaches the decomposition temperature described in [46], they have been exposed for long durations to temperatures beyond the scope of any studies conducted within this thesis. In conclusion, both the medium and high viscosity versions of the VersaSonic® acoustic coupling gels are sufficient for use in all experimentation preformed throughout the remainder of this thesis. Either viscosity can be utilized interchangeably. If the acoustic coupling gel is not specified during the experimental setups of the studies to follow, it should be assumed that either of these variations of VersaSonic® are used and the impact on which one is negligible.

CHAPTER FIVE

Expansion of Signal Interpretations

5.1 Second Quasi-isothermal Study

This chapter performs a quasi-isothermal investigation into the acoustic behavior of the machinist wax as a function of increasing temperature. This study is similar to that of Chapter Three, but it addresses the signal clarity issues presented in Chapter Four to allow for a clear signal that can be analyzed in depth. This chapter presents the concept of moment analysis to investigate the sensitivity of detecting thermal changes to changes in both the waveform as well as the higher order moments of the captured acoustic signal. This study collects a-scan information utilizing the through-transmission configuration with 25 mm (1”) diameter 0.5 MHz Olympus, or Panametrics equivalent, VideoScan transducers [31] the same as the experimental procedures displayed in Section 3.2. Data is collected using two separate containment vessels of different sizes to house the machinist wax. One is made of tin and is 203 mm (8”) long shown in Figure 5.1. The second container is made of polycarbonate and is 254 mm (10”) long and shown in Figure 5.2. The study subjects the vessel to a fixed temperature for several hours until thermal equilibrium within the wax is achieved. A-scans using through transmission along the long axis are performed and the acoustic signal is retained for later analysis. This process is then repeated by changing the temperature, waiting for thermal equilibrium, and then capturing additional a-scans. Of note, this test is performed for both increasing temperature steps and decreasing temperature steps, but in every instance the

interior temperature is monitored until the entire interior becomes isothermal. The results of characterization while the porous material is heated or cooled are individually reported on, and the results are different between the heating and cooling energy peaks noted in the DSC study of Section 3.1. This chapter showcases the proposed interpretations to signal analysis on the ultrasonic data from this study using the tin and polycarbonate containment vessels mentioned.

A more accurate dimensioning of the tin containment vessel is 200 mm x 125 mm x 78 mm (7.88” x 4.94” x 3.06”) with a wall thickness less than 1 mm (less than 0.03”). This containment vessel was filled to 80% capacity by volume with the machinist wax. Experimentation using the tin containment vessel attempts to characterize the machinist wax as the material is being heated. This is accomplished by initially placing the machinist wax inside an oven near 40℃ and remaining isothermal until thermal equilibrium is achieved. The oven used in the present study to simulate a system heating or cooling is the same one used in the quasi-isothermal study from Chapter Three. Thermal equilibrium is verified for this containment vessel through the use of four internal K-type thermocouples connected to a Graphtec midi LOGGER GL820. The thermocouples are positioned along the centerline of the container’s long axis with a 25 mm (1”) offset from each outer wall and 51 mm (2”) offsets between each thermocouple. Each internal thermocouple is elevated 13 mm (0.5”) from the base of the containment vessel. A symmetric internal thermocouple layout was arbitrarily chosen for the tin containment vessel. Figure 5.1 depicts the testing apparatus used for collecting ultrasonic data as the machinist wax experiences heating during the quasi-isothermal study. Thermocouples are utilized within this experiment for thermal quantification of the

internals of the porous media and to verify when the material is at thermal equilibrium. In addition to the four internal thermocouples, two external thermocouples are exposed to the system environment. The thermocouple data is recorded once all internal thermocouples are within 0.5℃ of one another. Ultrasonic data is also collected while the porous material is at thermal equilibrium. Through-transmission a-scans are collected along the container's long axis for set gain values of 0 dB, 10 dB, and 40 dB while the receiving transducer is connected to a preamplifier set to 50 dB. After data is collected for a set temperature, the oven temperature is increased in increments of 3 – 5℃ before remaining isothermal for a minimum of eight hours to ensure equilibrium is achieved throughout the material again. The process of collecting data during the isothermal instances experienced by the porous material and incrementing the oven temperature for holding is repeated until the oven temperature surpasses 90℃.

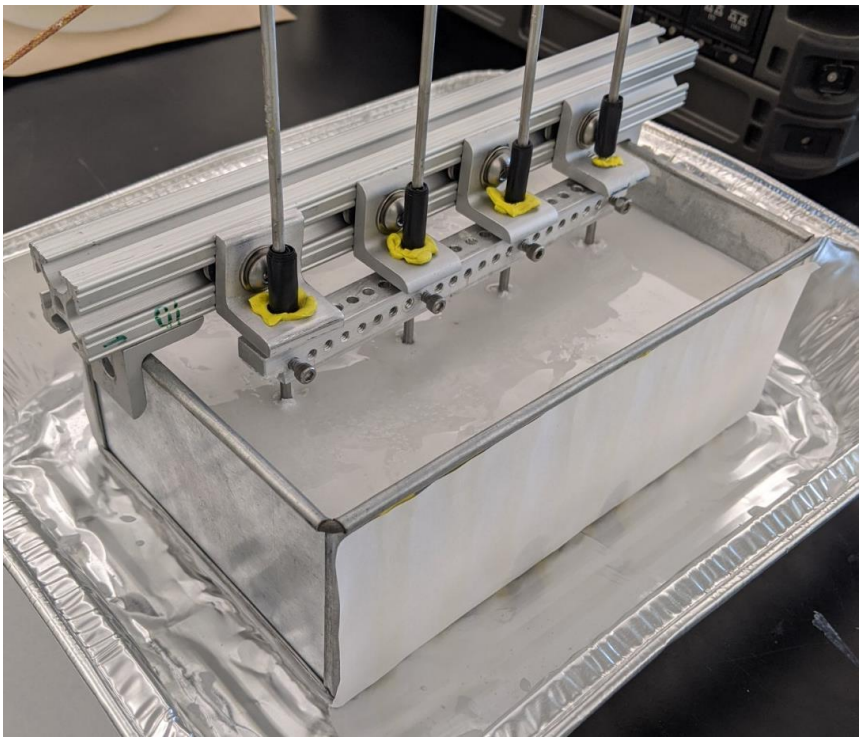

Figure 5.1. 200 mm x 125 mm x 78 mm (7.88” x 4.94” x 3.06”), tin containment vessel used in second quasi-isothermal study to analyze machinist wax during heating showing embedded thermocouple placement

The quasi-isothermal study involving the testing apparatus shown in Figure 5.1 exposes the porous machinist wax to temperatures ranging between 40℃ and 90℃. This range of temperatures includes the melting temperature of the material under study.

The machinist wax’s reaction to being cooled is captured with ultrasonic data while using the polycarbonate containment vessel. The more accurate dimensioning for the polycarbonate containment vessel is 252 mm x 111 mm x 102 mm (9.94” x 4.38” x 4.00”) with a wall thickness of 5 mm (0.19”). The machinist wax was poured into the polycarbonate housing at 80% capacity. The internal thermocouple layout returned to an asymmetric style utilizing three thermocouples of equal depth set 13 mm (0.5”) above the base of the container. Two thermocouples external to the material are used again to

observe the temperature of the system. The polycarbonate testing apparatus used during the quasi-isothermal study as the porous material is cooled is seen in Figure 5.2.

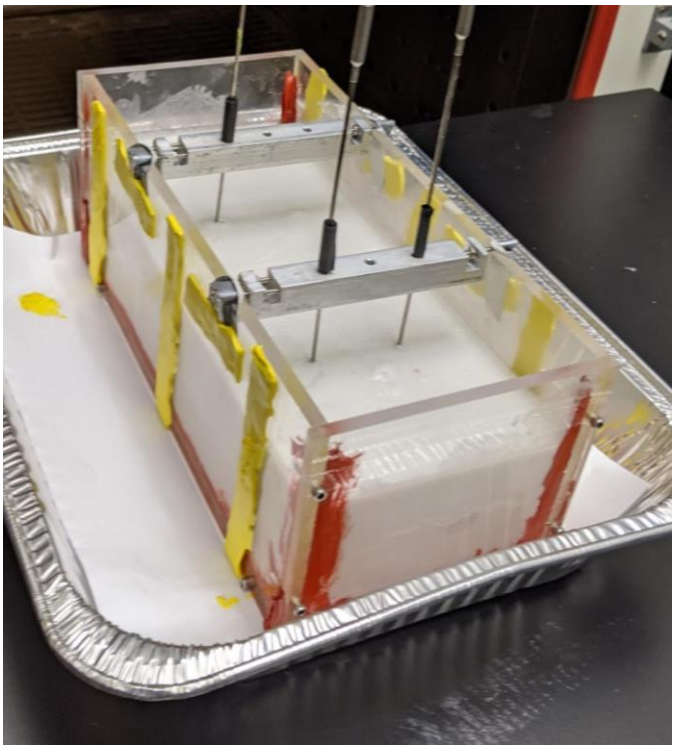

Figure 5.2. 252 mm x 111 mm x 102 mm (9.94” x 4.38” x 4.00”), polycarbonate containment vessel used in second quasi-isothermal study to analyze the machinist wax during cooling showing thermocouple placement and acoustic dampening strips

Experimentation using the polycarbonate containment vessel attempts to characterize the machinist wax as the material is being cooled. The container housing the machinist wax is initially placed inside the oven near 90℃ and held isothermally for a minimum of eight hours. The same experimental procedures for data collection are repeated for observing the machinist wax as it cooled. Ultrasonic data was only collected when the material was in thermal equilibrium as defined when all thermocouples within the vessel and in the surrounding air were reading values within 0.5℃ of each other. The oven temperature is decreased in step sizes of 3 – 5℃ from 90℃ to 40℃. The gain

values used during data collection were 0 dB, 10 dB, and 40 dB while the receiving transducer was connected to a preamplifier set to 50 dB.

Figure 5.3 and Figure 5.4 complete the quasi-isothermal study by characterizing the machinist wax using the onset for SoS as in Chapter Three. Remaining consistent with onset selection methods used in Chapter Three, the a-scan data was manually inspected, and the onset of each propagated waveform was selected by hand. The identified speed of sound is then obtained by following Equation 2.3 for both the heating and the cooling steps and plotted in, respectively, Figure 5.3 and Figure 5.4. Note the method used for onset selection throughout the remainder of this thesis is detection threshold for its consistency in selection which is not subjected to human error. Selecting the onset from each a-scan by hand is sufficient to recreate the plots of speed of sound as a function of temperature because the purpose is to show the discontinuity observed in Figure 3.9 remains in Figure 5.4 and now Figure 5.3 as the material is heated.

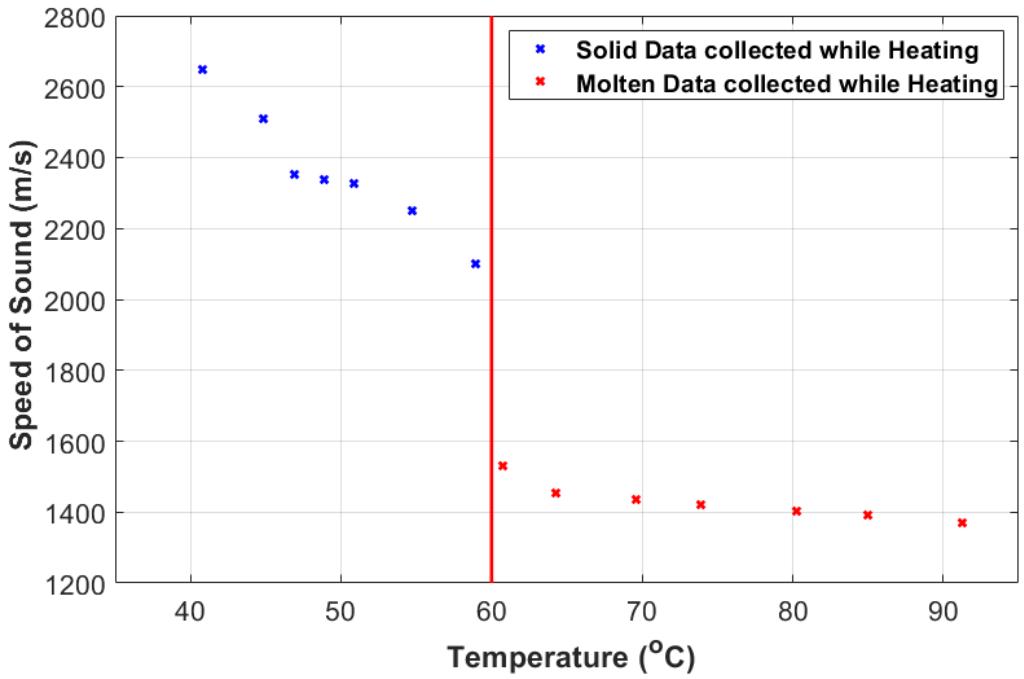

Figure 5.3. Speed of sound based on the onset to the time of flight as a function of temperature from isothermal step heating on the machinist wax, vertical line corresponds to the location of discontinuity during heating

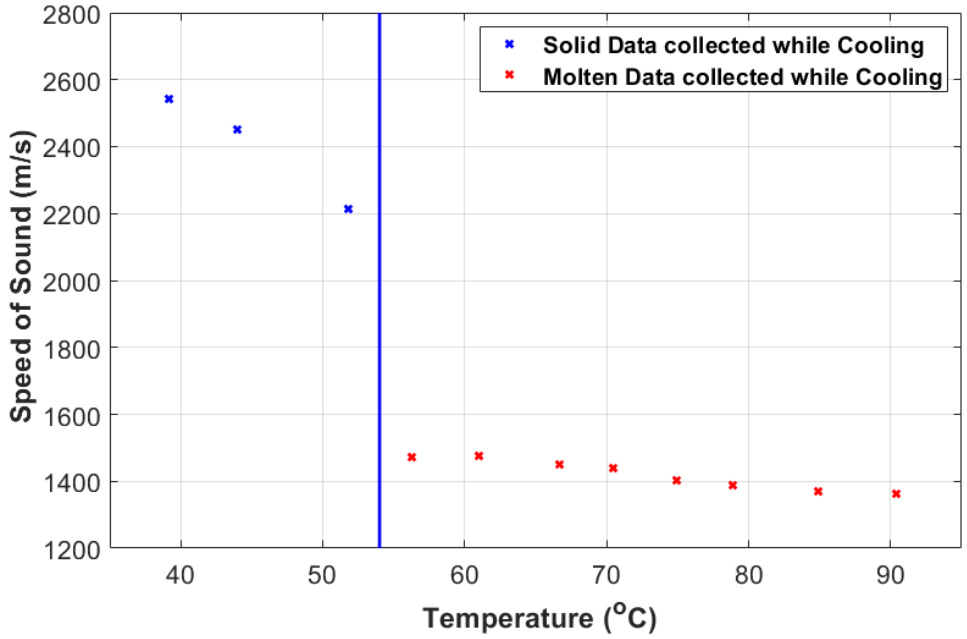

Figure 5.4. Speed of sound based on the onset to the time of flight as a function of temperature from isothermal step cooling on the machinist wax, vertical line corresponds to the location of discontinuity during cooling

Notice that the discontinuities in the identified speed of sound curves are around the transition temperatures identified from the energy peaks of the DSC testing of Section 3.1. This is the same observation as was indicated in the earlier isothermal study of Chapter Three. Also, notice the verification of a conclusion made previously, specifically the discontinuity in the plot experiences a horizontal shift to the right when the material is experiencing heating rather than cooling. From results shown, if the location of the discontinuity represents the transition temperatures of the porous material, then 60℃ corresponds to the melting temperature based on heating and 54℃ corresponds to the temperature of solidification when cooling. The values for the machinist wax's phase transition temperatures are very similar to the values determined by the DSC analysis, which were 62℃ and 45℃ for, respectively, heating and cooling. This issue where the speed of sound is a function of the heating path within the range of 54℃ to 60℃ poses a unique challenge, and whether the wax is increasing or decreasing in temperature will need to be identified to characterize the thermal state using sound within this narrow bound of temperatures. In addition, as will be shown in later sections, a difficulty arises when the acoustic path passes through a thermal gradient. The challenge in characterizing the internal thermal state is made difficult due to issues with signal attenuation and beam spread caused by internal scatter. Thus, additional signal interpretations beyond the signal onset are presented in the following section.

5.2 Energy Inspection

The previously suggested methods for material inspection using the onset to the time of flight to obtain the material's SoS led to discontinuities in curves created through least squares regression in Section 3.2 and now Section 5.1. However, Figure 3.10 leads

the observer to believe the signal should be interpreted based on the entirety of the parent signal and not the signal's onset alone. The first application of this concept is to consider how the parent signal's energy will come to be defined. Markova deals with this definition by relating the signal energy to the pressure of the signal in [32]. The signal's pressure is found by generating a synthetic waveform that can match the a-scan data collected. The resulting amplitude of the synthetic waveform represents the acoustic pressure of the signal at different places in time. By integrating the square of this pressure over time from zero to infinity, the energy of an a-scan is determined. There are a few reasons why this approach should be amended for the current studies. The use of a synthetic waveform is not preferred over the actual resulting waveform due to the possibility of omitting vital information in analysis. Markova's energy interpretation also relies on the assumption that multiple different waveforms are collected from an a-scan including pressure waves, shear waves, and pseudo-Rayleigh waves. Our studies include the dampening described in Section 4.1.2 in order to only analyze the longitudinal, or pressure, waves exclusively. Allowing the signal to experience all different forms of waveform interactions may be more realistic in regard to data collection in general, however, it is not conducive to the proposed methods of material characterization. The inclusion of all waveforms results in an addition or subtraction in amplitude along time as each waveform is layered over the other and allowed to crash into one another. Additionally, the a-scan data received during data collection presented in this thesis represents a voltage in time rather than a pressure in time. For clarification, Markova's definition of signal energy is perfectly well suited for applications in functions of time. Our studies focus on both time and temperature as well as the variety of paths created by

the signal scatter, so we instead focus on the energy of exclusively the captured signal. As the captured signal is a measurement of the instantaneous voltage created by the deformation of the piezo-electric transducer, the signal energy is defined in terms of the voltage and the resulting power. The energy has the following relationship to the electrical power:

$$E(T) = \int_{-\infty}^{\infty} P(t,T)\, dt \tag{5.1}$$

Where E represents energy, P represents power, t represents time in seconds, and T represents temperature in ℃.

In order to accommodate for a gated time which encompasses the parent signal, the definition for energy is recast as the following:

$$\tilde{E}(T) = \int_{t_i}^{t_f} P(t,T)dt \tag{5.2}$$

where t_i and t_f correspond to the starting and ending times of a gate which encompasses the parent signal in units of seconds, respectively, and $\tilde{E}(T)$ is the energy over the gated time range $t \in \{t_i, t_f\}$.

Equation 5.2 replaces the need for defining signal energy with the need for defining signal power. The signal power is defined as

$$P(t,T) \equiv A(t,T)^2 \tag{5.3}$$

where A represents the instantaneous amplitude of the captured waveform.

Using Equation 5.3, the normalized signal energy is defined as the following:

$$\bar{E}(T) = \frac{\tilde{E}(T)}{\max_T \tilde{E}(T)} = \frac{\int_{t_i}^{t_f} P(t,T)dt}{\max_T\left(\int_{t_i}^{t_f} P(t,T)dt\right)} \tag{5.4}$$

where $\bar{E}$ represents the normalized signal energy.

It is worth noting that this definition for signal energy is similar to the form suggested by Markova's [32] for the pressure wave analysis. The intention of creating this definition for normalized signal energy is to find a relationship to a material's internal temperature which can be described quantitatively. To understand the general relationship between signal energy and internal temperature, normalizing the energy between zero and one will prove beneficial. This normalization also removes the desire for the need for units as the result is unitless. Figure 5.5 and Figure 5.6 show the results of the normalized energy of the parent signal with respect to temperature for the machinist wax during its isothermal step heating and cooling, respectively. Note that no additional data was needed to generate these figures. The same sets of a-scan data used to create Figure 5.3 and Figure 5.4 were used to create Figure 5.*5* and Figure 5.*6* below. The only changes made involved how the signals were interpreted.

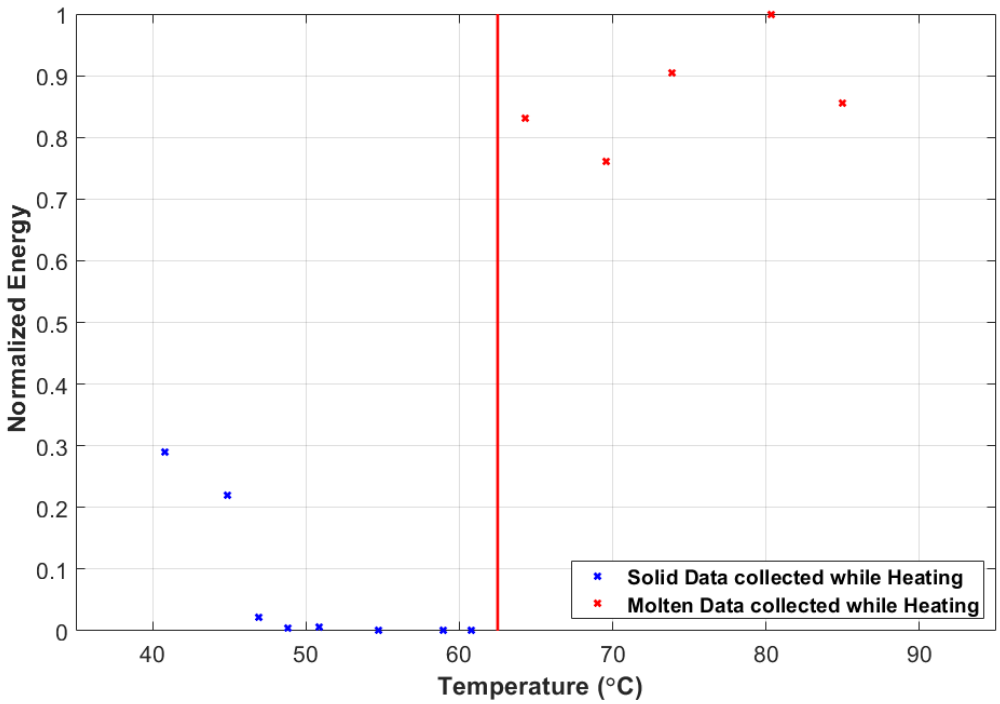

Figure 5.5. Normalized signal energy by temperature for machinist wax data collected from isothermal step heating

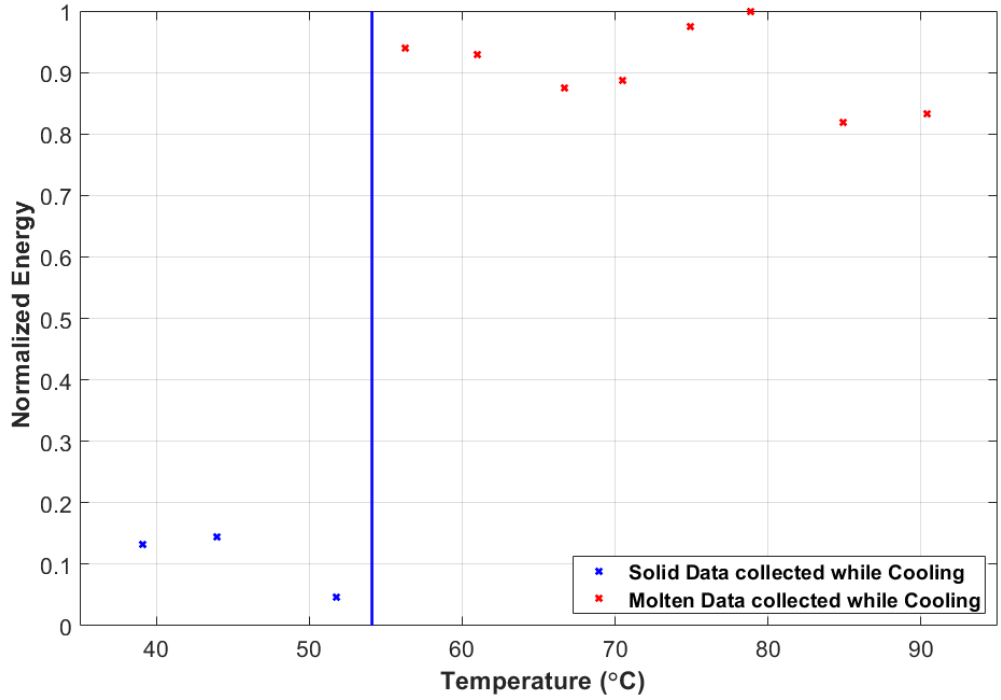

Figure 5.6. Normalized signal energy by temperature for machinist wax data collected from isothermal step cooling

Figure 5.5 and Figure 5.6 validate the hypothesis of a correlation between signal energy and the porous material's phase state. The normalized signal energy provides a determination of phase the studied material's phase state. Any data point below 50% of the maximum normalized energy is considered a solid, while data points above 50% of the maximum normalized energy are considered molten. The issue with this is that one must know a-priori the proper normalization factor to use. Thus, it is not an absolute measurement but a relative measurement where one can see passing through a transition by a shift in the energy, and then looking back one can identify the earlier states. Approximations for the studied material's transition temperatures may be defined based on the results from these plots. The estimates for transition temperatures are determined by identifying the last solid data point and the first molten data point in the figures and selecting a temperature between this range. The DSC determined transition temperature for solidification of the material cooling was previously accepted as 45℃ in Section 3.1. Based on the energy analysis, the temperature of solidification for the machinist wax is selected as 54.6℃. The previously determined melting point for this material while heated was accepted as 62℃ based on the DSC analysis performed in Section 3.1. Based on the energy analysis, the melting temperature for the machinist wax shifts to 62.5℃. These new values for transition temperature are crucial for defining a function of the material's internal temperature with a point of continuity. Unfortunately, these plots also identify the existence of a major discontinuity between transitions of phase for energy. The major discovery made while inspecting energy was the confirmation of a correlation between the behavior of the entire parent signal and temperature, not just the onset.

5.3 Moment Evaluations

The expansion of signal interpretation via the use of an energy analysis proved to be useful. However, the internal temperature is still unable to be directly quantified. Homogeneous materials such as the candle wax are able to be directly quantified by using the signal onset directly, but additional signal interpretations need to be considered for use on the machinist wax. The following expansions to signal interpretation covered in this section all include investigations surrounding statistical analysis. We will look to the resulting moments of the parent signal, specifically the first raw moment and the first, second, third, and fourth central moments will all be investigated. As the results will show, the first moment seems to be the best indicator for the temperature state of the machinist wax. The moment of a function is defined by the following general relationship (see e.g., [42]).

$$\mu_i = \int_{-\infty}^{\infty} (t-a)^i \, f(t) dt \tag{5.5}$$

where i corresponds to the order of the moment taken about location a, for some function that is dependent upon time $f(t)$.

Equation 5.6 differs from that in [42] by the addition of the shift factor, a, to allow for the moment about the location a whereas the form in [42] has the interpretation of the moment about the origin $t = 0$. The moments of a statistical distribution can be used to describe the shape of the distribution. Therefore, the moment about the origin (i.e., $a = 0$), is referred to as the first raw moment of the parent signal and is defined as the following:

$$\mu = \int_{t_i}^{t_f} (t-0)^1 \, f(t) dt = \int_{t_i}^{t_f} t \, f(t) dt \tag{5.6}$$

Notice in Equation 5.6 that the integral is evaluated over the range $t \in \{t_i, t_f\}$ instead of $t \in \{-\infty, \infty\}$. The signal of interest $f(t)$, if properly setup as in Section 5.2, would exist only within the gated region and would be zero elsewhere, thus the value of the integration outside of the gated region will be zero.

In our applications, $f(t)$ is the signal power defined in Equation 5.3 and the moment calculation is normalized using energy defined in Equation 5.2, thus the first moment is defined as

$$\mu(T) = \frac{1}{\tilde{E}(T)} \int_{t_i}^{t_f} tP(t,T)\, dt \tag{5.7}$$

In performing these operations on the parent signal, we are effectively determining the location of the mean of the signal in seconds. In other words, the first raw moment identifies the moment in time, $\mu(T)\ \epsilon\ \{t_i, t_f\}$, at which the signal power is equivalent on either side of this time. This is often referred to as the mean of a distribution. In engineering applications, we typically refer to the statistical mean as the centroid. The verbiage is used interchangeably for our applications. The desire for the parent signal's centroid is for it to lead to some relationship between internal temperature without the analysis issue posed by the discontinuity when using the signal onset analysis from Chapter Three. All proceeding moment calculations will be taken about the first raw moment value where $a = \mu(T)$. For example, the first central moment is obtained by repeating the calculation from Equation 5.7, with the exception that it will be about $\mu(T)$, the first raw moment. The first central moment should always return the zero value since the mean about the mean is zero. Performing the calculation merely acts as a good check for coding applications. The first central moment is represented by the following:

$$\mu_1(T) = \frac{1}{\tilde{E}(T)} \int_{t_i}^{t_f} (t - \mu(T))P(t,T)\, dt = 0 \tag{5.8}$$

The second central moment is often referred to as the variance. The variance refers to the width of the distribution from the average. In other words, the variance is a measure of the distance the distribution is spread from the mean, $\mu(T)$. The variance is defined as the following:

$$\mu_2(T) = \frac{1}{\tilde{E}(T)} \int_{t_i}^{t_f} (t - \mu(T))^2 P(t,T)\, dt \tag{5.9}$$

Additionally, the variance is the square of the standard deviation according to [42]. The standard deviation can then be found by

$$\sigma(T) = \frac{1}{\tilde{E}(T)} \sqrt{\int_{t_i}^{t_f} (t - \mu(T))^2 P(t,T)\, dt} \tag{5.10}$$

The third and fourth central moments regard utility in a similar manner. These statistical representations bring additional light to the nature of the distribution itself and are therefore less useful when described using units. The units of these moments have no physical meaning and are commonly divided out by the standard deviation to some power. The third central moment, called skewness, measures the weight of the distribution on either side of the mean. For example, if more data is represented to the right of the mean in the distribution, then the skewness is a positive value. The skewness is negative for distributions with more data represented to the left of the mean. The skewness is then zero for symmetric distributions about the mean. Skewness of some value in seconds to the third power is not as useful as a unitless skewness, so the skewness will always be divided by the previously calculated standard deviation to its third power.

The fourth central moment, called kurtosis, provides similar benefits for understanding of the overall distribution. The kurtosis value corresponds to the tails of a distribution being either thin or fat. Essentially, the value of the kurtosis is a comparison

for the “tailedness” of the distribution. Taking, for example, the kurtosis value of any univariate normal distribution as three [43], this value can be subtracted from the resulting kurtosis value and comparisons can be made on its distribution at the ends with relation to any univariate normal distribution. This generalization of kurtosis is often referred to as the excess kurtosis. Positive excess kurtosis, called leptokurtic, refers to thicker distribution tails. Negative excess kurtosis, called platykurtic, refers to the contrary with thinner distribution at the ends [43]. Similarly, to skewness, the units of kurtosis, or excess kurtosis, have no physical meaning and will therefore be divided out by the standard deviation to the fourth power. Equation 5.12 and Equation 5.13 will be used for computing the generalized variations of skewness and kurtosis, respectively.

$$\mu_3(T) = \frac{1}{\sigma^3 \tilde{E}(T)} \int_{t_i}^{t_f} (t - \mu(T))^3 P(t,T) dt \tag{5.11}$$

$$\mu_4(T) = \frac{1}{\sigma^4 \tilde{E}(T)} \int_{t_i}^{t_f} (t - \mu(T))^4 P(t,T) dt - 3 \tag{5.12}$$

Before discussing the findings revolving around the first raw moment of the parent signal, it will be beneficial to first see what the first, second, third and fourth central moments offer to better the understanding of the parent signal. Analysis using the central moments of longitudinal signals traversing through a material which experiences thermal changes has been conducted previously in [44]. The study conducted by Lau et al did not attempt to preserve the parent signal as demonstrated within Section 4.1. Additionally, their analysis observes the phase transition of a selected material by performing continuous ultrasonic testing while the material is not in thermal equilibrium. Our analysis is conducted on the ultrasonic data collected from the quasi-isothermal study described in Section 5.1. Lau concludes that the central moments are capable of identifying velocity changes which correspond to internal temperature changes or

transitions of material phase. By preserving the parent signal and analyzing a material which is in thermal equilibrium, additional information will become obtainable from the central moments beyond just the changes in velocity. Assumptions can be made about the changes in a waveform's general structure based upon the analysis of the central moments. Lau also comments on the ability of the central moments to identify the quality of the recorded signal. We will expand upon this claim in the following analysis using the central moments.

As stated previously, the first central moment should in fact return the zero value for all temperature scans collected during the quasi-isothermal study described in Section 5.1. While this won't necessarily contribute greatly to additional understanding of the parent signal, it will serve as a good check to ensure the mathematics and understanding behind these statistical moments are performing as we believe they should be. The result of using Equation 5.8 to calculate the first central moment of the parent signal returned the zero value for all temperatures collected during the quasi-isothermal study described in Section 5.1 while the machinist wax was both heated and cooled, as expected. This check essentially verifies that the location calculated for the first raw moment was done correctly. The first central moment involves shifting over to the location of the first raw moment, or the centroid of the parent signal, and calculating the first moment from that position. The value returned is the distance from the starting point to the centroid. Since the starting point is the centroid, the distance is zero.

The second central moment is used to find the standard deviation using Equation 5.10. Figure 5.7 and Figure 5.8 depict the standard deviation for the machinist wax as the material is heated and cooled, respectively.

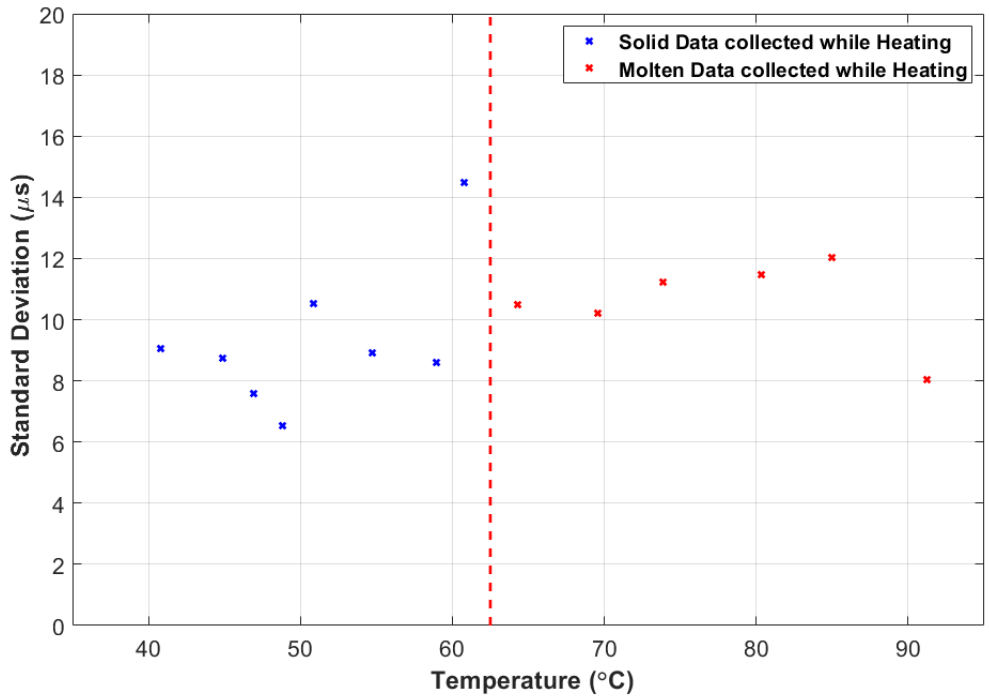

Figure 5.7. Standard deviation of machinist wax data collected during isothermal step heating, vertical line corresponds to melt temperature from normalized energy

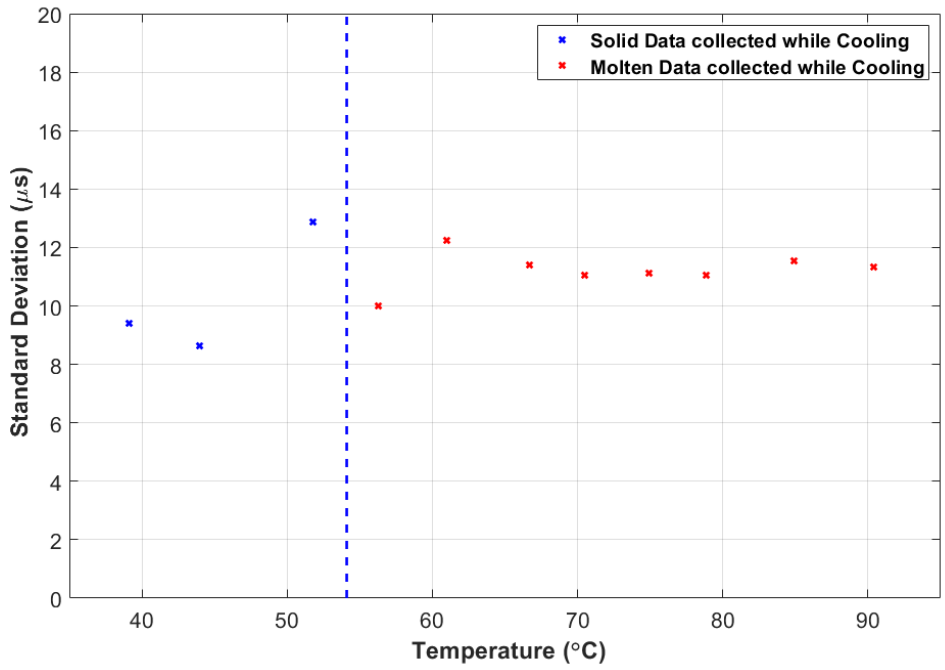

Figure 5.8. Standard deviation of machinist wax data collected during isothermal step cooling, vertical line corresponds to temperature of solidification from normalized energy

The following discussion is intended to propose areas of future work utilizing the central moments of a parent signal. For the purposes of this thesis, the central moments are not a reliable source for the quantification of temperature or phase state on the studied material. However, the analysis on central moments reveals several potential applications for future use including defining waveform structure and detecting waveform clarity.

The parent signal becomes a statistical distribution of the gated waveform's normalized power by using the equations defined in this section for the central moments. For example, the standard deviation of the gated parent signal represents the spread of data from the respective mean value, $\mu(T)$. The data is expected to have a spread about the mean since it is an oscillating soundwave with amplitude gradually dampening out over time. Values for the standard deviation are unfortunately capable of drawing several conclusions. For example, consider the information relayed in Figure 5.7 and Figure 5.8. The values of standard deviation remain fairly constant until a sudden increase preceding the transition temperature. Then the values for standard deviation return to a constant value that is higher in the molten region than in the solid region. A constant returned value for standard deviation means the distribution is consistently spread around the centroid. Having a higher average standard deviation in the molten regions of the collected data means the distribution from the centroid is spread wider in these regions. The change in the spread of the distribution between material phases implies a change in the structure of the waveform. Unfortunately, it is inconclusive what feature of the waveform is changing. Higher values for standard deviation can also imply a waveform is saturated with noise. As the distribution is spread further out, the peak of the distribution, which identifies the location of the centroid, is flatter. A signal highly saturated with

noise results in a flat distribution, or high standard deviation, because the resulting waveform amplitude is similar to the amplitude of the noise. This implies the standard deviation may also be used to compare the quality of data collected. Using the standard deviation alone suggests waveform structure and resolution are changing as temperature changes, but it is not currently capable of identifying what causes the changes. However, keep in mind the higher standard deviation at 61℃ shown in Figure 5.7. If the higher standard deviation for this temperature implies a decline in signal resolution causing a flatter distribution peak, then the tails of the distribution will also be fatter meaning the kurtosis at this temperature will be the lowest. Before looking at kurtosis, the skewness is plotted using Equation 5.11 for the third central moment. Figure 5.9 and Figure 5.10 depict the calculated skewness of the machinist wax data collected during heating and cooling, respectively.

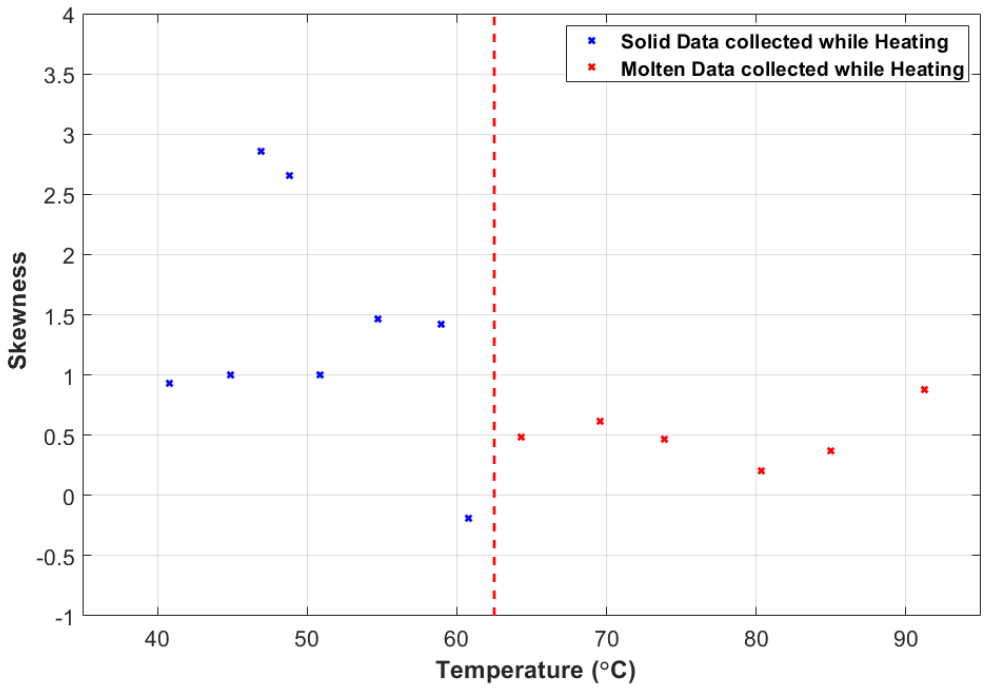

Figure 5.9. Skewness of machinist wax data collected during isothermal step heating, vertical line corresponds to melt temperature from normalized energy

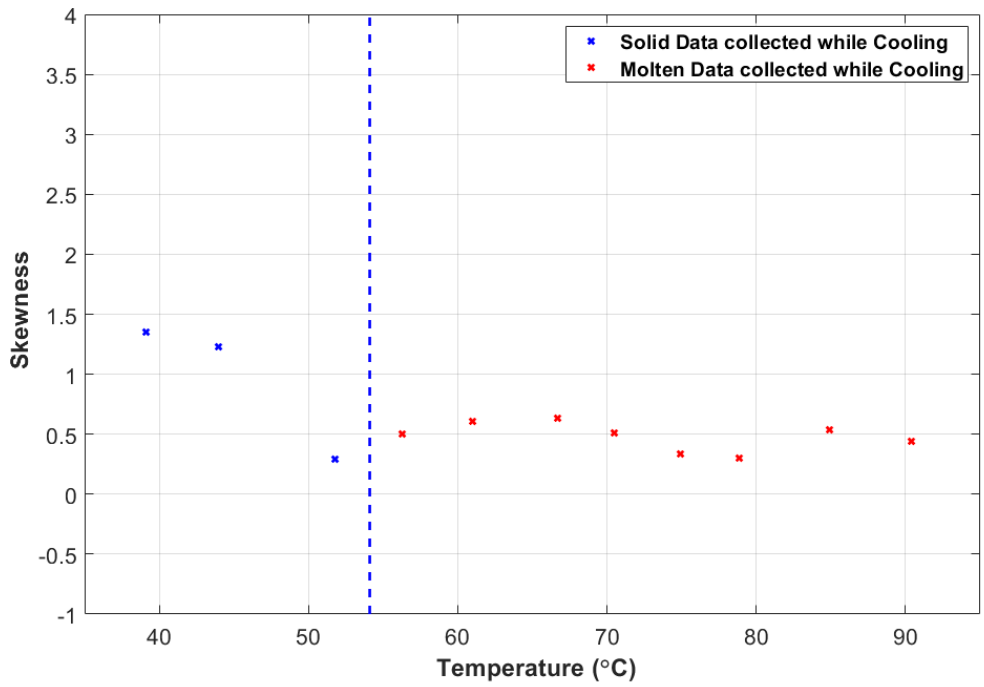

Figure 5.10. Skewness of machinist wax data collected during isothermal step cooling, vertical line corresponds to temperature of solidification from normalized energy

The observations made during the analysis of the parent signal's skewness are similar to the standard deviation. The positive values for skewness state that the majority of the distribution is to the right of the centroid. This observation is expected based on the structure of a typical soundwave. The oscillating waveform exponentially decays over time. Typical soundwave structure places the centroid at the front end of the statistical distribution meaning the majority of the distribution lies to the right of this point. However, while the skewness is also useful in determining what a parent signal's distribution looks like, only inferences are able to be made regarding why waveform structure is changing and what is causing the change. In the event that a negative skewness is reported, meaning the majority of the distribution is to the left of the centroid, it is equally possible to have assigned an early gate to the signal as it is to be

observing a waveform of nontypical structure. If the gate used to encompass the parent signal begins too early and ends too soon, the desired distribution will be skewed right. This creates a new distribution which doesn't have a centroid until later in time with the majority of the distribution located to the left of this location. Similarly, consider a waveform that includes peaks of similar amplitudes before decaying suddenly. A distribution of this type of waveform may lead to a majority of negative skewness values. In summation, the analysis on skewness is as inconclusive as the analysis on standard deviation. The provided information on waveform structure and signal strength is not specific enough to draw a single conclusion. While the statistical meaning of skewness is comprehensible, implying a definitive reason behind its alterations in parent signal analysis becomes difficult.

The fourth central moment, kurtosis, is the last of the central moments to be plotted and analyzed. Figure 5.11 and Figure 5.12 represent the kurtosis of the machinist wax calculated using Equation 5.12 as the material was heated and cooled during the quasi-isothermal study discussed in Section 5.1.

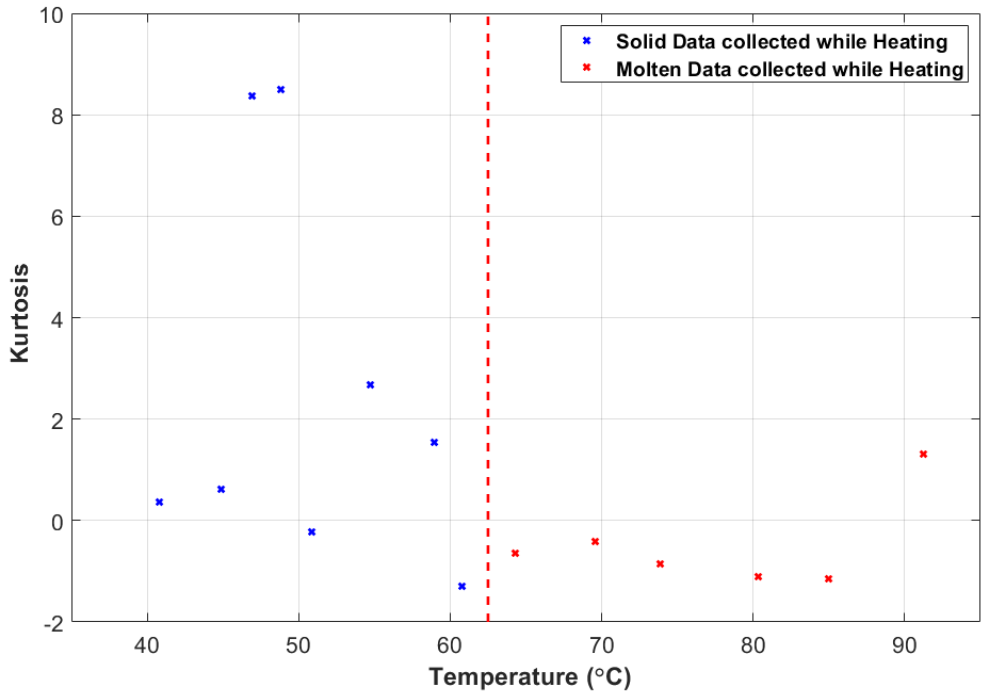

Figure 5.11. Kurtosis of machinist wax data collected during isothermal step heating, vertical line corresponds to melt temperature from normalized energy

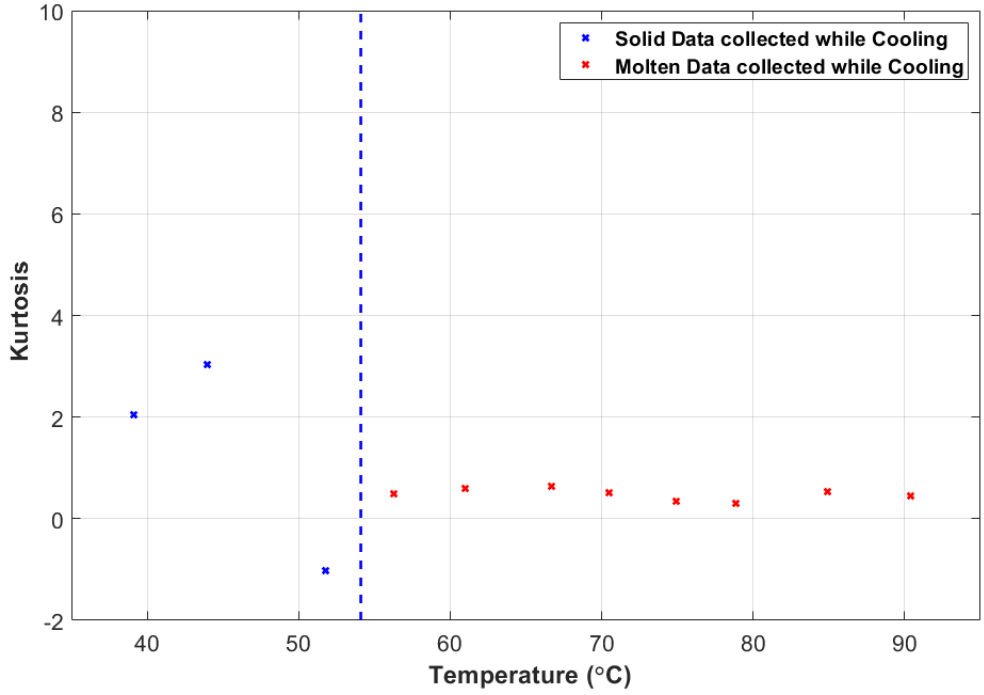

Figure 5.12. Kurtosis of machinist wax data collected during isothermal step cooling, vertical line corresponds to temperature of solidification from normalized energy

Initially note the lowest kurtosis value from Figure 5.11 is at 61℃. This note helps support the hypothesis made while analyzing the standard deviation. When comparing kurtosis values, a lower value implies the tails of the distribution are thin. The opposite is true for positive kurtosis values. When comparing central moment values, if a data set renders a high standard deviation and low kurtosis on average, a case can be made on the captured signal's relative resolution. In an extreme case, thin tail ends with a distribution over a broad range implies the shape of the distribution is very wide and not very tall. For the current application, this could imply the gated signal is majority static noise from the system. Turning attention to the two data points collected during heating prior to the 50℃ mark, a trend is observed. Each point is significantly higher than the rest for kurtosis and slightly higher for skewness. Statistically, this states that the distribution tails are significantly fatter in relation to the other data points, and a larger amount of the data is to the right of the centroid on average. Physically, this could potentially mean the parent signal at these temperatures exponentially decayed significantly faster than those of the other temperatures. For this to be true, the standard deviation of each of these two points needs to be lower than average. A lower average standard deviation states the deviation of the overall distribution from its centroid is lower which would occur for a spike in the signal amplitude which dies off quickly. Figure 5.7 supports this hypothesis as these temperature points provided the two lowest standard deviations. A definitive statement about waveform structure is still not possible from the provided moment data, however, combining the results from each central moment allows for an analyst to create better assumptions about the waveform's structure.

The power of the central moment analysis is using each of them together. A single moment by itself typically draws more questions than answers as seen in the previous discussion. The benefit behind this analysis technique is being able to answer some of the questions one central moment gave you by analyzing the next central moment. The central moments are potential resources when considering which data points to incorporate in an analysis and which ones experienced nonrepeatable discrepancies and should be redacted from the analysis. Performing these calculations also provides insight on the general alterations of a waveform's structure as data is collected. While the central moments may be useful in this manner, they lack the current ability to provide definitive results. They can assist in making assumptions about ultrasound data, but to verify these assumptions requires the use of additional analysis techniques left for future studies. Additionally, only vague identifiers are observed for the studied material experiencing structural alterations due to changing temperature. Regardless of the material being heated or cooled, the minimum skewness and kurtosis values were consistently located prior to phase transition. The same observation is made for the location corresponding to the maximum standard deviation. In conclusion, the central moments are not preferred for tracking the thermal changes of the studied material.

The first raw moment is the primary focus of these expansions to signal interpretation. By tracking the mean of each parent signal, the discontinuity found around the transition temperatures from Chapter Three and Section 5.1 will be shown to be avoided. This methodology used in signal analysis is able to not only take the signal onset into account but also the continuation of the signal's oscillations before dampening out. The first raw moment of the parent signal returns values of time in seconds for the

location of which the distribution is spread evenly. That is why this value is often referred to as the centroid. Figure 5.13 and Figure 5.14 depict the first raw moment of the machinist wax calculated using Equation 5.7 from data collected during the quasi-isothermal study as temperature was increased and decreased, respectively.

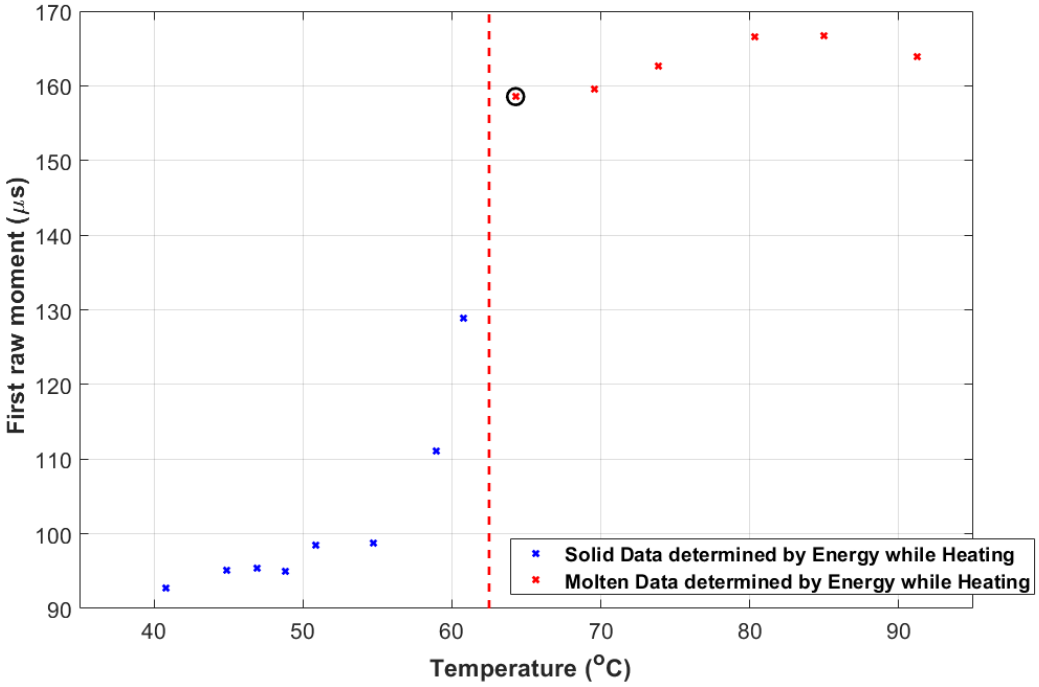

Figure 5.13. First raw moment of machinist wax data collected for quasi-isothermal test during heating across a 203 mm (8”) span

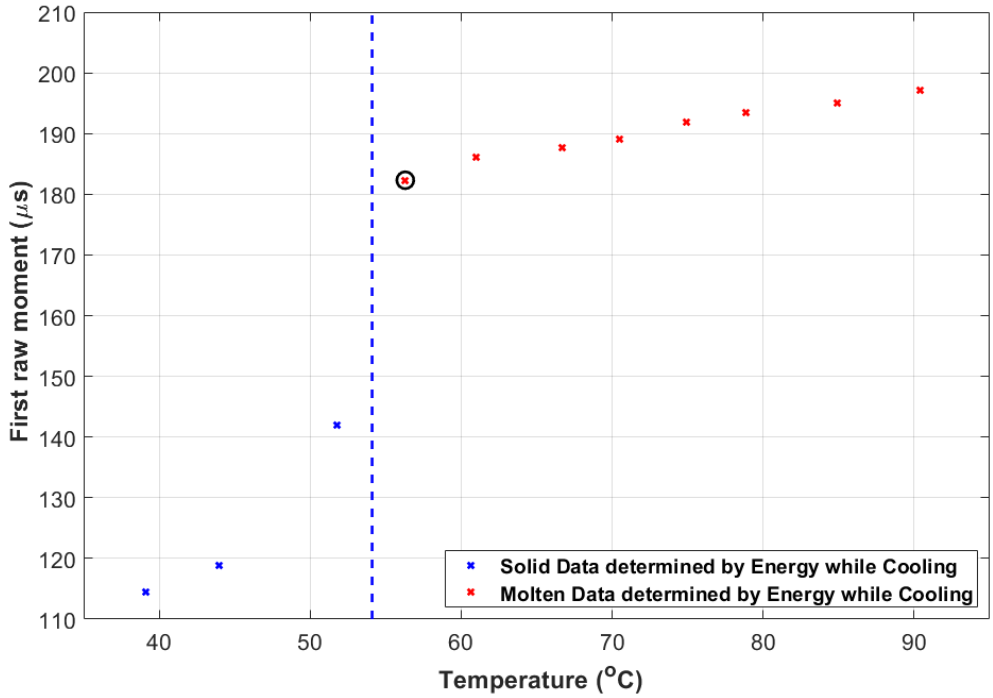

Figure 5.14. First raw moment of machinist wax data collected for quasi-isothermal test during cooling across a 254 mm (10”) span

Note that Figure 5.14 had to be vertically shifted for the time the signal spent within the polycarbonate walls based on the speed of sound found in [45], whereas Figure 5.13 did not require shifting since the containment vessel used for data collection had a negligible wall thickness. Notice there are two piecewise, continuous trends for both plots of data. The curves for characterizing the machinist wax during solid states, based on the energy analysis, both appear to be nonlinear, while the molten data is linear for each figure. The first molten data point after the energy determined transition temperature is highlighted. It is at this temperature where continuity for either piecewise function may be maintained. In order to provide the greatest representation for internal temperature of the machinist wax, the point of continuity is chosen to be set at the respective transition temperatures defined by the energy analysis. By taking the distance traveled through our

machinist wax and dividing it by the first raw moment, we obtain units for velocity. Performing this calculation produces a surrogate to the material property, speed of sound, which shall be referred to as the centroidal speed of sound (CSoS) in reference to the first raw moment. Figure 5.15 and Figure 5.16 depict the CSoS as a function of temperature for the machinist wax during heating and cooling, respectively.

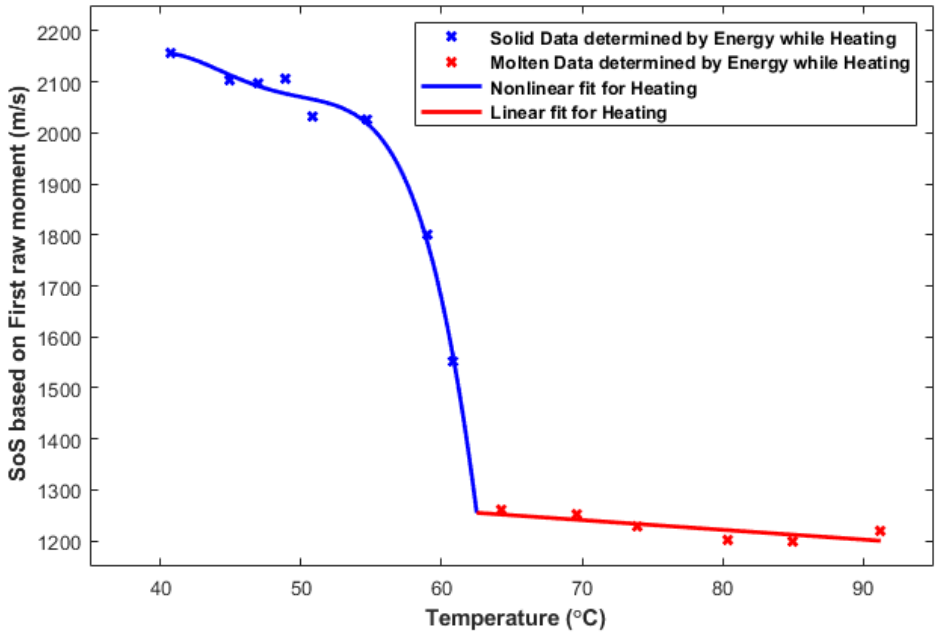

Figure 5.15. Centroidal speed of sound as a function of temperature for machinist wax during heating

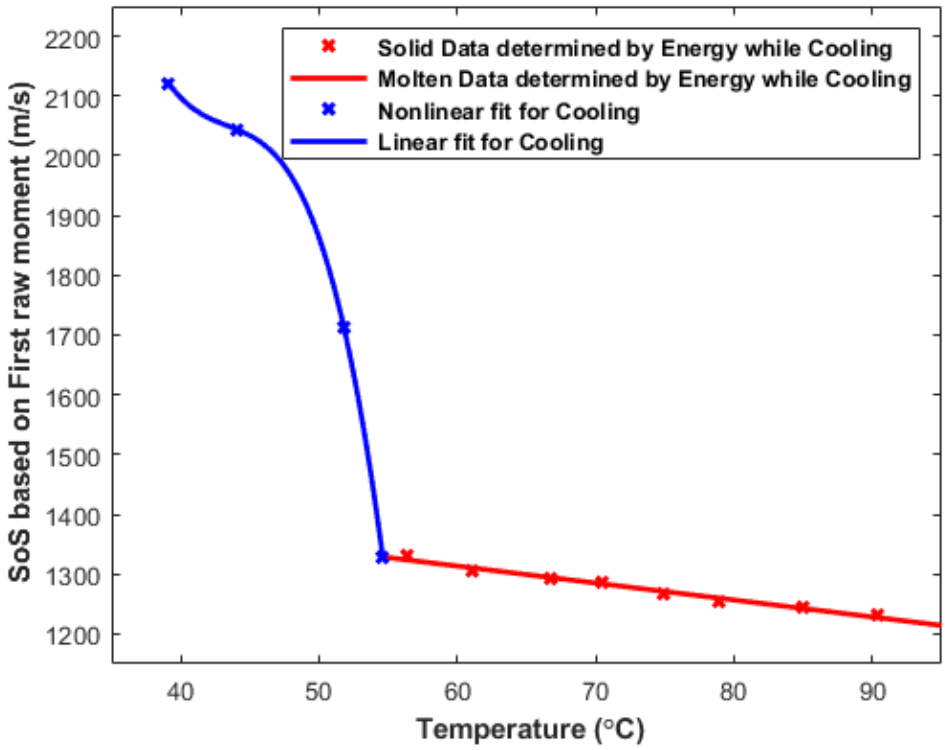

Figure 5.16. Centroidal speed of sound as a function of temperature for machinist wax during cooling

The nonlinear fits were created using least squares regression. Enough data was collected during the solid region for the machinist wax during isothermal step heating to create a fourth order polynomial. However, only three data points were collected for the solid region of the machinist wax during isothermal step cooling. The temperature of solidification determined by the normalized signal energy for this material is used as the point of continuity and acts as a fourth data point for this region. A third order polynomial is fit to the data for the machinist wax during isothermal step cooling in the solid region. Due to the fit in this region, the coefficients expressed in Equation 5.19 are likely to change based on any error in the collection of the ultrasonic data used to create the fit. However, the accuracy of this fit will be justified in Section 6.2 when it is used to quantify the internal temperature of our selected material during continuous cooling.

These functions of temperature are only good representations of the data at the ranges for which data was collected. Data was not collected at temperatures below 40°C due to the contraction this material experiences during solidification. Data collected once the material pulls itself from the walls of the containment vessel is meaningless. For industrial applications, the use of through-transmission ultrasound altogether at these temperatures is impractical. That being said, for the temperature ranges displayed in the above figures, two piecewise, continuous functions are created which relate the CSoS to the material's internal temperature. The functions are created for both the endothermic and exothermic reactions. Continuity for each function is found at the transition temperature determined from the energy analysis. In both cases, the cooler temperatures to the left of the continuity point, classifying the machinist wax as a solid, are represented by respective nonlinear functions. Simple linear functions represent the material to the right of this continuity during its molten phase. For both heating and cooling, least squares regression was utilized to fit the data to the form

$$\bar{c}_{solid\ heating}(T) = a_1 + b_1 T + c_1 T^2 + d_1 T^3 + e_1 T^4 \tag{5.13}$$

$$\bar{c}_{solid\ cooling}(T) = a_1 + b_1 T + c_1 T^2 + d_1 T^3 \tag{5.14}$$

$$\bar{c}_{molten\ heating/cooling}(T) = a_2 + b_2 T \tag{5.15}$$

Subject to the constraint

$$\bar{c}_{solid}(T_{melt}) = \bar{c}_{molten}(T_{melt}) \tag{5.16}$$

This equation is solved for the machinist wax during heating using least squares regression yielding coefficients of

$$a_1 = -75690 \text{ (m/s)} \qquad b_1 = 6705 \text{ (m/s°C)} \qquad c_1 = -215.3 \text{ (m/s°C}^2\text{)}$$

$$d_1 = 3.056 \text{ (m/s°C}^3\text{)} \qquad e_1 = -0.0162 \text{ (m/s°C}^4\text{)} \tag{5.17}$$

$$a_2 = 1375 \text{ (m/s)} \qquad b_2 = -1.912 \text{ (m/s°C)} \tag{5.18}$$

where the centroidal speed of sound, $\bar{c}_{solid}$ or $\bar{c}_{molten}$, will be in units of m/s and T is expressed in °C. $T_{melt} = 62.5$°C based on the energy analysis in Section 5.2. Figure 5.15 shows the fitted piecewise, continuous function.

The model is similarly solved for the machinist wax during cooling using least squares regression yielding coefficients of

$$a_1 = 38060 \text{ (m/s)} \qquad b_1 = -2474 \text{ (m/s°C)} \qquad c_1 = 56.85 \text{ (m/s°C}^2\text{)}$$

$$d_1 = -0.4370 \text{ (m/s°C}^3\text{)} \tag{5.19}$$

$$a_2 = 1484 \text{ (m/s)} \qquad b_2 = -2.837 \text{ (m/s°C)} \tag{5.20}$$

where $T_{melt} = 54.6$°C from the energy analysis performed in Section 5.2. Figure 5.16 shows the fitted piecewise, continuous function defined.

Equation 5.15 is recast as a function of the centroidal speed of sound using the coefficients from Equation 5.18 and Equation 5.20 for the internal temperature of the machinist wax during molten phases experiencing heating and cooling respectively as

$$T_{molten\ heating}(\bar{c}) = 719.1 - 0.5231\bar{c} \tag{5.21}$$

$$T_{molten\ cooling}(\bar{c}) = 523.0 - 0.3525\bar{c} \tag{5.22}$$

where Equation 5.21 is only applicable for $\bar{c} \leq 1255$ m/s and Equation 5.22 is only applicable for $\bar{c} \leq 1329$ m/s. Each centroidal speed of sound constraint corresponds to the material's transition temperatures determined during the energy analysis.

Temperature as a function of centroidal speed of sound during the solid phases is not solved analytically as the molten phases are. The solid regions are defined by third and fourth order polynomials and are solved using a numerical solver embedded in MATLAB's coding software [47]. The fzero command found in MATLAB locates the

closest zero value of a function from a desired starting point using several numerical methods including bisection, secant, and inverse quadratic interpolation [47]. The function given to MATLAB's fzero command is of the form

$$g(\bar{c}, T) = \bar{c} - \bar{c}_{solid}(T) \tag{5.23}$$

where $\bar{c}$ represents the centroidal speed of sound in m/s obtained from data collection and $\bar{c}_{soild}(T)$ represents the respective Equation 5.13 or Equation 5.14 with the appropriate coefficients applied from either Equation 5.17 or Equation 5.19 depending on the machinist wax heating or cooling, respectively.

Finding the roots of this function will return multiple solutions for the internal temperature which correlate to the entered value for CSoS. Of these solutions, only one is a purely real solution that is within the temperature range supported by collected data. The fzero command in MATLAB accepts an initial starting location to find the nearest zero value. By using a temperature within the range tested, 40℃ and 90℃, the location of the zero is not imaginary and is within the desired range. Therefore, the internal temperature of the machinist wax as a function of centroidal speed of sound while this material is solid in phase is defined as

$$T_{solid}(\bar{c}) = fzero\big(g(\bar{c}, T), T_{range}\big) \tag{5.24}$$

where the solutions to internal temperature of the machinist wax as a solid, $T_{solid}(\bar{c})$, are in ℃ and T_{range} represents any value of temperature in ℃ within the range tested.

With this information, one can successfully identify the internal temperature of the machinist wax along a straight line without the need to access the vessel which contains it. These sets of equations currently only apply to the machinist wax. However, future work may allow materials of different internal structures to be characterized using

the CSoS analysis methodology described in this thesis. Materials similar in structure to the studied machinist wax have been notorious for their illusiveness to characterization, and the CSoS is an innovative tool which may be used for the thermal characterization described. Every material will react differently, but the contributions of this thesis include a new methodology in which to pursue material inspection. After the successful thermal characterization of the machinist, the quasi-isothermal studies can come to a close in order to create a new set of studies which revolve around the applicability of the findings. Using several through-transmission channel lines across a rectangular geometry, the CSoS is used to quantify the effective internal temperature without the need to physically access the respective containment vessel in Chapter Six. Being able to thermally characterize the machinist wax using the CSoS brought this goal a giant step closer.

During the larger studies for applicability described in Chapter Six, it was hypothesized that the centroid experienced shifting due to pressure applied at the transducers. In order to verify pressure caused some centroidal shift, a final study was performed.

5.4 Centroidal Shifting based on Transducer Pressure

To confirm the hypothesis about transducer pressure, a simple test was organized. One of the quasi-isothermal containers used in previous studies was used to bring the machinist wax to a molten state. This study does not intend to quantify temperature, but to observe the impact of a centroidal shift on temperature overall. A-scan data was collected using through-transmission on a pair of 0.5 MHz transducers. The gain was set to 0 dB with the receiving transducer connected to a preamplifier set to 50 dB. All scans collected were done so by holding the transducers in hand. As each scan was collected,

the pressure was gradually increased. Figure 5.17 shows the correlation between the first raw moment as pressure increases for four varying pressure states. Applied pressure state one correlates to barely holding the transducers in place on the sides of the container walls. At applied pressure state two, two fingers are used to apply pressure to the transducers. Pressure state three corresponds to using both hands to press the transducers against the container walls. At the applied pressure state four, the transducers are forced tightly to the sidewalls.

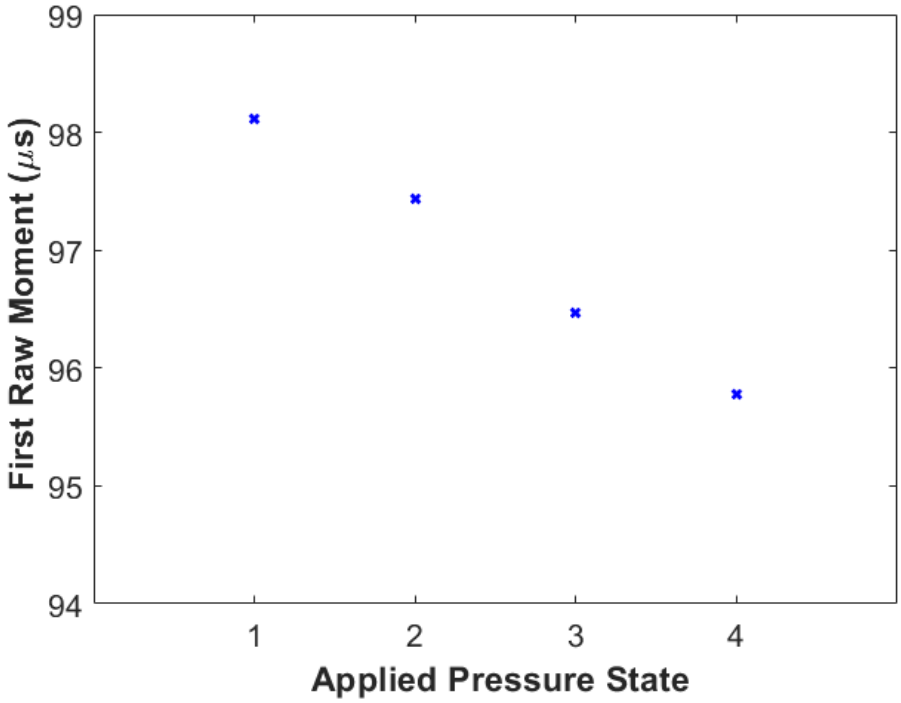

Figure 5.17. Centroidal shifting due to increasing transducer pressure

Figure 5.17 proves that as transducer pressure is increased, the centroid of the parent signal arrives earlier in time. The decrease seen in this plot is only by a few microseconds, but it is important to see how this change will affect temperature during a molten state. Once molten, the CSoS has a linear relationship to temperature as seen in

Equation 5.15. It is convenient to use the molten data since it won't matter how hot the actual material is. The scaling of temperature will be maintained equal to the scaling of the centroid regardless. In order to observe the scaling of temperature, we first use Equation 5.22 for our molten material and calculate the temperature for each data point. The temperature values are subtracted by the minimum to express the direct impact transducer pressure can have on the accuracy of the effective internal temperature of the medium. Figure 5.18 depicts the temperature scaling caused by increasing transducer pressure.

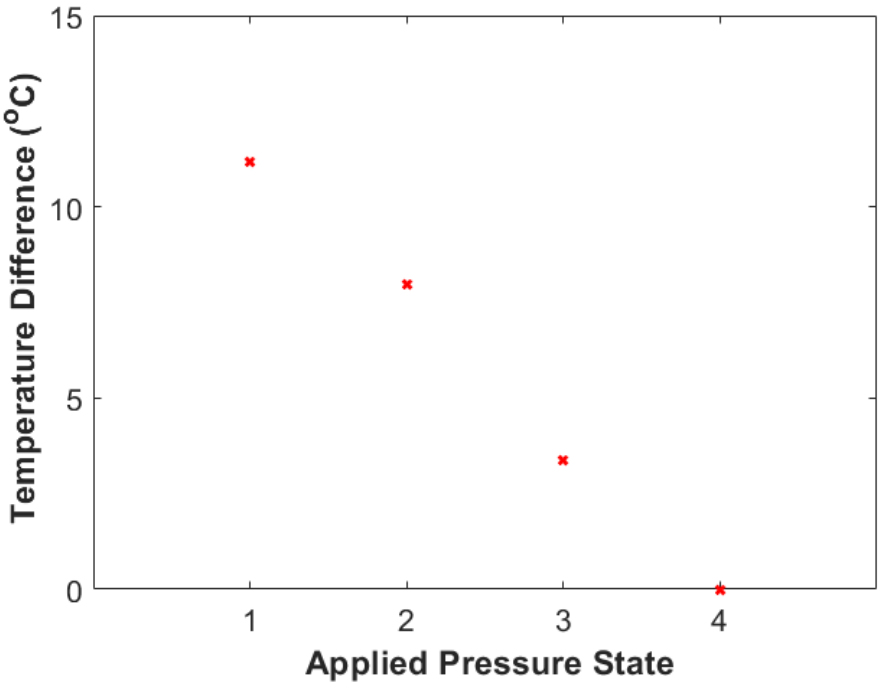

Figure 5.18. Temperature shifting due to increasing transducer pressure

Even with the slightest shifting of the centroid by a few microseconds, the accuracy of the calculated effective internal temperature can vary over 10℃. It is also observed from repeated testing that the further away a material is from equilibrium, the

greater the impact pressure has on centroidal shifting. The data used to create Figure 5.17 and Figure 5.18 was collected when the medium was not in thermal equilibrium. The quasi-isothermal studies only collected data once all locations within the medium were within 0.5℃ of each other. That is the reason pressure played no noticeable change between repeated experimentation during those studies. For the studies examined in the following chapter, the temperature difference from one location within the medium to the next will vary by 5℃ or more. Chapter Six will show how maintaining a proper pressure for each transducer can increase the accuracy of thermal quantification using the CSoS. Ideally, a testing apparatus should be constructed which is conducive to such pressure maintenance. Results from ideal pressure attribution and nonideal pressure attribution shall be examined.

Thus far, the centroid's behavior has proven useful for characterizing materials during times of thermal equilibrium. The characterization methodology needs validation during less convenient thermal scenarios which are likely to occur in an industry setting. The use of the centroid needs to be applicable. The next series of studies shall attempt to prove the applicability of the centroidal speed of sound.

CHAPTER SIX

Highly Porous Material Acoustic Quantification for 2D Geometry

6.1 Experimental Overview

The intent of Chapter Six is to demonstrate the applicability of the findings from Chapter Four and Chapter Five. In order to pursue this feat, the Chapter Six introduces a study which attempts to determine the effective internal temperature of the machinist wax and a two-dimensional temperature profile along channel lines without accessing the internals of the container housing the material. Multiple containers of differing geometric shape were tested on, but an in-depth analysis of only one is examined within this thesis. This chapter will focus on using a rectangular box to contain the machinist wax. The ability to plot the internal temperature profiles along channel lines of a rectangular plane geometry shall be examined. In addition, this rectangular setup will have two separate methods of heating. Each study will include experimental procedures for validation. This includes the use of several K-type thermocouples which are inserted top-down into the machinist wax, similar to the quasi-isothermal studies. The values obtained from the internal sets of thermocouples are not used to assist in calculating the internal temperature from ultrasound, they are for validation only. There will also be external thermocouples which are adhered to the sides of each containment vessel near the transducer locations. This creates the ability to formulate thermal boundary conditions around the exterior of the container. These boundary conditions are necessary for a greater understanding of the internal thermal activity. The way in which these boundary

conditions will be utilized shall be explained in further detail later within this chapter. For now, several considerations are necessary to discuss before delving deeper into the analysis.

Since each study focuses on applicability, a considerable increase to containment vessel size was made in comparison to the prior studies listed within this thesis. Additionally, this larger system is not heated by system surroundings, but by internal heating sources. Each study collects data continuously as opposed to only at times of equilibrium. In fact, the system will rarely, if ever, be in thermal equilibrium. The first consideration takes each of these factors into account and looks at what components will be necessary to achieve such a system for analysis. Extensive testing on the machinist wax during the quasi-isothermal tests revealed this material's reluctance to fully melt. That being said, the internal heating sources would need to be capable of reaching a heat sufficiently higher than the material's melt temperature. This way, the material located at the outer walls of the containment vessel is also capable of becoming fully molten. Insulation is applied to the testing apparatus exterior in order to assist in bringing the material to a fully molten state. Referring back to Chapter Four, this addition of insulation not only allowed the system to heat properly, but also assisted in surface wave dampening in the process. The testing apparatus is properly dampened in a similar manner following the guidelines expressed in Chapter Four. With the considerations of heating and dampening addressed, comes additional concerns. For a system which will be experiencing extremely high temperatures for extended periods of time, hardware limitations are an imperative consideration. One of these problems was preemptively addressed during Chapter Four. The TGA analysis from the preceding chapter verified

that the use of the VersaSonic® coupling gel at either viscosity will be sufficient for the studies in question. The maximum input temperature for either of these studies is 230°F. This input temperature corresponds to the temperature at the heater cores. The cores do not maintain this initial input temperature for the entire duration of a test. The cores are certainly not equivalate in temperature to the container walls where the transducers and coupling gels are located. The temperature at these walls is known to reach a maximum of 80°C. The TGA results from Section 4.2 show the VersaSonic® coupling gels far outlasting this requirement. However, according to information found in [31], the transducers used within these studies are not intended for continuous use above 50°C. Continuously collecting data along a container wall whose temperature is 80°C is clearly an issue. In response to this, a buffer will be used to absorb a great deal of the heat that would normally be placed on the transducers in use. Following the lead of Taylor Jeffrey in her thesis [7], a sheet of ultem material is cut to shape in order for account for heat absorption.

It is important to discuss the different ways the ultrasound data will be expressed during these studies. A common method for expressing data collected through means of ultrasound includes the use of b-scans. Traditionally, b-scans look at the change in a-scan data along a displacement through a material (see e.g., [18]). Typical b-scan plots include the gated time of the a-scan signal versus displacement along a part. The amplitude of each a-scan is reflected by color plot intensity. However, for the purposes of the proceeding studies, the b-scans included in analysis will not track each a-scan over a displacement, but over the time elapsed during testing. This allows the observer to witness changes in the a-scan data collected for the duration of each study. A similar

technique is used for monitoring the cure cycle of epoxy resins (see e.g., [29]). Therefore, the axes will be represented as gated a-scan time versus time into experimentation, or global time. For each b-scan plot, a-scan time is represented in microseconds while the global time is in hours. An example of how b-scans are used for these testing purposes is depicted in Figure 6.1.

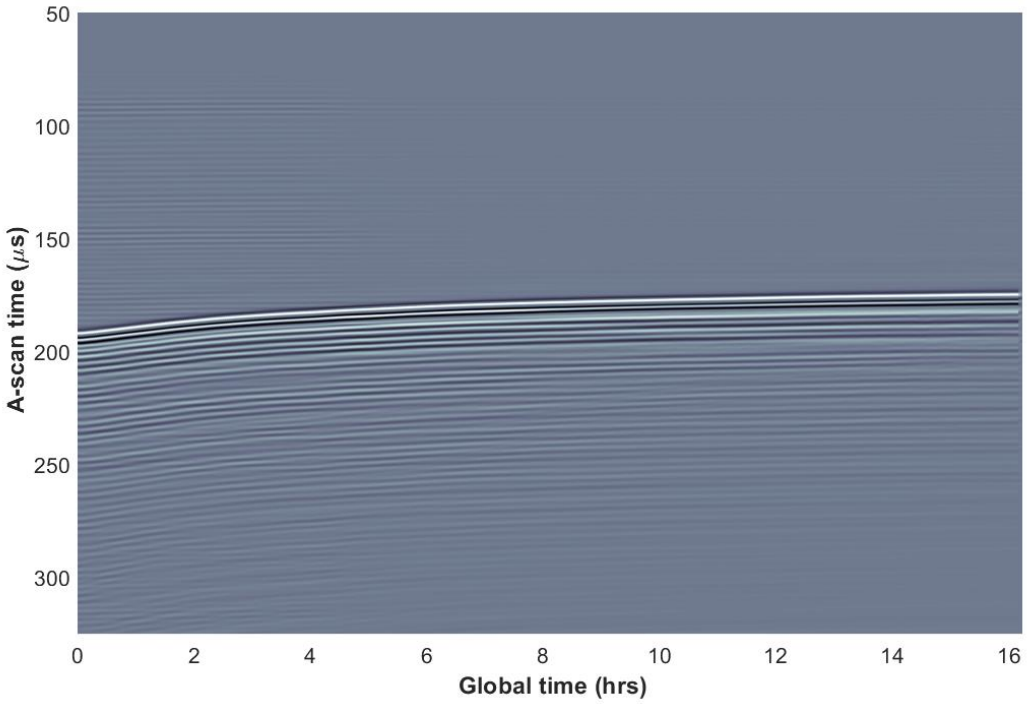

Figure 6.1. Example of b-scan variant used during the continuous thermal studies

Each a-scan is aligned with time for the duration of the test. The a-scan data is oriented in such a way that the lower values for signal flight time are positioned at the top the plot. With this being the case, it can be observed that the signal onset experienced a rapid decrease in ToF over a short duration before decreasing gradually. Since material speed of sound is faster in solids as opposed to liquids, it can be concluded that the material is cooling. In addition to the signal onset, the resulting oscillations of each signal

can be qualitatively observed to assist in gating the desired parent signal. If the signal is lost during testing, the loss tells the analyst that at this time the material pulled itself from the container walls. The machinist wax cools to the point where it contracts off the sides of the container while solidifying. Once this occurs, the remaining ultrasound data past that point is useless. Ultrasound data will only be analyzed for times prior to losing signal. All of this information is obtainable without the need for calculations or prior knowledge of the testing procedures. B-scans are extremely useful during these studies for this reason. They can be thought of as the baseline for analysis. If something unexpected is represented in data, it is always beneficial to return to the b-scans to ensure data was collected as intended. For this reason, the b-scan data is plotted for each study on every channel.

In addition to b-scans, the normalized signal energy is also represented for each study. The normalized energy will look very different for these studies if compared to the quasi-isothermal studies. They also tell the analyst slightly different information. Figure 6.2 depicts the normalized energy for a single channel during a similar study.

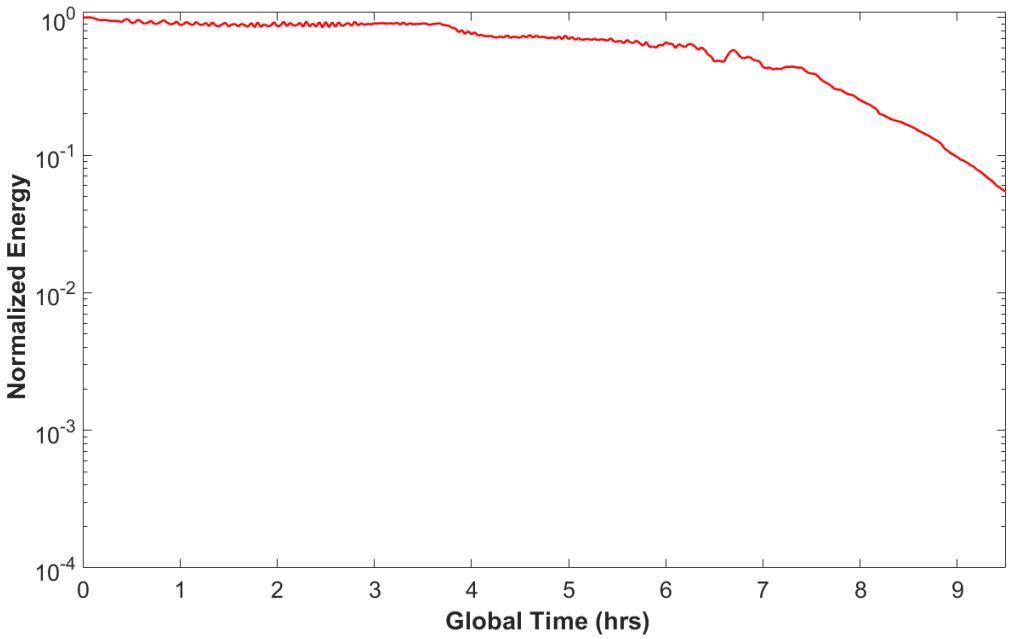

Figure 6.2. Example of normalized energy during continuous thermal study

During the quasi-isothermal studies, the energy data was either above or below the 50% marker and the state of the material was then identified. In the case where energy is continuously recorded for the entire duration of a test, attention is shifted to noticeable deviations in behavior. For example, Figure 6.2 shows the normalized energy maintaining some set value until nearly four hours into testing. At this time, a noticeable deviation occurs. The deviation from the norm may be either positive or negative, it correlates to the same meaning regardless. The authors propose the deviation marks the time at which the material begins to change its phase somewhere along the channel pathway. The direction of the slope after the deviation tells the analyst if the material's phase transition corresponds to solidifying or melting. Since the normalized energy begins to decrease after this deviation, the material is solidifying.

In conjunction with energy, the first raw moment for each channel is also recorded for all studies. The remaining moments are not included in the analysis of these studies because they are not necessary for quantifying the internal temperature.

During the quasi-isothermal tests, the data was collected during times of equilibrium and used to create the centroidal speed of sound relationships with temperature defined in Equation 5.21, Equation 5.22, and Equation 5.24. Using the centroidal speed of sound to quantify the internal temperature of our porous material in this manner returns an approximation for the average temperature of the studied material along the acoustic pathway prescribed by the pair of transmit and receive transducers. For the experimentation conducted within this chapter, the internal temperature of our studied material will not be near thermal equilibrium as it was when collecting the data used to define the relationships between centroidal speed of sound and temperature. The continuous ultrasonic testing will capture waveforms for the machinist wax as the material varies in internal temperature all along the channel lines. Equation 5.22 and Equation 5.24 are used in Section 6.2 and Section 6.3 to quantify the internal temperature of the machinist wax as the material continuously cools, however, the temperature values returned using these equations will give an average, or effective, temperature for the material across the acoustic pathway the signal traverses. The term “effective temperature” used in the following discussions is referring to the average temperature of the material across the channel lines that is calculated using Equation 5.22 and Equation 5.24. The effective temperature is then used in conjunction with Equation 6.1 to give an approximation of the temperature profile along the channel lines. The inclusion of the external boundary conditions represented by external surface thermocouples creates the

opportunity to represent the internal temperature beyond just a singular effective temperature.

$$T(s) = \frac{1}{2}[2\chi[-e^{-\left(\frac{d\, l_w}{2}\right)^2} + e^{-(d\, s)^2}] + T_{wr} - \frac{2\, s\, T_{wr}}{l_w} + T_{wt} + \frac{2s\, T_{wt}}{l_w}] \qquad (6.1)$$

where $T(s)$ represents the temperature profile for multiple points along the desired acoustic pathway, d represents an inverse delay constant, l_w represents the total distance travelled by the signal, and T_{wt} and T_{wr} represent the thermal boundary conditions set by the external surface thermocouples located at the transmit and receive transducers respectively. The χ variable controls the height of the temperature profile peak and is continuously iterated over to create a family of possible temperature profiles while s identifies the location along the acoustic pathway where $s = 0$ corresponds to the center of the respective pathway.

Equation 6.1 is used in conjunction with the calculated effective temperature to create an approximation for the expected temperature profile along the acoustic pathways. Equation 6.1 is better understood in two separate parts. The first part is controlled by χ, and gives the curvature of the temperature profile. The second part represents the boundary condition considerations. Figure 6.*3* gives an example of four iterations of χ for a fabricated scenario not based on data collected during actual experimentation.

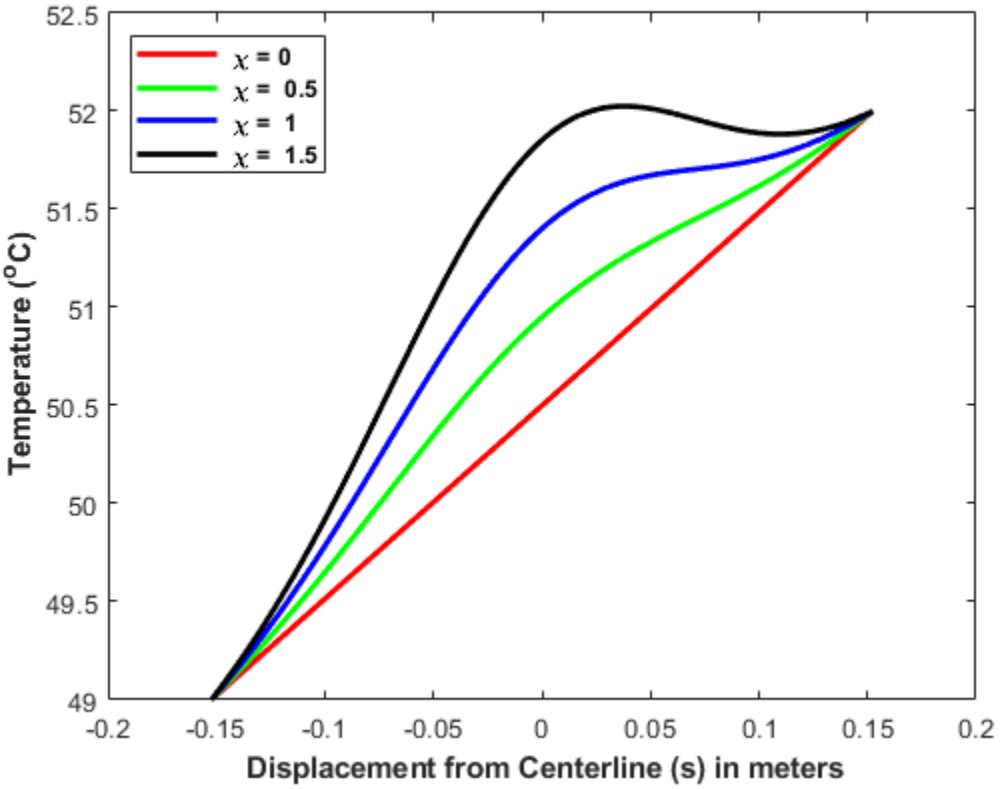

Figure 6.3. Temperature profile iterations of chi variable across a 305 mm (12”) hypothetical acoustic pathway

For this example, the temperature at the receiving transducer is 49℃ and the temperature at the transmitting transducer is 52℃. Without the consideration of Equation 6.1 which relies on χ, the linear relationship is observed for the approximated temperature profile when $\chi = 0$. With each iteration of higher values of χ, the curvature of the temperature profile in heightened and a family of functions is created. The calculated effective temperature is then used to determine which temperature profile approximation from the family of functions is the best fit. The inclusion of Equation 6.1 allows the analyst to expand their understanding of the internal temperature from a single effective temperature point to a two-dimensional representation of the temperature along that channel line. The following section will explain in detail the results of quantifying

the internal temperature of an inaccessible, porous medium entirely from ultrasound using the centroidal speed of sound relationship defined in Section 5.3.

Each study for applicability utilizes the same rectangular containment vessel made of sixteen-gauge sheet metal, specifically carbon steel. The exact dimensions of this containment vessel are 256 mm x 156mm x 154mm (10.06” x 6.13” x 6.00”) with a wall thickness of 2 mm (0.06”). A single plane of transducers is positioned 51 mm (2”) down from the top of the containment vessel. The transducers are aligned down the length of the container to collect data across the 156 mm (6.13”) span. The studies will attempt to quantify the temperatures within a two-dimensional rectangular plane representing a horizontal slice of the medium at a depth of 51 mm (2”) using ultrasound. A total of four channels are used during testing. Each channel uses through-transmission to collect the a-scan data. This equates to a total of eight transducers in use. Preamplifiers are used for all receiving transducers set to the maximum setting of 50 dB. Each a-scan is collected at set gain values of 0 dB, 10 dB, and 20 dB. A top-down diagram of the transducer channel and internal thermocouple layout is depicted in Figure 6.4.

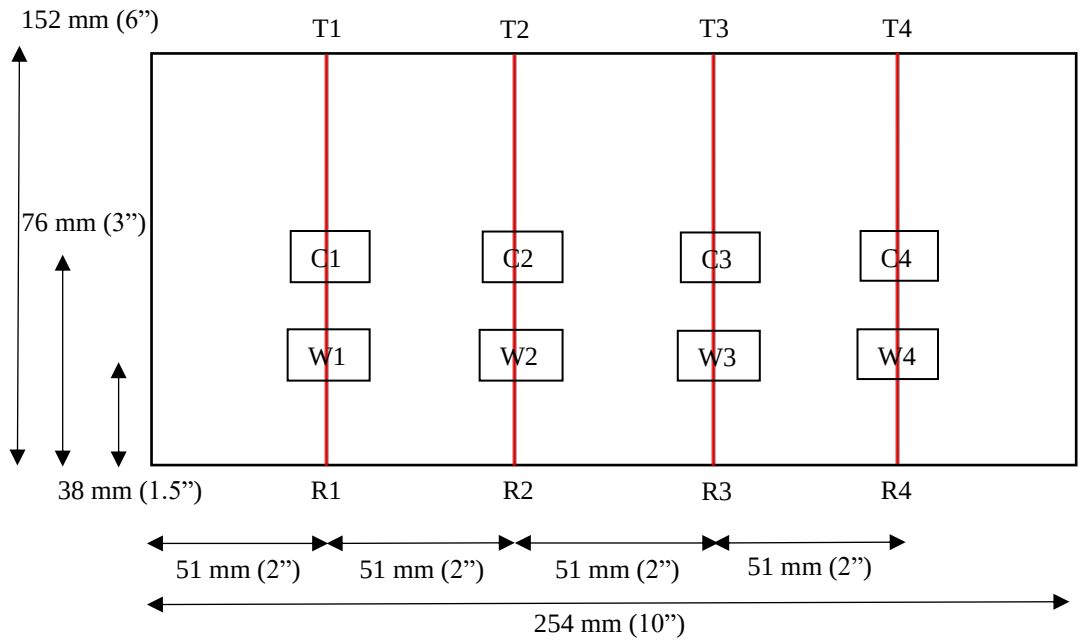

Figure 6.4. Top-down view of rectangular plane geometry including transducer channel and internal thermocouple layout

The internal thermocouples represented by C1 – C4 are aligned directly through the center of the long axis. A single additional row of internal thermocouples represented by W1 – W4 are offset from the wall of receiving transducers by 1.5”. These eight thermocouples which are internal to the system shall not be used to calculate the internal temperature of the material, they are only used for validation. There are an additional eight thermocouples which are external to the system. These external thermocouples are positioned directly below each transducer and read the temperature of the container wall surface at those positions. For this system, two aluminum heater blocks are used to bring the machinist wax to its molten state. The larger of these heater blocks has dimensions 102 mm x 102 mm x 13 mm (4.0” x 4.0” x 0.5”) while the smaller has dimensions 76 mm x 102 mm x 13 mm (3.0” x 4.0” x 0.5”). Each heater contains a thermocouple and is positioned within the system as shown in Figure 6.5.

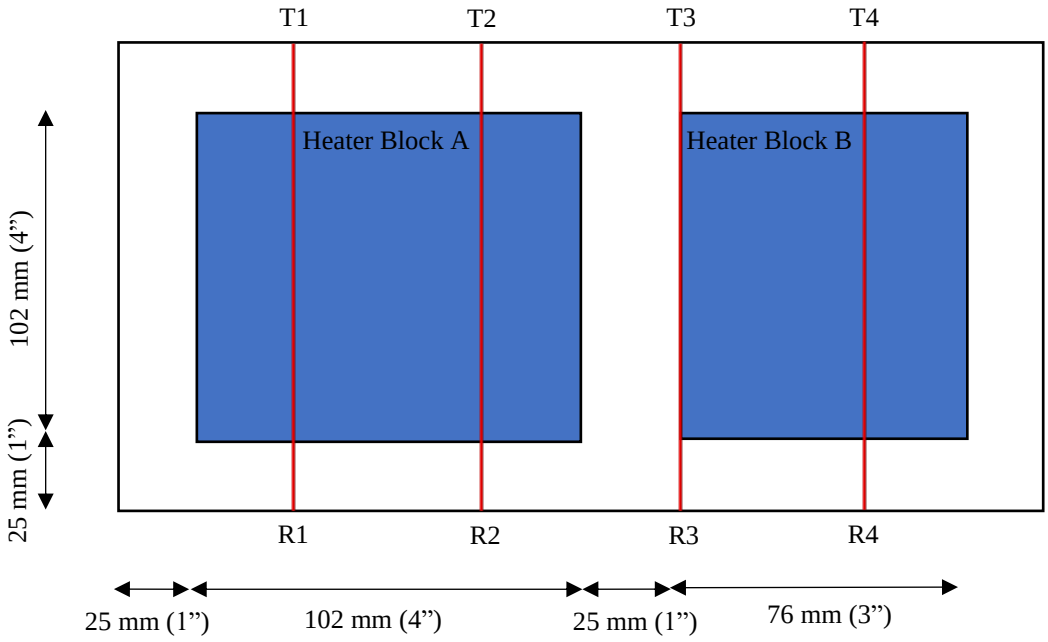

Figure 6.5. Top-down view of internal heating layout of testing apparatus

The larger of the heater block assemblies shall be referred to as “Heater Block A” while the smaller shall be “Heater Block B” for the remainder of this thesis. By using differently sized heater block assemblies, we are able to simulate both thermally uniform and nonuniform heating and cooling scenarios for the machinist wax. The final testing apparatus is depicted in Figure 6.6 and Figure 6.7.

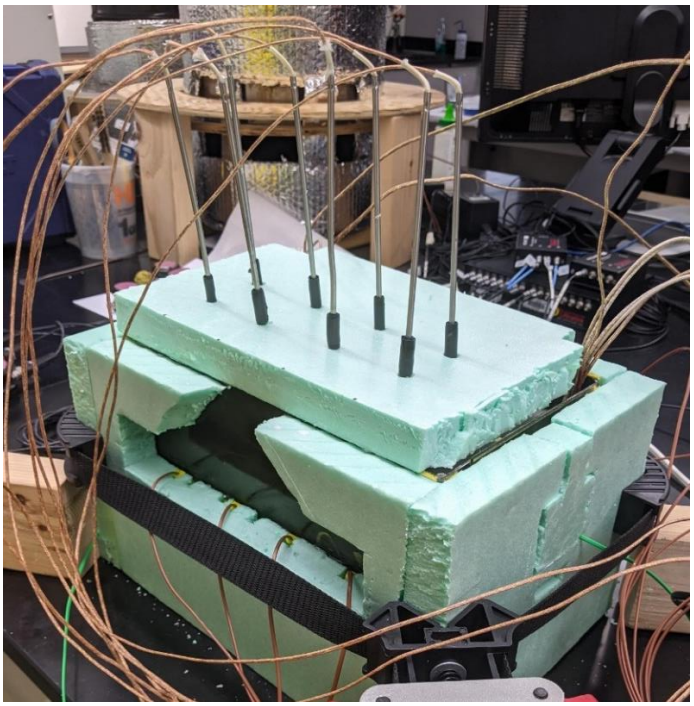

Figure 6.6. Overview – Rectangular setup

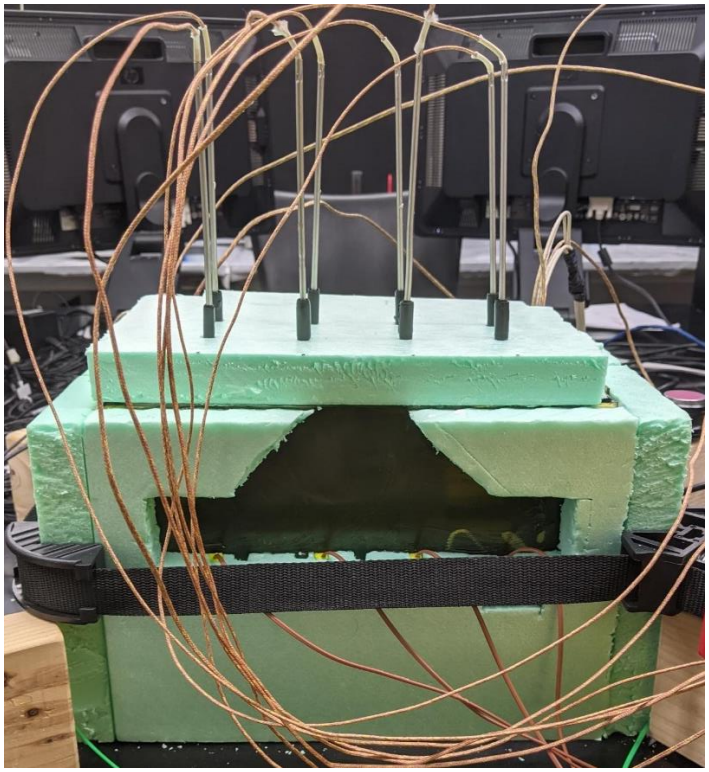

Figure 6.7. Front view – Rectangular setup

6.2 Acoustic Quantification for Porous Machinist Wax during Uniform Cooling

The first study utilizing this testing apparatus attempted to calculate the internal temperature of the machinist wax without accessing the medium as the machinist wax uniformly cooled. Simulating this case within the testing apparatus involved bringing both heater block assemblies to 110℃ (230℉). The heaters held this temperature for greater than twenty-four hours to ensure the machinist wax was completely molten prior to testing. Data collection began as soon as the heater block assemblies were shut off simultaneously. This first study collects data during the uniform cooling of the machinist wax from a molten state until the signal is lost on all channels. Once the material has cooled sufficiently, the machinist wax contracts itself from the sides of the containment vessel and the acoustic transmissions are no longer obtainable. After sound propagation is not no longer possible, the test is effectively terminated. The time at which this event occurs is observable from the b-scans plotted for each channel at a set gain of 10 dB seen in Figure 6.8.

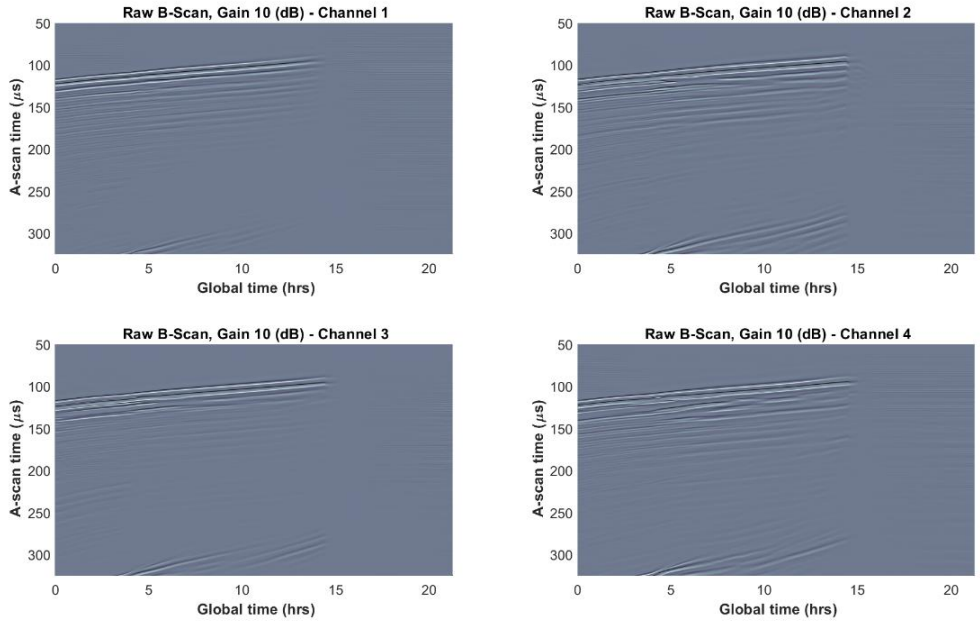

Figure 6.8. B-scan data for all four channels during uniform cooling

Based on the b-scan data obtained, the acoustic signal's ability to traverse through the machinist wax is inhibited prior to fifteen hours into testing. Therefore, the only data that should be considered for this test will encompass testing times prior to fifteen hours. For the purpose of the uniform cooling study, fourteen hours of testing time is considered during analysis. The b-scan also qualitatively indicates that the material under study is cooling. The onset to the time of flight is observed to decrease as the test is carried out. A decreasing time of flight indicates our porous material is transitioning from a molten to a solid state, or in this case, cooling. In order to observe the cooling effect of this material quantitatively, the data acquired from the thermocouples is represented in Figure 6.9. The entirety of the thermocouple data across all eighteen channels collected during the uniform cooling study is depicted.

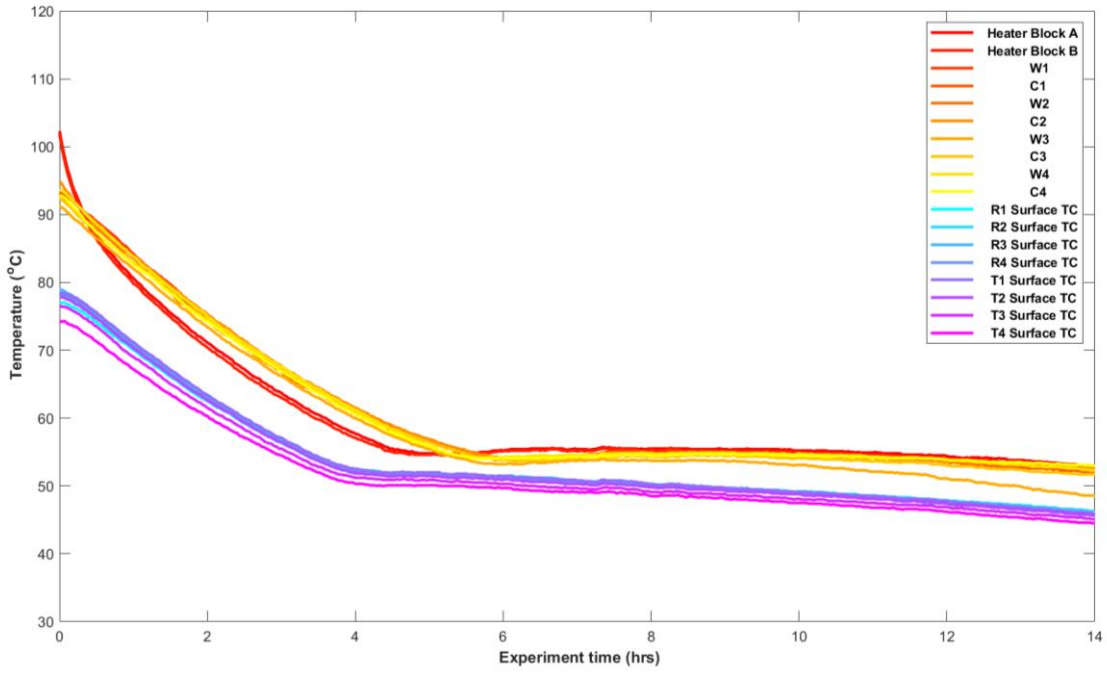

Figure 6.9. All thermocouple data for uniform cooling

From this plot, it is beneficial to observe how the bulk temperatures react with respect to the natural cooling process taking place during experimentation. Notice for each bulk temperature profile, the trend begins with a steep descent before stabilization around some temperature. Recalling the analysis of this material found in Chapter Three, this behavior is as expected. The molten data should represent some constant, linear change with temperature as cooling begins. At the transition temperature, the material attempts to undergo a change of state. Based on the DSC analysis performed on this material in Chapter Three, this material changes phase state suddenly between one temperature and the next. Behavior such as this is unlike the gradual phase change seen in the homogeneous candle wax. Due to this characteristic, the machinist wax requires additional time to complete the phase transformation and holds isothermally at the transition temperature. This behavior is reflected in Figure 6.9 when the material's

temperature becomes isothermal based on the thermocouple data. Displaying all the thermocouple data within a single plot is useful for observing bulk responses but proves to be cumbersome. Taking a closer look at only the thermocouples used in validation provides better insight to what the ultrasound data should reflect. Figure 6.10 and Figure 6.11 represent the internal thermocouples 1.5” offset the receiver wall and along the center of the containment vessel, respectively.

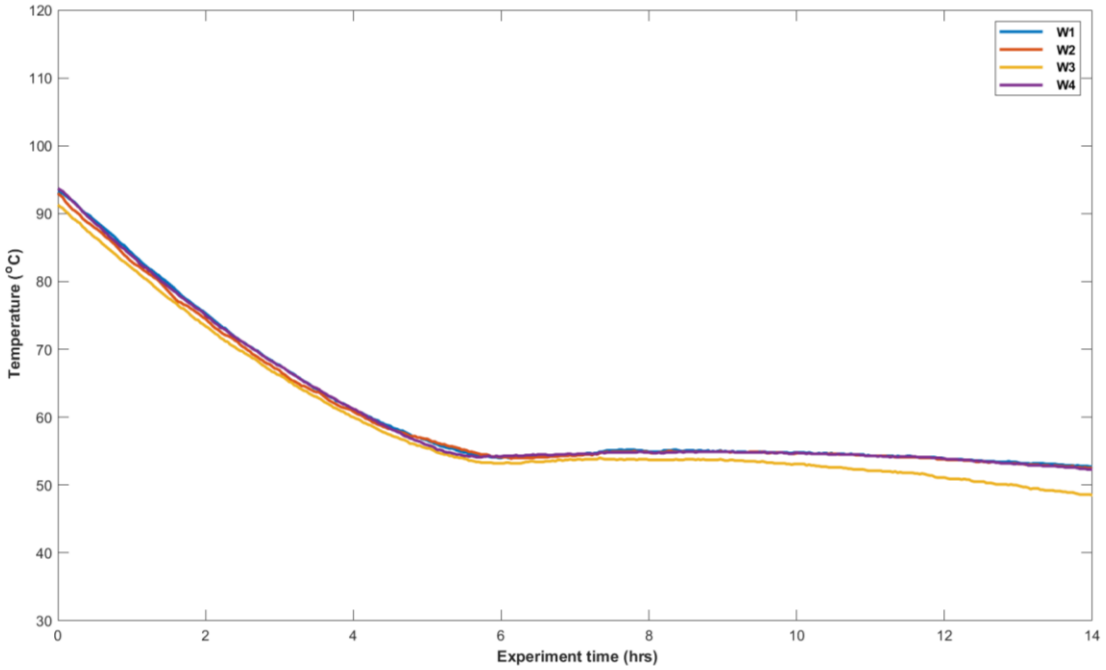

Figure 6.10. Internal wall offset thermocouples for uniform cooling

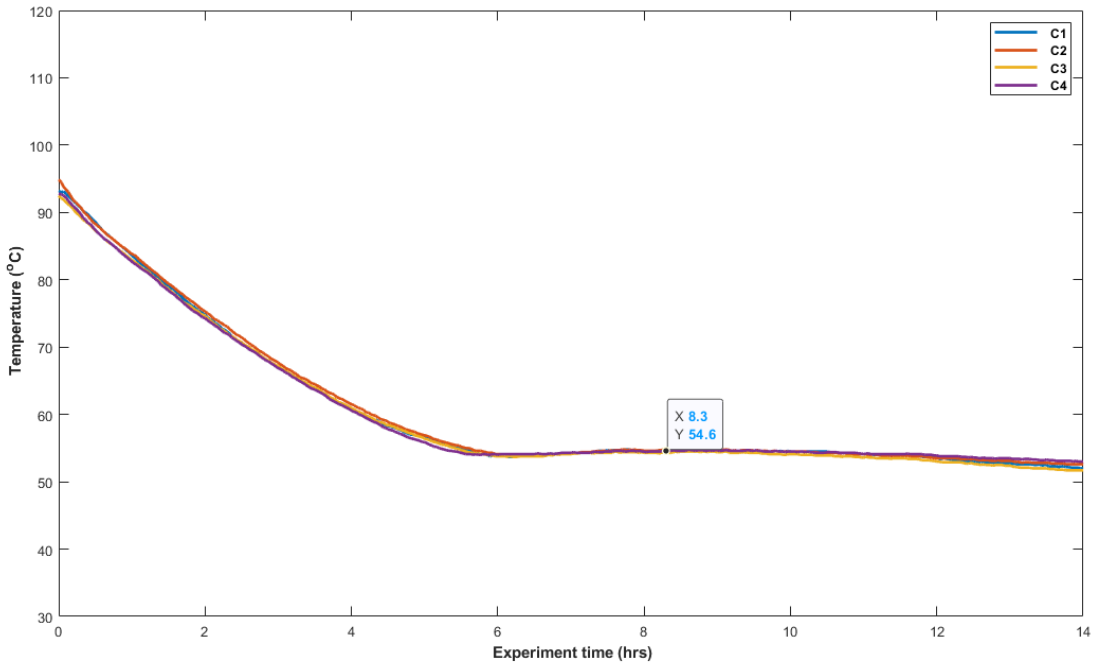

Figure 6.11. Internal thermocouples along centerline for uniform cooling

According to the internal thermocouples used in validation, the temperature of each channel should remain very similar throughout the duration of the test. A single outlier to this statement can be examined along the third channel offset to the wall of receiving transducers. This is the only deviation in relative temperature from one channel to the next, therefore, channel three should be slightly cooler on average than the other channels later in time. Note that the centroidal speed of sound is expected to return an effective temperature along the entire channel line. The difference should be less drastic than what is depicted in Figure 6.10 since Figure 6.11 shows channel three is in sync with all other channels. Additionally, the steady decline of temperature should experience stabilization at 54.6℃ just prior to six hours into testing based on both figures. In conjunction with highlighting the internal thermocouples, it can also be useful to single out the external thermocouples on a separate plot for drawing expectations based on the

boundary conditions. The surface thermocouples are represented exclusively in Figure 6.12 and are labeled based on the transducer boundary condition they represent.

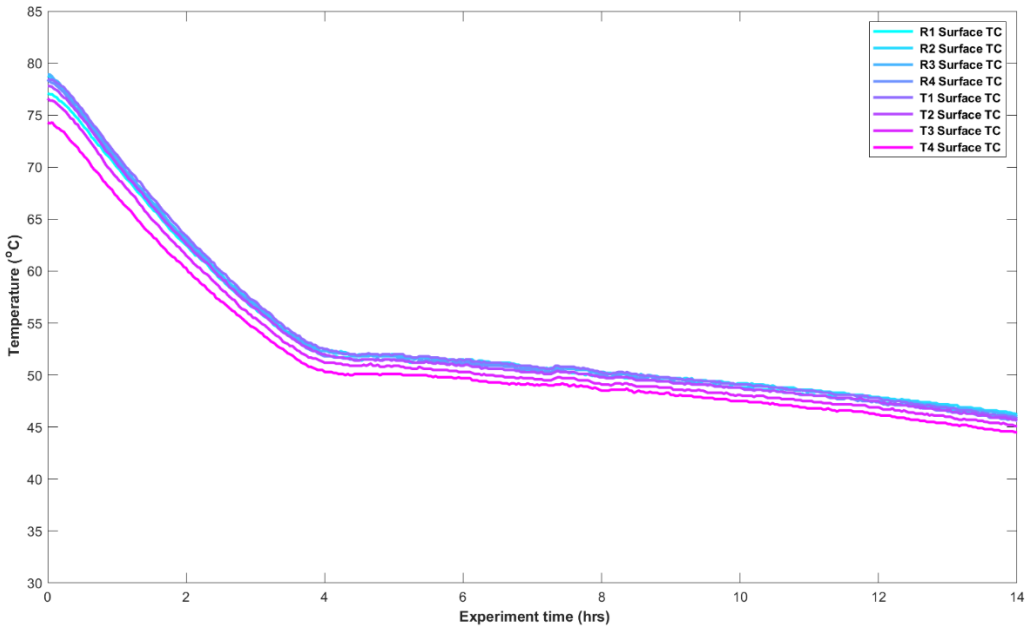

Figure 6.12. Surface thermocouples for uniform cooling

The surface temperature plot gives the analyst information regarding the beginning of solidification at the boundary. As expected, these thermocouples are the first ones to reach a stable temperature before the slow decay begins. The temperature stops its rapid descent at the boundary of the container near four hours into testing. At this time, the temperature stabilizes because the medium at these locations has arrived at the transition temperature and started to solidify. For the energy analysis to be validated in this study, it is expected to see a deviation in energy near four hours along all channels. The normalized energy for each channel is shown in Figure 6.13.

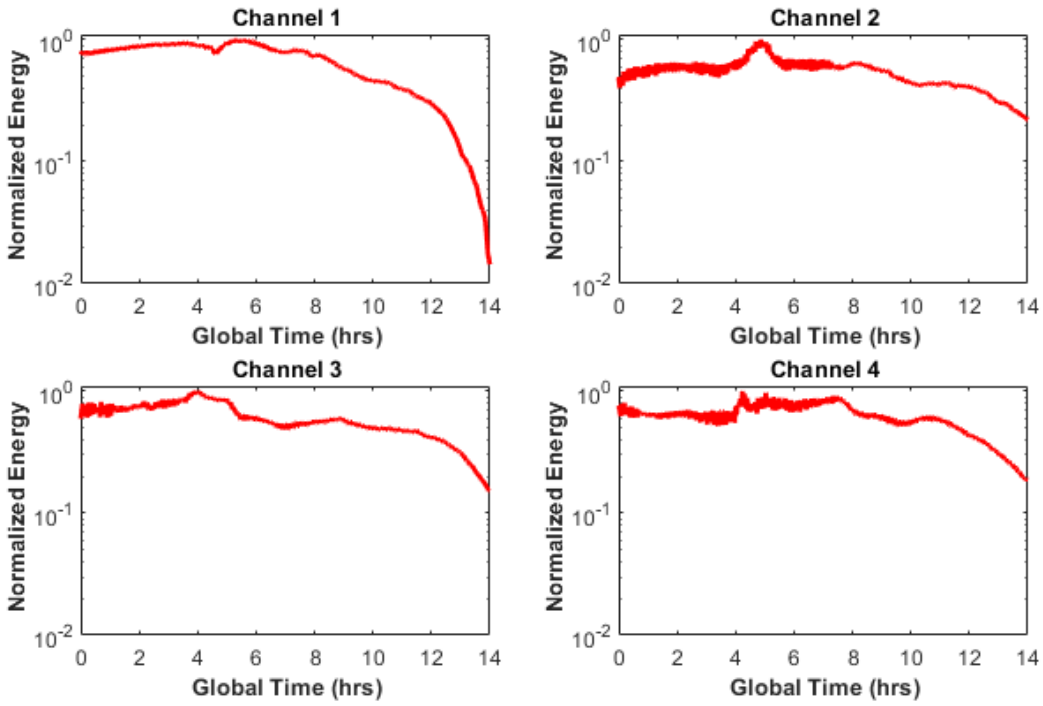

Figure 6.13. Normalized energy for all channels during uniform cooling

The general trend revealed by the plots for normalized energy identifies energy as maintaining some set higher value for the majority of the test. There exist two deviations from this trend which are expressed in each channel. A sudden rise or fall occurs in each plot that is followed by a negative slope which grows increasingly negative with time. For all channels, the onset of the sudden rise or fall occurs near the fourth hour. This first deviation correlates to the time during testing which the material initially begins to harden. This hardening refers to the beginning of phase transition for the material along the corresponding acoustic pathway as implied from Figure 6.12. Notice the time at which the external boundary conditions of the material initially stabilize from their previous decline. The time of both events are almost an exact match. It is therefore assumed by the authors that after four hours of testing, the material reached its transition

temperature around the perimeter of the containment vessel and energy was capable of recording the time of this event. Over the duration of testing, the majority of the material evaluated along each channel also reached this transition temperature and began the solidification process. This process is witnessable by observing the second aforementioned deviation. The normalized energy begins to decrease at an increasing rate corresponding to more of the material reaching this transition temperature. While the normalized energy is unable to quantify the internal temperature of the material, it is able to identify key occurrences during the material's transition from one state of matter to the next. This utility found within the normalized energy is perfect for applications which do not require a quantitative representation of the enclosed material's behavior. If the objective of material inspection is to identify the phase transition of the material, then using the proposed inspection methodology of solving for the normalized energy can provide a solution for the machinist wax of irregular porosity. The analysis of signal energy accomplishes this without needing to access the contained medium under question. However, going beyond the qualitative understanding of phase and quantifying the internal temperature requires the use of the raw first moments. Each raw first moment is recorded as the experiment transpired for all channels and plotted in Figure 6.14.

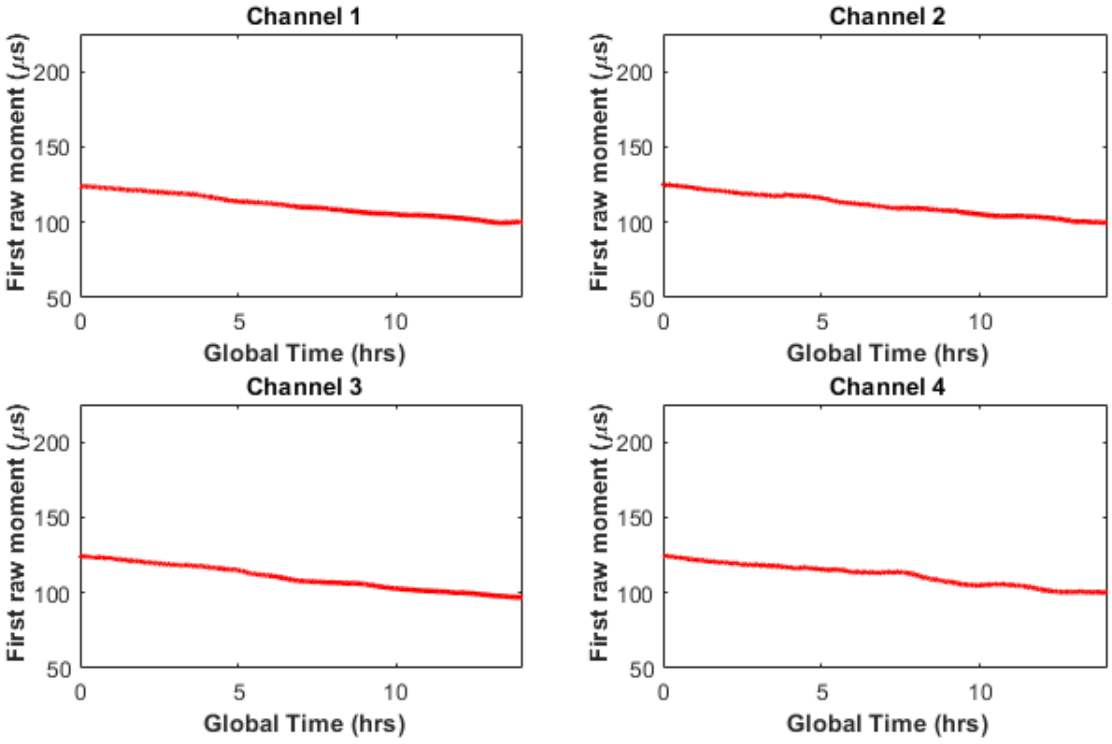

Figure 6.14. First raw moment for all channels during uniform cooling

The first raw moments depicted above show seemingly linear trends. The results shown in Figure 6.14 are as expected because the internal thermocouple data showed the material dropping to the transition temperature and holding near that value throughout experimentation. Recalling Equation 5.15 from Chapter Five, molten data for this material experiences a linear relationship between the CSoS and the internal temperature while cooling until it reaches 54.6℃. At this transition temperature, the same relationship becomes nonlinear, encompassing smaller changes in temperature for greater alterations of the centroid. The observations made using Figure 6.14 show the first raw moments of each channel contain a linearly decreasing trend throughout testing and this trend is as expected. Thermocouple data shows internal temperature seemingly holding isothermally after reaching the transition temperature, however this isn't quite the case. In reality the

internal temperature is changing, it is only doing so at a much slower rate than before the transition temperature. So, witnessing the first raw moment behave continuously is expected. It is this continuous behavior that we desired to capture from the very beginning. The constraint defined in Equation 5.16 characterizes this material's relationship between speed of sound based on the centroid and temperature to be continuous. Before 54.6℃, a linear decrease in the moment correlates to a linear decrease in temperature, but after 54.6℃ that correlation changes. This behavior is equally reflected by the information received from the thermocouples used in validation. This being the case, the first raw moment of each channel should decrease linearly with time. This is exactly the behavior that is represented within Figure 6.14 and serves as a pre-validation step before quantifying the internal temperature of the material. Once the first raw moment for all channels was determined to be reflective of information provided by the internal thermocouples, that data was converted over to the CSoS. The effective internal temperature was then solved for using Equation 5.22 or Equation 5.24. The effective internal temperature of the machinist wax along all channels is quantified for the duration of the test and represented in Figure 6.15 using only ultrasound.

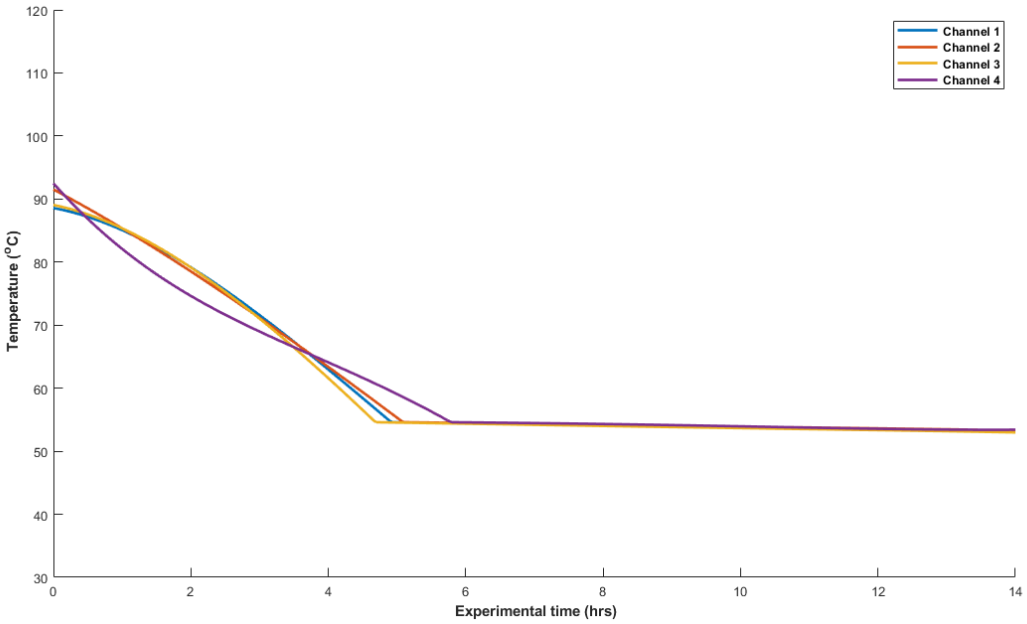

Figure 6.15. Effective internal temperature of machinist wax for all channels during uniform cooling

Recall the internal temperature of the machinist wax based on thermocouple data from Figure 6.10 and Figure 6.11. The results portrayed in Figure 6.15, using data collected entirely from ultrasound, reflect a near perfect combination of both figures. The greatest margin of error between thermocouple data and ultrasound occurs two hours into testing. This error resembles a maximum of a 5℃ difference between any of the channels. Other than this minor difference, the similarities are abundant. The beginning of the test shows all channels closely packed around 90℃ for either interpretation. The first, second, and third channels arrive at the transition temperature closer to five hours into testing using ultrasound. These same channels arrive closer to six hours based on the thermocouple data. However, the temperature difference between interpretations at the fifth hour for these channels is still less than 5℃. Channel four arrived at the transition temperature near identical in time for the thermocouple data and the ultrasonic

interpretations. Additionally, it was determined previously that all channels should be represented closely together after arriving at the transition temperature. The only exception was channel three, who should be slightly cooler near the end of the test. While the difference is small, channel three does in fact possess a deviation from the other channels near the end of the test and is cooler on average based on the ultrasound data. All of these similarities between interpretations are quite impressive, but they pale in comparison to the final discovery. The transition temperature determined during the quasi-isothermal energy analysis in Chapter Four is 54.6℃. This is the same temperature value where all channels eventually stabilize near the sixth hour of testing based on both thermocouple and ultrasonic data. The thermocouple data only relays temperature to the tenth of a degree Celsius. Not only did every channel equilibrate at this value to this exact tenth of a degree, but this in turn implies that a more accurate approximation for the transition temperature is 54.6℃. This suggests the energy analysis from Chapter Five is capable of determining the temperature of solidification for the porous machinist wax with a greater accuracy than that of the DSC analysis in Chapter Three which reported this material's solidification temperature to be 45℃. The transition temperature was calculated from energy by simply identifying the first solid and last molten data points and selecting a temperature between this temperature range. There is now a case to be made that energy can return the transition temperature of a material with a rivaled accuracy to that of DSC analysis.

Equation 6.1 is combined with a constraint determined from repeated testing with the containment vessel to allow for additional representations of the ultrasound data. It is shown in Figure 6.16 and Figure 6.17 that the approximated temperature profiles are

constrained to a maximum temperature value. This constraint is based upon numerous tests using the described testing apparatus and machinist wax. Repeated testing indicates this material's peak temperature for the approximated profile should be 15℃ higher than the temperature at the boundaries after the profile assumes the temperature is above the melting temperature. Any time during testing can be used to obtain the temperature profile along the distance of a channel line. Equation 6.1 is repeatedly iterated for differing values of χ until the profile approximation best fits the effective temperatures found for each channel line. For the purposes of this thesis, the temperature profiles along each channel will be examined for four hours into testing in Figure 6.16 and for twelve hours into testing in Figure 6.17. The flat peak temperatures of these approximated profiles are thought of as melt fronts. The length of the melt front is observed to decline further into testing as expected for the material continuously cooling.

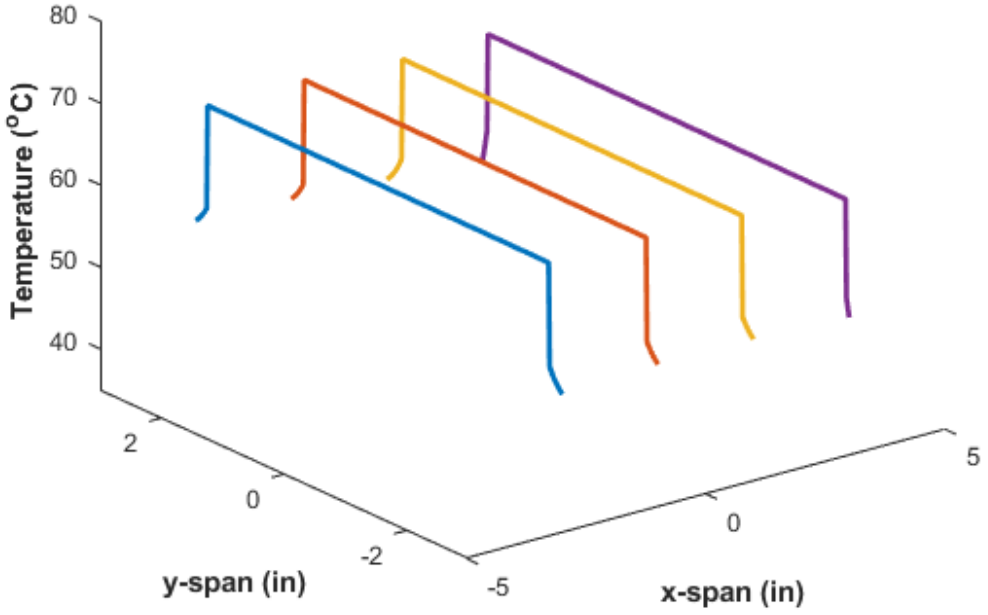

Figure 6.16. Temperature profile along each channel four hours into uniform cooling

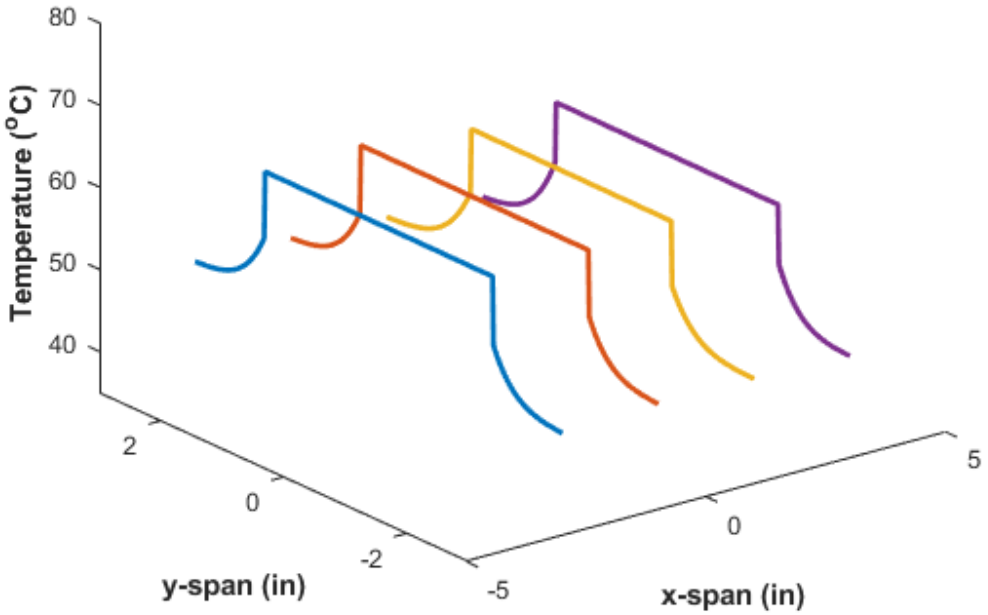

Figure 6.17. Temperature profile along each channel twelve hours into uniform cooling

At four hours into testing, the energy analysis implies this is the first instance which all channels have begun the solidification process. Figure 6.16 shows the first instance at which the temperature profile is no longer a flat line of molten temperatures. Temperatures near the furthest edges of the container are quantified to be at or below the transition temperature. This corresponds to the material solidifying around the edges first. Intuitively this behavior is expected. As the medium cools, it is expected to cool from the outside inward toward the heat sources located at the medium's core. Transitioning forward in time to the twelfth hour of testing, this melt front is seen to regress inward. Additionally, the overall maximum temperature experienced in each channel has also decreased. At the twelfth hour of testing, the third channel should be the coolest, meaning that it should also have the shortest melt front. This is visibly the case displayed in Figure 6.17. These behaviors are validated across all thermocouple data and the previous effective temperature data gathered from ultrasound.

6.3 Acoustic Quantification for Porous Machinist Wax during Nonuniform Cooling

The CSoS has now been shown to be applicable for quantifying the internal temperature and phase transition of an inaccessible porous machinist wax as it experiences some thermally uniform change. The experimental procedure from this study can be slightly altered in order to better observe the restraints of the CSoS. Recall the impact pressure has on centroidal shifting observed from the study conducted previously in Section 5.4. The impact of pressure is amplified for materials which are not in thermal equilibrium. The uniform cooling study experienced significant difficulty when applying the appropriate pressure to each transducer. Although this cooling process occurred uniformly, this is very different than collecting data which is in thermal equilibrium. It is observed from the thermocouple data that the internal temperature along each channel could vary by several degrees Celsius at any given location. The next study shall attempt to observe the internal temperature of the machinist wax as the material experiences nonuniform cooling. This gives pressure an even greater impact on centroidal shifting. Without a testing apparatus that is setup with the intention of applying highly specific pressures to each transducer, the accuracy of the data is expected to decline. However, the centroid is still capable of quantifying temperature. Instead of building such a device, it will prove to be beneficial to observe the results of a test where pressure is only loosely monitored. Observing the results of a nonuniform cooling test which has improper transducer pressure will assist in the affirmation of our new methodology as well. It shall be seen that general thermal behavior by channel is still observable. The accuracy of the readings will simply decline.

Nonuniform cooling of the material shall be simulated by bringing both heater block assemblies to 110℃ (230℉) and isothermally maintaining this heat for greater than twenty-four hours. This step effectively brings the material to a fully molten state just as before. Immediately preceding the start of data collection, Heater Block A is turned off completely and Heater Block B is turned down to 82℃ (180℉). Due to a limitation of the heater block assembly's controller box, turning down the temperature for Heater Block B effectively turns off this heating source. It will turn itself back on once the temperature of Heater Block B drops below the desired 82℃ (180℉). It will continue turning itself on an off as the temperature is below or above 82℃ (180℉), respectively. It is important to understand how this behavior is capable of effecting the normalized energy. It is expected that each channel will experience some degree of difficulty tracking the energy because of this. Note that this is a byproduct of the method used to simulate a nonuniformly cooling material. In an actual scenario, this effect would not likely be present. Also recall from discussions within Section 5.3, the first raw moment does not rely on information from the previous scan. The factors impacting energy will not necessarily directly influence the location of the centroid. The data analysis for the nonuniform cooling study was carried out in the same manner as the preceding study. The first step involved observing the b-scan data shown in Figure 6.18.

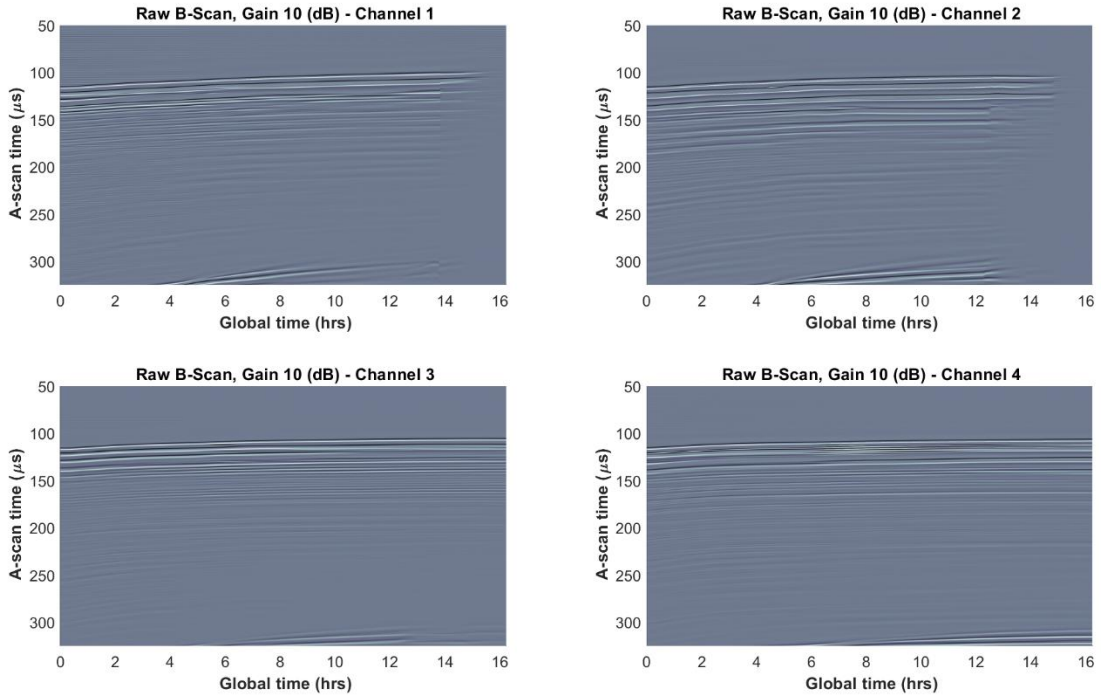

Figure 6.18. B-scan data for all channels during nonuniform cooling

The signal is lost on channels one and two around fifteen hours into testing, so data will only be analyzed for the first fourteen hours of the test. The fact that channels three and four maintained a signal throughout the entire duration of the test is as expected. These channels sit directly above Heater Block B which never dropped considerably below 82°C (180°F). Heater Block B produced enough heat along the channel lines of Channel Three and Channel Four to ensure the material did not cool to the point where it contracted off the sides of the container walls. Observing the thermocouple data in Figure 6.19 offers a quantitative understanding for how the test thermally operates. All thermocouple data is plotted for the nonuniform cooling of the porous machinist wax.

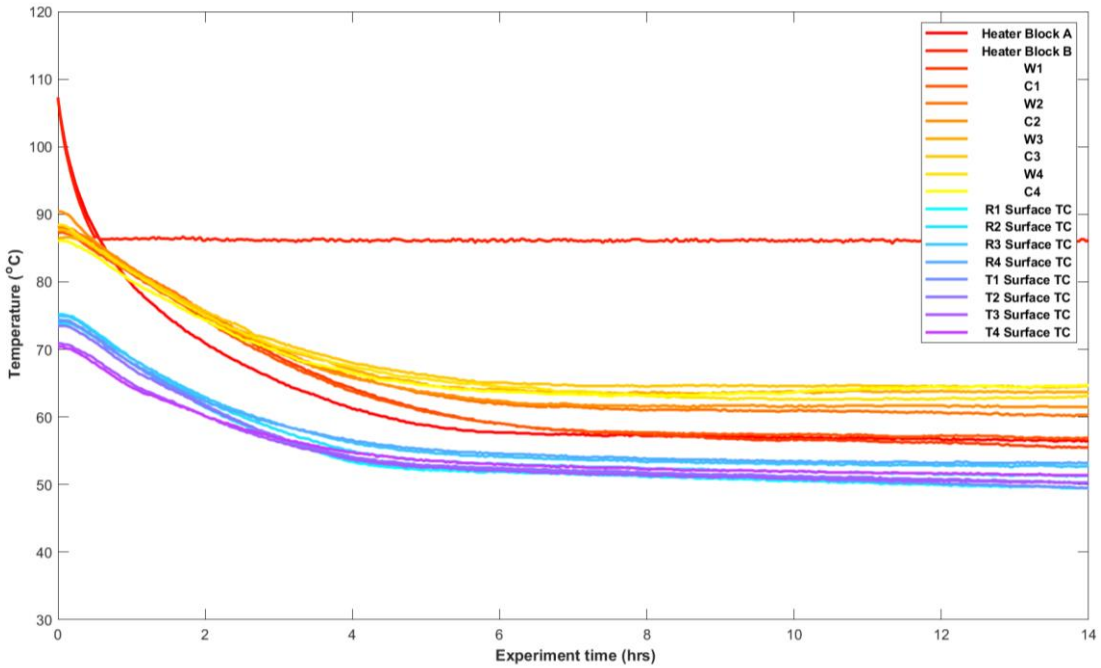

Figure 6.19. All thermocouple data for nonuniform cooling

The thermocouple data is spread across a large range of temperatures at any given time during testing. Due to the spread of data, the bulk temperature relationships are more difficult to define that in the previous study. Each channel line differs in temperature between surface, centerline, and wall offset temperature. The takeaway from Figure 6.19 is understanding the difficulty in deciding an expected effective temperature based on this data. The centroid is expected to experience equal difficultly. In order to make assumptions on the expected internal temperature values, the internal thermocouples are plotted separately similar to the previous study in Section 6.2. Figure 6.20 and Figure 6.21 plot the internal thermocouples from the receiver wall offset and along the centerline of the container, respectively.

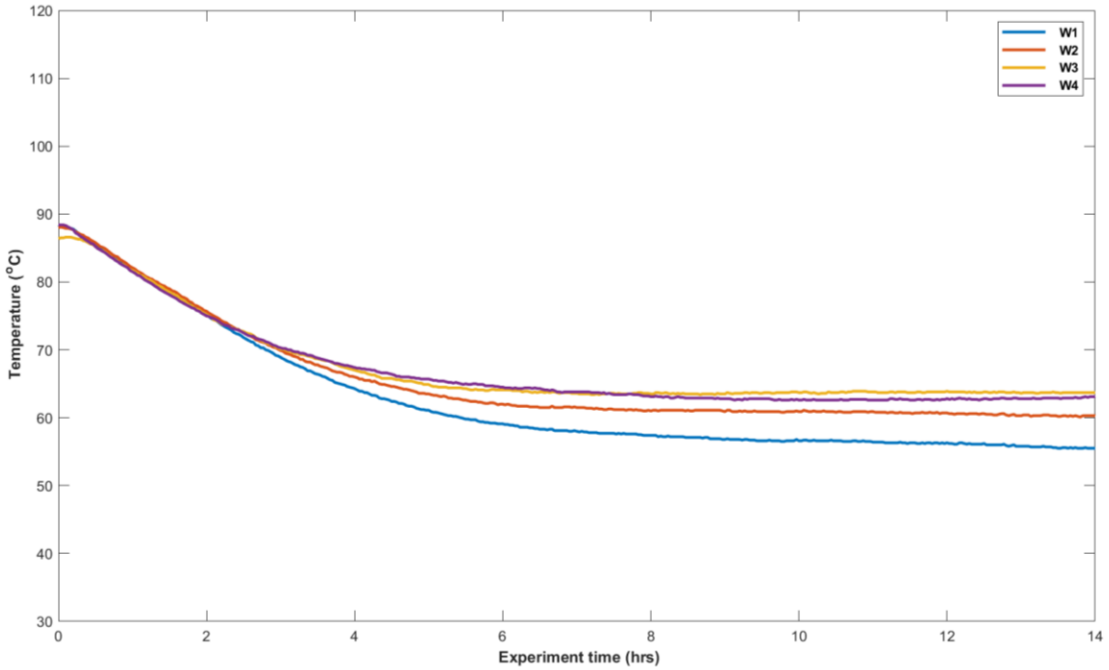

Figure 6.20. Internal wall offset thermocouples for nonuniform cooling

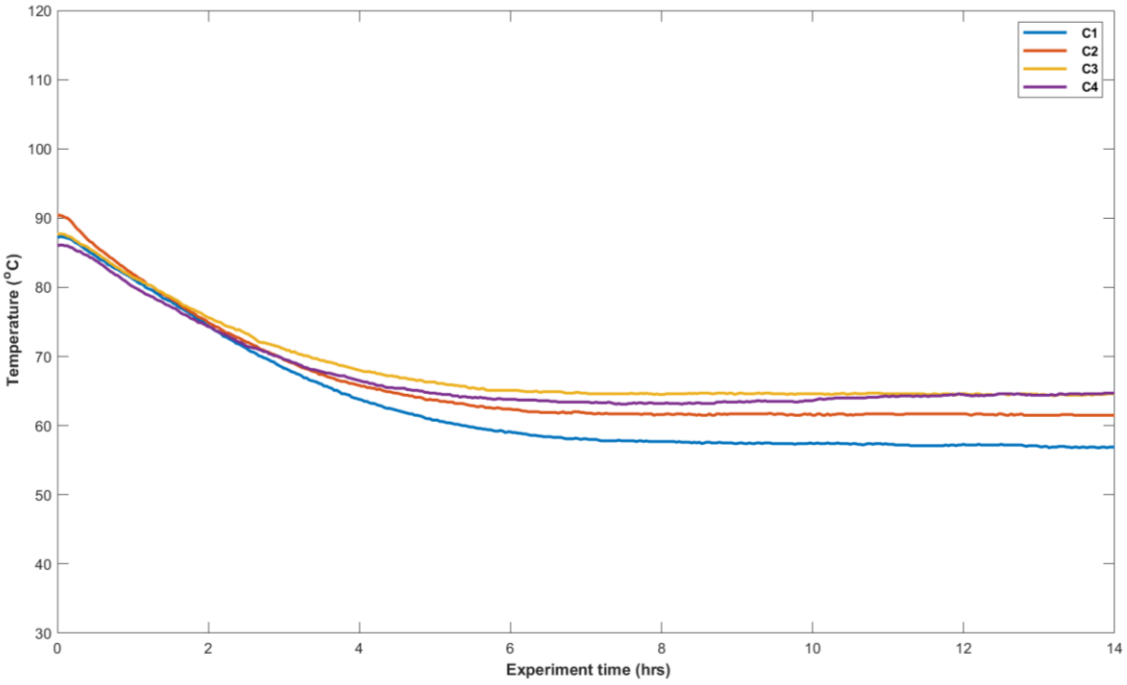

Figure 6.21. Internal thermocouples along centerline for nonuniform cooling

Representing the thermocouples internal to the desired medium on separate plots assists to identify what results are expected from ultrasound data. According to the data from Figure 6.20 and Figure 6.21, the first transducer channel is the coolest of the channels and reaches a stabilization temperature between the eighth and tenth hours. Note the stabilization temperatures in this case are not the material's temperatures of phase transition. Locations throughout the machinist wax reach stabilization based on the distance away from Heater Block B which continuously propagates heat into the system. Temperatures along the first channel line stabilized at the lowest average temperature slightly above the transition temperature as they are the furthest from the heat source. Locations along the second channel line experience the second lowest average temperature followed by channels three and four who share a seemingly equivalent average temperature. Due to the difficulty of quantifying an exact expected average temperature per channel across all time, qualitative trends of these figures are noted instead. If the ultrasonic data is capable of quantifying the internal temperature while this material experiences nonuniform cooling, there are several slope trends to be expected regardless of the attention paid to pressure. Initially, all ultrasonic channels should reflect a similar internal temperature. Later in experimentation, Channel One should be the coolest, followed by Channel Two, leaving Channel Three and Channel Four as the hottest channels and near equal in value. Since Heater Block B is continually introduces heat into the system, the internal temperature of the material decreases at a slower rate than in the uniform cooling study from Section 6.2. The negative slopes of effective internal temperature are expected to gradually stabilize above the materials transition temperature for all channels using the ultrasound data.

Before moving onto normalized energy, the external thermocouple data is displayed in Figure 6.22. As mentioned previously, the stabilization of temperatures no longer corresponds to the studied material experiencing phase transition due to the constant heating provided by Heater Block B. Figure 6.22 labels the surface thermocouples based on which transducer they are positioned beneath.

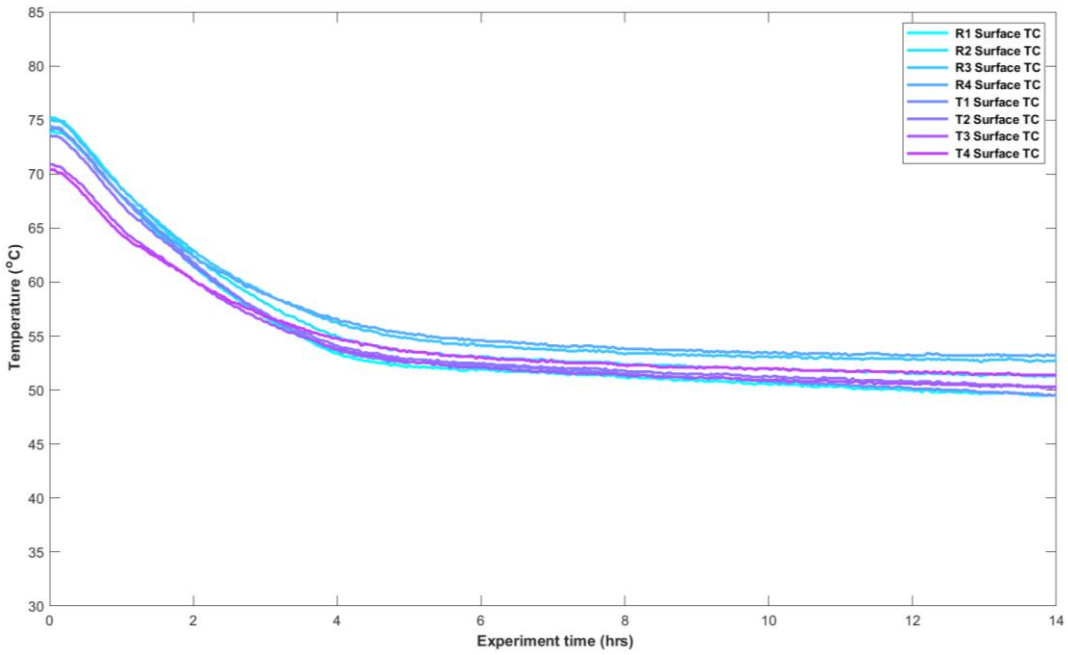

Figure 6.22. Surface thermocouples for nonuniform cooling

There exists a clear stabilization of temperature near four hours of testing. For Channel One and Channel Two, the temperature at the boundary drops below the transition temperature near the fourth hour, and energy is expected to identify this occurrence. Channel Three and Channel Four are thermally different on the transmit and receive sides of the container. The boundary temperatures on the transmit side of these channels stabilize and drop below the transition temperature near the fourth hour. However, the receive side of the container does not drop below the transition point until

closer to the sixth hour for these channels. Energy is expected to identify the beginning of solidification for these channels at a time between the fourth and sixth hour

After understanding how the ultrasonic data is expected to behave, the normalized energy is evaluated. The normalized energy for all channels is depicted in Figure 6.23 for the duration of the test.

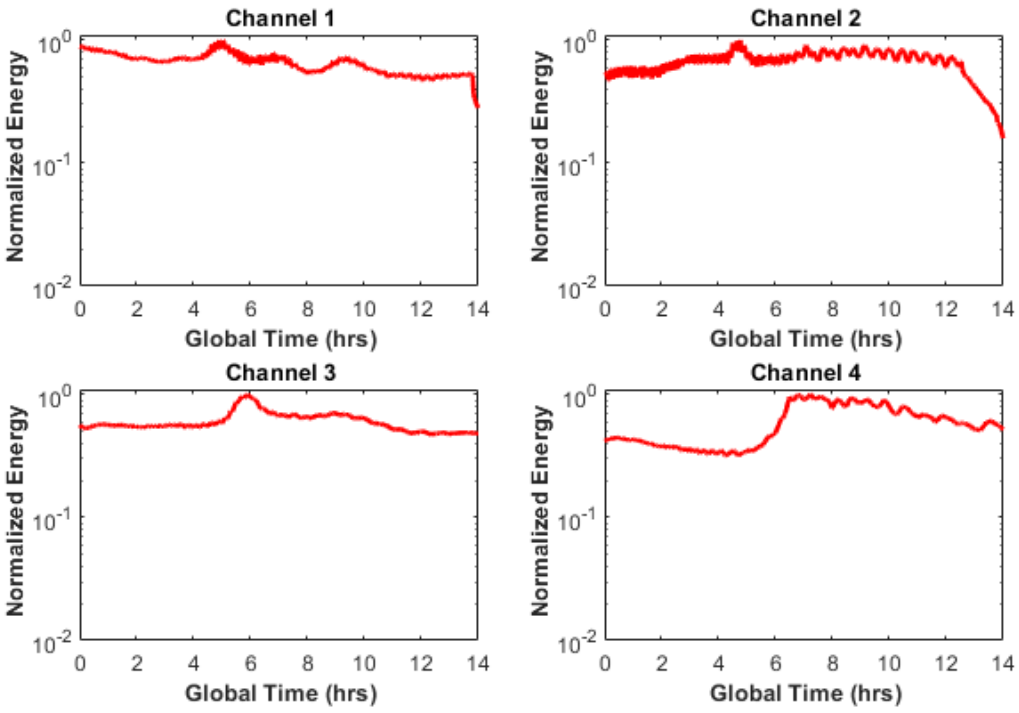

Figure 6.23. Normalized energy for all channels during nonuniform cooling

As hypothesized the normalized energy encountered several issues due to the method used for simulating a thermally nonuniform cooling distribution. However, despite the clear irregularities seen in the energy evaluation, one consistency remains. There remains an initial spike in energy across each channel. The onsets of these spikes still correlate to the beginning of solidification of the material along that channel just as observed in the previous study. Channel One and Channel Two experience this onset first

near the fourth hour in agreement with the discussed thermocouple data. Channel Three and Channel Four experience a similar onset near the fifth hour of testing which is in agreement with the previous hypothesis. The analysis on signal energy is still able to identify information regarding the studied material's phase state during nonuniform cool and constant heat generation. Therefore, the authors propose the use of an ultrasonic signal's energy for investigating changes of state on select materials experiencing thermally nonuniform alterations. Conclusive evidence is not currently available to verify if the proposed inspected method pertains to a particular class of material systems. However, the success of this method is noted for the studied material which possesses irregular porosity. The first raw moment for all channels experiencing nonuniform cooling is depicted in Figure 6.24 for the duration of the test.

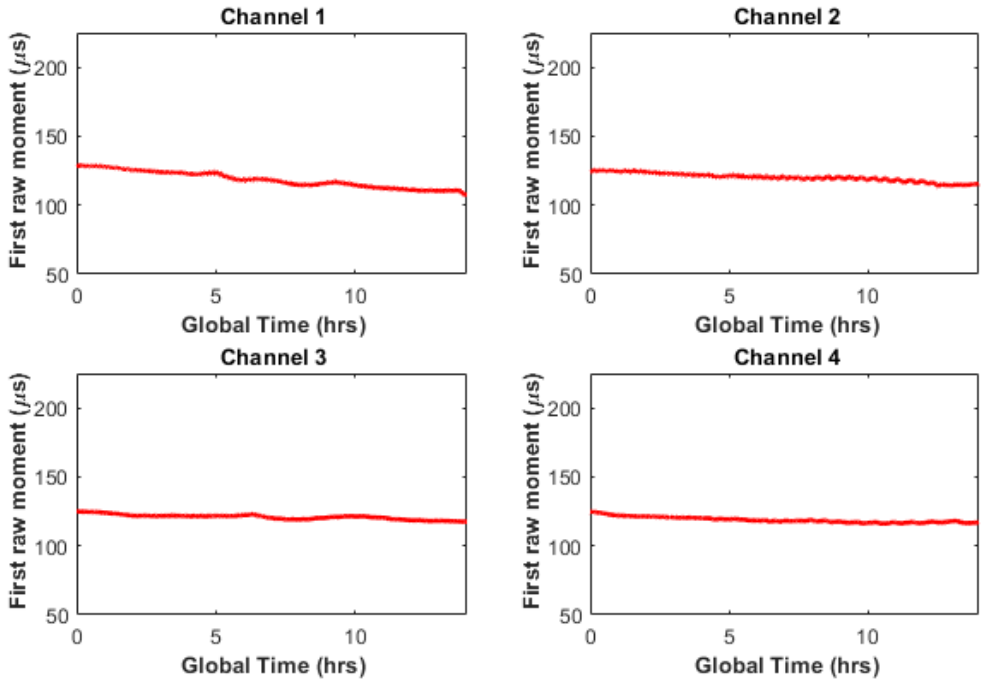

Figure 6.24. First raw moment for all channels during nonuniform cooling

The centroid is expected to decrease at a slower rate than in the previous test and stabilize out at some value based on the distance from Heater Block B. For this test, the thermocouple data showed each channel stabilizing above the transition temperature. In order to accomplish this, the centroid must also stabilize. This is a requirement of the centroid since the material is expected to be molten throughout the duration of testing. Equation 5.15 defines a linear relationship between the studied material's speed of sound based on the centroid and temperature while the material is above 54.6℃. Therefore, the first raw moment is expected to reflect similar slopes in comparison to the trendlines observed in the thermocouple data. Channel Two, Channel Three, and Channel Four all potentially reflect the desired outcome. Channel One continues a downward trend throughout testing which likely means it reaches the transition temperature at some point. This information is not in agreement with the thermocouple data. In order to fully investigate the outcome of the nonuniform cooling test, the first raw moments must be converted to the CSoS and the internal temperatures quantified along all channels. The results for the effective internal temperature along each channel for the machinist wax while experiencing a thermally nonuniform cooling are depicted in Figure 6.25.

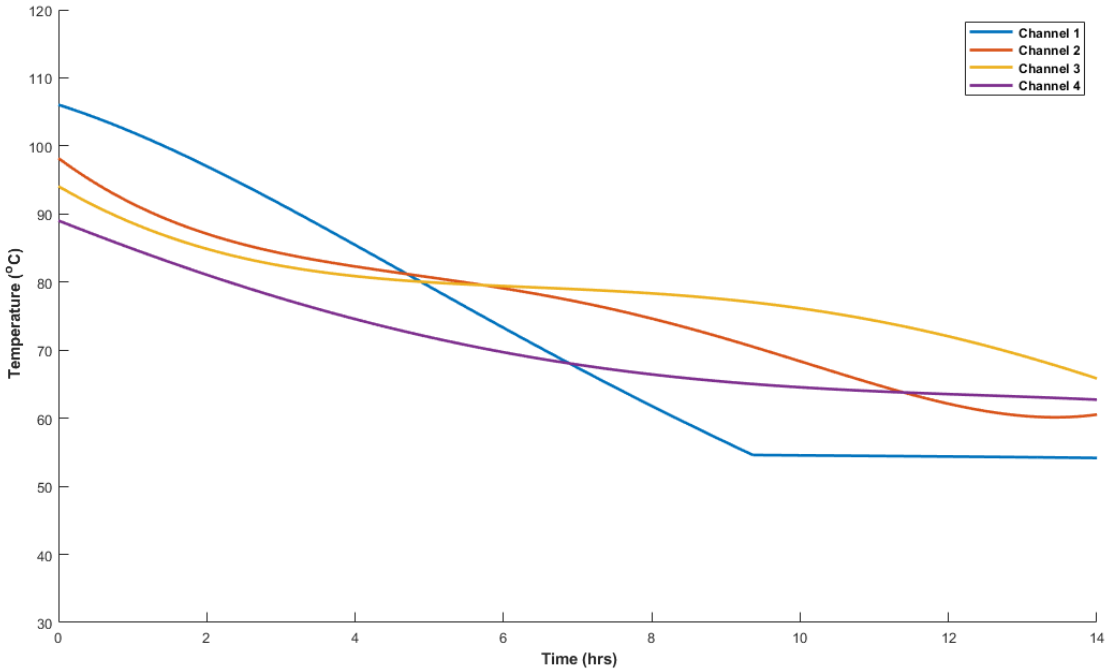

Figure 6.25. Effective internal temperature of machinist wax for all channel during nonuniform cooling

The results from the nonuniform cooling study are not as accurate as the results from the previous study as hypothesized. The sensitivity to the amount of pressure placed on each transducer is amplified when dealing with multiple thermal gradients. This test included a wide range of temperature values which the acoustic signal passed through before arriving on the other side for each scan. While this dataset reflects larger quantitative error, notice how qualitatively similar this interpretation is to the data in the thermocouple plots by observing the individual channels. This is especially the case toward the end of the data set. The stacking order from coolest to hottest channels corrects itself at this point. Only Channel One arrived at the transition temperature when it was not supposed to. All other channels stabilized at some value very close in agreement with the thermocouple data. To this point, the thermocouple data did not

reflect an average stabilizing temperature for Channel One that was drastically different than what is reflected as the effective temperature based on ultrasound data. The error for this Channel One reduces after reaching stabilization. The CSoS is capable of tracking the general thermal alterations of a thermally nonuniform material, but the quantitative representation can often be scaled incorrectly. This effect is highlighted at the beginning of testing. Considering pressure has the ability to scale the centroid, it is believed that Channel One, Channel Two, and Channel Three were attributed too high of a pressure for this study. According to the pressure study from Section 5.4, applied transducer pressure is inversely related to the centroidal value. Therefore, higher pressures may return higher values for internal temperature for these three channel lines. It is further hypothesized that the ultrasonic interpretations to the data became gradually more accurate due to the loss of surface tension on the transducers from the coupling gels. This minuet pressure change is all that is necessary to improperly scale the centroid for materials not in thermal equilibrium. Another reason pressure is likely the issue is because Channel Four reflects a near identical match to the presented thermocouple data. Temperatures for Channel Four differ between ultrasound and thermocouple data by less than 0.5°C at both the beginning and ending of testing. Additionally, all slopes which represent the temperature of Channel Four are also nearly identical. For a channel to be this accurate, it is difficult to conclude this method of analysis is not applicable for quantifying the temperature of thermally nonuniform materials. There exists too much evidence to the contrary. To this point, it is believed that in dealing with such a scenario, the quantitative accuracy of the proposed inspection method may be increased by utilizing a setup which controls transducer pressure. In conclusion, it is the belief of the authors that the CSoS has the potential to

quantify the effective internal temperature of the studied material which is thermally nonuniform if high attention is paid to transducer pressure. Since this study includes a setup which does not hold paramount the pressures applied to each transducer, the results of the temperature profiles are similarly skewed. For this reason, the temperature profiles are being omitted from this study to avoid redundancy in explanation.

CHAPTER SEVEN

Conclusion

The intent of this thesis was to present a new methodology to characterize the internal thermal state of materials containing a high degree of irregular porosity using ultrasound. Industries such as the petro-chemical industry, food industry, and polymer processing industry could benefit from harnessing the ability to quantify the internal temperature of a desired material without needing to access the medium. Characterizing homogeneous materials for this purpose was possible prior to the time of writing this thesis as described in [4-7]. The traditional inspection methodologies regarding the characterization of homogeneous materials have been demonstrated in Chapter Three using the onset to the time of flight for calculating the material's speed of sound. The candle wax represented a homogeneous material which experienced very few complications in characterization. Two linear functions that are continuous at the material's transition temperature were created for the material's speed of sound based on onset as a function of internal temperature. The machinist wax provided an example of the need for additional inspection methodologies and ultrasonic signal interpretations after performing the identical analysis. The machinist wax was unable to be fully characterized using the acoustic onset alone. Discontinuities in the speed of sound and temperature relationships obtained while using the previously proposed method of characterization for homogeneous materials on the machinist wax, leaving gaps in what could be thermally quantified. Thus, the proposed inspection methods shifted their focus

from the signal's onset to the parent signal itself. The parent signal came to be defined as the resulting longitudinal signal gated in time from the initial onset to the time at which its amplitude returns the baseline noise signal.

Shifting the focus from the acoustic signal's onset created a list of experimental requirements that could previously be ignored. Methods for maintaining the resolution of the desired parent signal were proposed and their impact was shown in Chapter Four. The first consideration for increasing the signal resolution was how to ensure no reflection waves, or echoes, were present in the desired parent signal. Understanding how long the parent signal is going to resonate after the onset to the time of flight is important to consider when determining channel distances. This is an important stipulation unique to using the centroid for characterization. The centroid cannot be used to quantify temperature for materials over shorter distances because of this. Understanding of signal resolution was then expanded upon by developing new ways to dampen out surface waves. Surface waves are not a unique issue to the centroid, but they can interfere with the accuracy of the estimates. Experimentation led to the development of a process to attribute to the containers which house the medium of interest. Surrounding the transducers with several thin layers of gum-tape made by ACP Composites [48], or a similarly tenacious material, and applying a covering across the surface greatly reduced surface wave interference. Lastly, the importance of selecting an appropriate acoustic coupling gel was relayed. Advisable TGA tests to perform when selecting an appropriate coupling gel were proposed. One of the quickest ways for a signal to lose its resolution is for the coupling gel to deteriorate during scanning. Using the ASTM E2550 standard [46] was suggested for identifying decomposition temperatures in acoustic gels across the

temperature ranges desired for use during ultrasonic testing. An additional consideration for future work can be made regarding the coupling gels. The surface tension of these gels which grips the transducers should be considered because of the impact it has on transducers pressure. After signal resolution was optimized for analyzing the entire parent signal, new interpretations of ultrasonic signals useful for material characterization were investigated.

The first contribution provided by this thesis was the discovery of the utility for an ultrasonic signal's normalized energy being useful in the thermal characterization of the selected porous material. Compared to the results from the DSC machine in Chapter Three, the energy analysis in Chapter Five provided increased accuracy in approximating the transition temperatures of the machinist wax. Additionally, DSC analysis loses accuracy due to sample sizing and ambiguous interpretation as suggested in [21]. DSC plots provide additional information beyond the transition temperature, but because of this, identifying the exact point of phase transition becomes subject to interpretive error. In comparison, obtaining the machinist wax's transition temperatures from the energy analysis was simplistic in calculation. When calculating the transition temperature of a material using the proposed energy analysis from quasi-isothermal data, the accuracy may be increased by collecting ultrasonic data at smaller increments of temperature. The inspection method proposes data points which return normalized energy values below 50% are considered solid while the data points above 50% are considered molten. The temperature where the data transitions from solid to molten was considered the transition temperature based on this methodology. Results from Chapter Six lead the authors to also propose signal energy may be beneficial for analyzing the thermal alterations of phase for

materials which are not in equilibrium while continuously collected ultrasonic data. The proposed methodology suggests as the normalized energy deviates from a constant value, the studied material has begun changing phase. Results from Chapter Six suggested energy was capable of identifying this phase change regardless of the medium cooling uniformly or nonuniformly.

Since energy couldn't quantify temperature as intended, the focus shifted to the additional information that could be provided by the central moments of the parent signal in Section 5.3. Aside from the first central moment, all other central moments gave some indication that a transition of phase was about to occur. For the standard deviation, derived from the variance, the maximum value indicated the beginning of transition. For skewness and kurtosis, the minimum value gave this indication. The problem is that each central moment has a unique meaning corresponding to the distribution of the parent signal. By themselves, the central moments rendered more questions than answers. It is very possible to have a maximum standard deviation which does not correlate to the transition temperature due to arbitrary loss of signal. It is concluded from the analysis listed within this thesis that these moments are not able to track the thermal alterations of phase state to the same capacity as the normalized energy. This is also where the strengths of the central moments were discovered, however. Observing the second, third, and fourth central moments in unison provides a wealth of information regarding the quality of the data that was collected. The central moments can assist in identifying signal resolution, signal shape, poor gating, and multiple other irregularities which deal with the quality of the a-scan. While the central moments may be useful in this manner, they lack the current ability to provide definitive results. They can assist in making assumptions

about ultrasound data, but to verify these assumptions requires the use of additional analysis techniques left for future studies. The authors propose an analysis using these moments on a-scan data can lead to an increased understanding of the behavior of the parent signal as well as give the analyst confidence in the data that is represented.

The main contribution provided within this thesis resides in the discovery of the newfound utility of the first raw moment for thermal characterization of materials. The onset to the time of flight was unable to generate a continuous function for internal temperature in Chapter Three for the highly porous material. The focus shifted to analyzing the entirety of the parent signal. This resulting signal was then converted to the effective power and the first raw moment was calculated. For the selected range of temperatures which crossed the transition temperature threshold, this material inspection methodology proved capable of generating two functions for internal temperature which were continuous at the transition temperatures during both the heating and cooling of this material.

The relationships defined in Section 5.3 for calculating the internal temperature of the machinist wax were created using data collected during the quasi-isothermal study presented in Section 5.1. The quasi-isothermal study discussed in Section 5.1 utilized a system capable of bringing the material near thermal equilibrium. The data collection process was discovered to be simplified for materials experiencing thermal equilibrium. The amount of pressure applied to the transducers used in data collection causes centroidal shifting as seen in Section 5.4. The shifting that occurs causes the effective temperature calculations from Equation 5.22 and Equation 5.24 to lose their accuracy. The impact of pressure becomes heightened for materials further away from thermal

equilibrium. This factor made data collection difficult during the nonuniform cooling experiment preformed in Section 6.3.

In realistic scenarios, most materials will not be experiencing thermal equilibrium while data collection occurs. For this reason, it was imperative to show the centroid was still capable of quantifying the effective internal temperature of the selected material not at thermal equilibrium. The studies within Chapter Six provided experimentation to observe the effectiveness of the newly proposed material inspection methodology and its applicability. The test analyzed in Section 6.2 collected ultrasonic data as the machinist wax uniformly cooled while maintaining a consistent, low transducer pressure. This test provided an example of the potential accuracy achievable using the proposed methodology for material characterization on the porous machinist wax. The effective temperature returned from ultrasound was compared to internal K-type thermocouple data. The greatest source of error was 5°C nearly two hours into testing after comparing the thermocouple and ultrasonic data. At several select points in time, both sources were in agreement to the tenth of a degree Celsius. Calculating the effective temperature is sufficient for providing an example of the usefulness of the centroidal speed of sound. However, the temperature profile along channel pathways was also calculated as an example of alternative representations for the internal temperature made possible by the centroidal speed of sound. Equation 6.1 was used within the MATLAB coding software to take the effective temperature, calculated using the relationships defined in Section 5.3, and generate an approximated temperature profile along channel lines.

The test for applicability included in Section 6.3 was intended to show the reader how improper transducer pressure will affect the accuracy of the effective internal

temperature approximation using the proposed methods. This test collected data as the machinist wax cooled nonuniformly. Improper pressure was attributed to the transducers during testing and the results were observed. Even though the calculated effective temperature lost accuracy, the centroidal speed of sound proved capable of tracking the general thermal alterations experienced throughout the selected porous material.

The centroidal speed of sound is proposed by the authors as a surrogate to the material property, speed of sound, which has been previously based upon the onset to the time of flight of an ultrasonic signal. The centroidal speed of sound is instead based upon the first raw moment of a parent signal. The centroidal speed of sound may be capable of thermally characterizing materials of several different internal structures. However, the present data is only capable of concluding that the proposed methodology is successful for thermally characterizing the selected material of randomly dispersed porosity studied within this thesis. Future work should be focused on the limitations of the proposed material inspection methodology. Other material structures should be analyzed to observe how the behavior of the centroid changes. Additionally, the factors which influence centroidal shifting, such as pressure, need to be fully analyzed and quantified for increased accuracy in the purposed methodology. Finally, a correlation between acoustic coupling gels and gradual centroidal shifting due to changes in surface tension should be observed.

BIBLIOGRAPHY

[1] P. B. Nagy, L. Adler, and B. P. Bonner, “Slow wave propagation in air-filled porous materials and natural rocks,” Appl. Phys. Lett., vol. 56, no. 25, pp. 2504–2506, Jun. 1990, doi: 10.1063/1.102872.

[2] M. Nori and R. Venegas, “Sound propagation in porous materials with annular pores,” The Journal of the Acoustical Society of America, vol. 141, no. 6, pp. 4642–4651, Jun. 2017, doi: 10.1121/1.4986939.

[3] J. Krautkrämer, “Determination of the size of defects by the ultrasonic impulse echo method,” Br. J. Appl. Phys., vol. 10, no. 6, pp. 240–245, Jun. 1959, doi: 10.1088/0508-3443/10/6/302.

[4] S. L. Stair, “Nondestructive Inspection and Characterization of Complex Engineering Materials via Ultrasound Techniques,” Ph.D. dissertation, Department of Mech. Eng., Baylor Univ., Waco, TX, 2017.

[5] C. M. Gregg, “The Observation of Phase State and Temperature Using Noninvasive Ultrasonic Waves,” M.S.M.E. thesis, Department of Mech. Eng., Baylor Univ., Waco, TX, 2017.

[6] E. W. Jost, “Non-Destructive Inspection Approach Using Ultrasound to Identify the Material State and Internal Temperature for Amorphous and Semi-Crystalline Materials,” Honors thesis, Baylor Univ., Waco, TX, 2018.

[7] T. D. Jeffrey, “Characterization of the Internal Temperature and Phase State of Amorphous Materials Using Ultrasonic Non-Destructive Evaluation,” M.S.M.E. thesis, Department of Mech. Eng., Baylor Univ., Waco, TX, 2019.

[8] C. Li, L. Huang, N. Duric, H. Zhang, and C. Rowe, “An improved automatic time-of-flight picker for medical ultrasound tomography,” Ultrasonics, vol. 49, no. 1, pp. 61–72, Jan. 2009, doi: 10.1016/j.ultras.2008.05.005.

[9] L. Svilainis, "Review of high resolution time of flight estimation techniques for ultrasonic signals," *2013 International Conference NDT*. 2013. pp. 1–12.

[10] F. Tariq, N. Naz, R. A. Baloch, and Faisal, “Characterization of Material Properties of 2xxx Series Al-Alloys by Non Destructive Testing Techniques,” J Nondestruct Eval, vol. 31, no. 1, pp. 17–33, Mar. 2012, doi: 10.1007/s10921-011-0117-5.

[11] G. D'Arrigo and A. Paparelli, "Sound propagation in water–ethanol mixtures at low temperatures. I. Ultrasonic velocity," The Journal of Chemical Physics, vol. 88, no. 1, pp. 405–415, Jan. 1988, doi: 10.1063/1.454616.

[12] X. Li, G. Ghoshal, R. J. Lavarello, and M. L. Oelze, "Exploring potential mechanisms responsible for observed changes of ultrasonic backscattered energy with temperature variations: Changes in ultrasonic backscattered energy with temperature," Med. Phys., vol. 41, no. 5, p. 052901, Apr. 2014, doi: 10.1118/1.4870964.

[13] R. Jia, Q. Xiong, G. Xu, K. Wang, and S. Liang, "A method for two-dimensional temperature field distribution reconstruction," Applied Thermal Engineering, vol. 111, pp. 961–967, Jan. 2017, doi: 10.1016/j.applthermaleng.2016.09.174.

[14] C.-Y. Yang, "Solving the two-dimensional inverse heat source problem through the linear least squares error method," International Journal of Heat and Mass Transfer, vol. 41, no. 2, pp. 393–398, Jan. 1998, doi: 10.1016/S0017-9310(97)00125-7.

[15] M. Herskowitz, S. Levitsky, and I. Shreiber, "Attenuation of ultrasound in porous media with dispersed microbubbles," Ultrasonics, vol. 38, no. 1–8, pp. 767–769, Mar. 2000, doi: 10.1016/S0041-624X(99)00156-0.

[16] L.W. Schmerr, "An Ultrasonic System" and "Reflection and Transmission of Bulk Waves," in *Fundamentals of Ultrasonic Nondestructive Evaluation: A Modeling Approach*, 2nd ed. New York, NY, USA: Springer, 2016, ch. 1, pp. 1–11. ch. 6, pp. 113–188.

[17] G. L. Workman, D. Kishoni, and P. O. Moore, "Ultrasonic Wave Propagation" and "Instrumentation for Ultrasonic Testing," in *Nondestructive Testing Handbook: Volume 7 Ultrasonic Testing*, 3rd ed. Columbus, OH, USA: American Society for Nondestructive Testing, 2007, ch. 2, pp. 35–57. ch. 5, pp. 177–199.

[18] Z. Zhang, M. Liu, Q. Li, and Y. Ang, "Visualized characterization of diversified defects in thick aerospace composites using ultrasonic B-scan," Composites Communications, vol. 22, p. 100435, Dec. 2020, doi: 10.1016/j.coco.2020.100435.

[19] Olympus, "Ultrasonic Transducers Technical Notes," datasheet, 2019.

[20] S. A. Lopez-Haro, A. Vera, and L. Leija, "Evaluation of an ultrasonic propagation speed measurement system in the temperature range from 20℃ to 45℃," in 2010 Pan American Health Care Exchanges, Lima, Peru, Mar. 2010, pp. 85–89. doi: 10.1109/PAHCE.2010.5474594.

[21] X. Jin, X. Xu, X. Zhang, and Y. Yin, “Determination of the PCM melting temperature range using DSC,” Thermochimica Acta, vol. 595, pp. 17–21, Nov. 2014, doi: 10.1016/j.tca.2014.09.004.

[22] GRAPHTEC, “GL820 midi LOGGER: USER’S MANUAL,” GL820-UM-151, datasheet, Jan. 2005.

[23] TA Instruments, “TGA Thermogravimetric Analyzer: Q Series, Getting Started Guide,” datasheet, 2001 [Revised June 2006].

[24] F. Lanza di Scalea and S. Salamone, “Temperature effects in ultrasonic Lamb wave structural health monitoring systems,” The Journal of the Acoustical Society of America, vol. 124, no. 1, pp. 161–174, Jul. 2008, doi: 10.1121/1.2932071.

[25] R. Karli, A. Bouchalkha, and K. Alhammadi, “Investigation of electromagnetic (EM) wave attenuation in oil pipeline,” in 2017 International Conference on Electrical and Computing Technologies and Applications (ICECTA), Ras Al Khaimah, Nov. 2017, pp. 1–4. doi: 10.1109/ICECTA.2017.8251982.

[26] P. F. Pires, J. M. S. S. Esperança, and H. J. R. Guedes, “Ultrasonic Speed of Sound and Derived Thermodynamic Properties of Liquid 1,1,1,2,3,3,3-Heptafluoropropane (HFC227ea) from 248 K to 333 K and Pressures up to 65 MPa,” J. Chem. Eng. Data, vol. 45, no. 3, pp. 496–501, May 2000, doi: 10.1021/je9902950.

[27] F. Lionetto, A. Tarzia, and A. Maffezzoli, “Air-Coupled Ultrasound: A Novel Technique for Monitoring the Curing of Thermosetting Matrices,” IEEE Trans. Ultrason., Ferroelect., Freq. Contr., vol. 54, no. 7, pp. 1437–1444, Jul. 2007, doi: 10.1109/TUFFC.2007.404.

[28] F. Lionetto and A. Maffezzoli, “Monitoring the Cure State of Thermosetting Resins by Ultrasound,” Materials, vol. 6, no. 9, pp. 3783–3804, Sep. 2013, doi: 10.3390/ma6093783.

[29] Y. Zhang et al., “Research on epoxy resin curing monitoring using laser ultrasonic,” Measurement, vol. 158, p. 107737, Jul. 2020, doi: 10.1016/j.measurement.2020.107737.

[30] P. A. Oliveira, R. M. B. Silva, G. C. Morais, A. V. Alvarenga, and R. P. B. C.-Félix, “Speed of sound as a function of temperature for ultrasonic propagation in soybean oil,” J. Phys.: Conf. Ser., vol. 733, p. 012040, Jul. 2016, doi: 10.1088/1742-6596/733/1/012040.

[31] Olympus, “Panametrics-NDT™: Ultrasonic Transducers,” 920-041C-EN, datasheet, 2008.

[32] I. Markova, G. Ronquillo Jarillo, and M. Markov, “Energy of acoustic signals in a borehole,” Geophysical Prospecting, vol. 67, no. 3, pp. 508–518, Mar. 2019, doi: 10.1111/1365-2478.12750.

[33] J. Zhou, N. Wu, and X. Wang, “Water temperature measurement using a novel fiber optic ultrasound transducer system,” in 2015 IEEE International Conference on Information and Automation, Lijiang, China, Aug. 2015, pp. 2316–2319. doi: 10.1109/ICInfA.2015.7279672.

[34] K. Ono, “A Comprehensive Report on Ultrasonic Attenuation of Engineering Materials, Including Metals, Ceramics, Polymers, Fiber-Reinforced Composites, Wood, and Rocks,” Applied Sciences, vol. 10, no. 7, p. 2230, Mar. 2020, doi: 10.3390/app10072230.

[35] U. Techavipoo, T. Varghese, Q. Chen, T. A. Stiles, J. A. Zagzebski, and G. R. Frank, “Temperature dependence of ultrasonic propagation speed and attenuation in excised canine liver tissue measured using transmitted and reflected pulses,” The Journal of the Acoustical Society of America, vol. 115, no. 6, pp. 2859–2865, Jun. 2004, doi: 10.1121/1.1738453.

[36] A. Abbate, J. Frankel, and P. Das, “Wavelet Transform Signal Processing Applied to Ultrasonics,” in Review of Progress in Quantitative Nondestructive Evaluation, D. O. Thompson and D. E. Chimenti, Eds. Boston, MA: Springer US, 1996, pp. 741–748. doi: 10.1007/978-1-4613-0383-1_97.

[37] I. W. Selesnick, “Hilbert transform pairs of wavelet bases,” IEEE Signal Process. Lett., vol. 8, no. 6, pp. 170–173, Jun. 2001, doi: 10.1109/97.923042.

[38] C. Zhou, Y. Wang, C. Qiao, S. Zhao, and Z. Huang, “High-accuracy ultrasonic temperature measurement based on MLS-modulated continuous wave,” Measurement, vol. 88, pp. 1–8, Jun. 2016, doi: 10.1016/j.measurement.2016.03.037.

[39] Magnaflux, “Ultragel II: Product Data Sheet” datasheet, [Revised Jan. 2021].

[40] Echo Ultrasonics, “EchoPure™: Phased Array, Cold Weather, Warm Welds,” 6635-01-565-2310, datasheet, [Revised Apr. 2019].

[41] Echo Ultrasonics, “VersaSonic®: Multipurpose High Temperature, Ultrasonic Couplant,” datasheet, [Revised Jun. 2019].

[42] R. V. Hogg, J. McKean, and A. T. Craig, “Probability and Distributions,” in *Introduction to Mathematical Statistics*, 6th ed. Upper Saddle River, NJ, USA: Pearson Education, 2005, ch. 1, pp. 62.

[43] H.-Y. Kim, “Statistical notes for clinical researchers: assessing normal distribution (2) using skewness and kurtosis,” Restor Dent Endod, vol. 38, no. 1, p. 52, 2013, doi: 10.5395/rde.2013.38.1.52.

[44] S. J. Lau, D. G. Moore, S. L. Stair, and C. L. Nelson, “Application of temporal moments and other signal processing algorithms to analysis of ultrasonic signals through melting wax,” in *AIP Conference Proceedings*, Minneapolis, Minnesota, 2016, p. 180006. doi: 10.1063/1.4940636.

[45] A. R. Selfridge, “Approximate Material Properties in Isotropic Materials,” IEEE Trans. Son. Ultrason., vol. 32, no. 3, pp. 381–394, May 1985, doi: 10.1109/T-SU.1985.31608.

[46] E37 Committee, “Test Method for Thermal Stability by Thermogravimetry,” ASTM International. doi: 10.1520/E2550-17.

[47] “Root of nonlinear function - MATLAB fzero.” https://www.mathworks.com/help/matlab/ref/fzero.html (accessed Jun. 24, 2021).

[48] ACP Composites, “Yellow Sealant Tape,” No. 49881, datasheet, 2014, [Revised Jan. 2015].